SOME ORTHOSILICATES AND THEIR HYDRATES

JUNE, 1967

NO. 19

by

L. E. CAMPBELL

Joint
Highway
Research
Project

PURDUE UNIVERSITY
LAFAYETTE INDIANA

Final Report

SOME ORTHOSILICATES AND THEIR HYDRATES

TO: G. A. Leonards, Director
Joint Highway Research Project

FROM: H. L. Michael, Associate Director
Joint Highway Research Project

June 20, 1967

File: 4-6-11

Project: C-36-47K

The attached research report entitled "Some Orthosilicates and Their Hydrates" is the Final Report on the HPR Part II research project "Properties of Some Silicates Related to Cements and Their Hydrates". The research was conducted and the report written by Mr. Larry E. Campbell, Graduate Instructor in Research, on our staff. Professor W. L. Dolch has supervised and guided the research and the preparation of the report for the Project.

The plan of study for this researchwas approved to be effective July 1, 1964. Mr. Campbell also used the report as his dissertation for a Ph.D. from the Department of Chemistry at Purdue. The report will be forwarded to the ISHC and the BPR for their comments and approval.

Respectfully submitted,

Harold L. Michael

Harold L. Michael
Associate Director

HLM:jrw

Attachment

Copy:
F. L. Ashbaucher
W. L. Dolch
W. H. Goetz
W. L. Grecco
G. K. Hallock
R. H. Harrell
V. E. Harvey
J. F. McLaughlin
F. B. Mendenhall
R. D. Miles
J. C. Oppenlander
C. F. Scholer
M. B. Scott
W. T. Spencer
F. W. Stubbs
H. R. J. Walsh
K. B. Woods
E. J. Yoder

Final Report

Some Orthosilicates and Their Hydrates

by

Larry E. Campbell
Instructor in Research

Joint Highway Research Project

Project: C-36-47K

File: 4-6-11

Prepared as Part of an Investigation

Conducted by

Joint Highway Research Project
Engineering Experiment Station
Purdue University

in cooperation with the

Indiana State Highway Commission

and the

U. S. Department of Transportation
Federal Highway Administration
Bureau of Public Roads

The opinions, findings and conclusions expressed in this publication are those of the authors and not necessarily those of the Bureau of Public Roads.

Not Released for Publication

Subject to Change

Not Reviewed By
Indiana State Highway Commission
or the
Bureau of Public Roads

Purdue University
Lafayette, Indiana
June 20, 1967

ACKNOWLEDGMENTS

The author wishes to thank Dr. A. F. Clifford, his major professor and Dr. W. L. Dolch, co-chairman of his advisory committee for their interest, assistance and advice throughout this study. Thanks also to the other members of his advisory committee Dr. J. W. Richardson and Dr. M. E. Lipschutz.

The research was conducted in the laboratories of the Joint Highway Research Project which also, along with the U. S. Bureau of Public Roads supported the research. Their generous support is appreciated.

Mr. Mark Montgomery and James V. Barnes assisted in many of the experiments.

Special thanks go to Dr. L. E. Copeland of the Portland Cement Research Association and Dr. S. A. Diamond of the School of Civil Engineering at Purdue for the helpful discussion of the findings of this study.

Digitized by the Internet Archive
in 2011 with funding from
LYRASIS members and Sloan Foundation; Indiana Department of Transportation

http://www.archive.org/details/someorthosilicat00camp

TABLE OF CONTENTS

Page

LIST OF TABLES v

LIST OF FIGURES vi

ABSTRACT x

INTRODUCTION. 1

LITERATURE SURVEY 4
  Barium Silicates and Barium Silicate Hydrates . . 4
  Strontium Silicates and Strontium Silicate Hydrates 8
  Calcium Silicates and Calcium Silicate Hydrates . 10
  Cadmium Silicates and Cadmium Silicate Hydrates . 15
  Infrared Studies on Orthosilicates and Some Silicate Hydrates. 15
  Heterogeneous Kinetics. 21
  Aqueous Silicate Ions 24

EXPERIMENTAL. 26
  Preparation of Compounds. 26
  Characterization of Compounds 29
  Measurement of Kinetic of Reaction of Anhydrous Compounds. 31

DATA 35
  X-Ray Diffraction 35
  Infrared Spectra. 35
  Differential Thermal Analysis 35
  Electron Micrographs. 35
  Adsorption Data on Anhydrous Silicates. 35
  Kinetic Measurements. 60

DISCUSSION OF RESULTS 81

SUMMARY OF RESULTS. 124

CONCLUSIONS. 126

BIBLIOGRAPHY. 127

Page

APPENDIX A 131
Description of BET Method and Apparatus for Krypton Adsorption Isotherms and Surface Areas 131

APPENDIX B 138
Description of Circuit for Measuring Resistances and Converting High Frequency A.C. to D.C. Suitable for Sargent SR Recorder 138

APPENDIX C 141
Application of Halford's Method to Prediction of Infrared Selection Rules for Orthosilicates 141

VITA 150

LIST OF TABLES

Table Page

1. Structural Data for Orthosilicates and Some Silicate Hydrates. 5

2. Calculated and Observed Frequencies for Silicate Ions. 18

3. Fundamental Vibrations of the Tetrahedral Ion. . 19

4. X-Ray Diffraction Data.. 36

5. X-Ray Diffraction Data for the Hydrates of the Orthosilicates. 37

6. Chemical Analysis of the Silicate Hydrates.. . . 88

7. Results of Krypton Adsorption Specific Surface Area Measurements. 88

8. Results of Chemical Analysis of Solutions After Reaction at 25.0°C.. 90

9. Measured Values of Equivalent Conductance of Silicate Hydrates. 91

10. Calculated Values of k for Ba_2SiO_4.. 102

11. Calculated Values of k for Sr_2SiO_4. 102

12. Calculated Values of k for β-Ca_2SiO_4.. 114

13. Calculated Values of k for γ-Ca_2SiO_4.. 119

Appendix

C-1. Space Group and Unit Cell Population for Some Orthosilicates. 143

C-2. Splittings of T_d Modes under Lower Symmetry Restrictions. 148

LIST OF FIGURES

Figure Page

1. Mole Ratio of CaO to SiO_2 in Solid Against Concentration of Calcium Ion in Solution (millimoles/liter). 14

2. Silicate Groupings (A) Isolated Unit; (B) Dimer; (C,D) Rings; (E) Infinite Chain; (F) Infinite Band; (G) Infinite Sheet. 16

3. Apparatus for Measuring Reaction Kinetics. . . 34

4. Infrared Spectra of A) Ba_2SiO_4 and B) $BaH_2SiO_4 \cdot aq$. 39

5. Infrared Spectra of A) Sr_2SiO_4 and B) $SrH_2SiO_4 \cdot aq$. 41

6. Infrared Spectra of A) β-Ca_2SiO_4 and B) $CaH_2SiO_4 \cdot aq$. 43

7. Infrared Spectra of A) γ-Ca_2SiO_4 and B) CaH_2SiO_4 aq. 45

8. Infrared Spectra of A) Cd_2SiO_4 and B) CdH_2SiO_4 aq. 47

9. Differential Thermal Analysis Results (A) Hydrate of Sr_2SiO_4, (B) Hydrate of Ca_2SiO_4 and Ca_2SiO_4, (C) Hydrate of Ba_2SiO_4, (D) Hydrate, CdH_2SiO_4. 48

10. Differential Thermal Analysis Results (A) Ba_2SiO_4, (B) Sr_2SiO_4, (C) Cd_2SiO_4 (D) γ-Ca_2SiO_4, (E) β-Ca_2SiO_4.. 49

11. Electron Micrograph of Hydrate of Ba_2SiO_4 (47000X). 51

12. Electron Micrograph of Hydrate of Sr_2SiO_4 (47000X). 53

Figure Page

13. Electron Micrograph of Hydrate of β-Ca_2SiO_4 (47000X). 55

14. Electron Micrograph of Hydrate of γ-Ca_2SiO_4. . 57

15. Electron Micrograph of $CdH_2SiO_4 \cdot aq.$ (47000X). . 59

16. Fraction Reacted of Ba_2SiO_4 vs. Time for Several Values of Sample Size (C_o). 63

17. Fraction Reacted of Ba_2SiO_4 vs. Time for Several Values of Initial $Ba(OH)_2$ Concentration. . 64

18. Fraction Reacted of Ba_2SiO_4 vs. Time for Several Values of Sample Specific Surface Areas (S_o) but constant (C_o).. 65

19. Fraction Reacted of Ba_2SiO_4 vs. Time for Various Temperatures but Constant Sample Size and Surface Areas.. 66

20. Fraction Reacted of Sr_2SiO_4 vs. Time for Several Values of Sample Sizes (C_o). 67

21. Fraction Reacted of Sr_2SiO_4 for Several Values of Initial $Sr(OH)_2$ Showing vs. Time for Concentration. 68

22. Fraction Reacted of Sr_2SiO_4 vs. Time for Different Surface Areas (S_o). 69

23. Fraction Reacted of Sr_2SiO_4 vs. Time for Several Values of Temperature (T). 70

24. Concentration of $Ca(OH)_2$ and CaH_2SiO_4 in Solution as Function of Time for the Reaction of β-Ca_2SiO_4. 71

25. Fraction Reacted of β-Ca_2SiO_4 vs. Time for Several Values of Sample Sizes (C_o).. 72

26. Fraction Reacted β-Ca_2SiO_4 vs. Time for Several Valuesof Initial $Ca(OH)_2$ Concentration. 73

27. Fraction of β-Ca_2SiO_4 vs. Time for Several Values of Specific Surface Area (S_o). 74

28. Fraction Reacted of β-Ca_2SiO_4 vs. Time for Several Values of Temperature (T). 75

Figure Page

29. Data for γ-Ca_2SiO_4 Showing Concentration of Species in Solution vs. Time for Various Value of C_o. 76

30. Fraction Reacted of γ-Ca_2SiO_4 vs. Time for Several Values of Sample Sizes (C_o). 77

31. Fraction Reacted of γ-Ca_2SiO_4 vs. Time for Several Values of Initial $Ca(OH)_2$ Concentration (C_i).. 78

32. Fraction Reacted of γ-Ca_2SiO_4 vs. Time for Several Values of Specific Surface Areas (S_o).. 79

33. Fraction Reacted of γ-Ca_2SiO_4 vs. Time for Several Values of Temperature (T). 80

34. Fraction of Anhydrous Ba_2SiO_4 Remaining as a Function of Time for Varying Sample Sizes. . (C_o).. 94

35. Fraction of Anhydrous Ba_2SiO_4 Remaining as a Function of Time for Various Values of Specific Surface Areas (S_o). 95

36. Fraction of Anhydrous Ba_2SiO_4 Remaining as a Function of Time for Varying Temperatures. . . 96

37. Fraction of Anhydrous Sr_2SiO_4 Remaining as a Function of Time for Various Sample Sizes (C_o).. 97

38. Fraction of Anhydrous Sr_2SiO_4 Remaining as a Function of Time for Various Specific Surface Area. 98

39. Fraction of Anhydrous Sr_2SiO_4 Remaining as a Function of Time for Various Temperature.. . . 99

40. Rate Constant Dependence on Temperature for Ba_2SiO_4.. 104

41. Rate Constant Dependence on Temperature for Sr_2SiO_4. 105

42. Reaction of β-Ca_2SiO_4 with Water at 25.0°C, Effect of Sample Size. 107

Figure Page

43. Reaction of β-Ca_2SiO_4 with Water at 25.0°C, Effect of Surface Area. 108

44. Reaction of β-Ca_2SiO_4 with Water, Effect of Temperatures. 109

45. Reaction of γ-Ca_2SiO_4 with Water, Effect of Sample Size.. 110

46. Reaction of γ-Ca_2SiO_4 with Water, Effect of Surface Area (S_o).. 111

47. Reaction of γ-Ca_2SiO_4 with Water, Effect of Temperatures. 112

48. Reaction of β-Ca_2SiO_4 with $Ca(OH)_2$ Solutions at 25.0°C. 115

49. Reaction of γ-Ca_2SiO_4 with $Ca(OH)_2$ Solutions at 25.0°C. 116

50. Rate Constant Dependence on Temperature for β-Ca_2SiO_4. 117

51. Activation Energy for γ-Ca_2SiO_4.. 118

Appendix

A-1. Gas Adsorption Apparatus. 133

A-2. Krypton Adsorption Isotherm for Ba_2SiO_4, Fineness Fraction No. 1.. 134

A-3. Krypton Adsorption Isotherm for Sr_2SiO_4, Fineness Fraction No. 1.. 135

A-4. Krypton Adsorption Isotherm for β-Ca_2SiO_4, Fineness Fraction No. 4.. 136

A-5. Krypton Adsorption Isotherm for γ-Ca_2SiO_4, Fineness Fraction No. 2.. 137

B-2. Bridge Circuit for Resistance Measurement of Solution. 139

C-1. Symmetry Modes for an Isolated XY_4 Molecule.. 149

ABSTRACT

Campbell, Larry Edwin. Ph.D., Purdue University, June 1967, Some Orthosilicates and their Hydrates, Major Professor: Alan F. Clifford.

The reactions of several alkaline-earth orthosilicates with water were studied. The compounds used were the orthosilicates of barium, strontium, and calcium, the last in both the β and γ phases. The objectives of the study were to determine the processes of the early hydration reactions of these substances, to determine the activation energies involved, and to relate any differences to structural differences in the compounds. A secondary objective was to study the final products of the reaction.

The anhydrous silicates were prepared by ignition of silicic acid and the appropriate carbonate in a tube furnace in the usual way. The silicates were then separated into several size fractions by sedimentation in ethanol. The specific surface area of each fraction was determined by krypton adsorption measurements.

The anhydrous silicates were mixed with an amount of water large enough so that, at least for an appreciable initial time, no saturation of the water with dissolved species occurred. Under these conditions the reaction was

studied without the rate-controlling diffusion conditions that are present in such more concentrated systems as, for example, portland-cement concrete.

The reaction was followed conductimetrically, and the values obtained were recorded by means of appropriate circuiting. The well-stirred system was sampled from time to time and the samples were analyzed for reaction products.

The reaction variables controlled were the sample size, the initial concentration of the alkaline-earth hydroxides in solution, the temperature, and the specific surface area of the orthosilicates.

A consideration of the equivalent conductances of the various products that could have been formed by the reaction showed that the species produced in solution in all cases was the dibasic orthosilicate ion, $H_2SiO_4^{-2}$.

A consideration of various models for the progress of the reaction led to the postulation of the following process: 1) protonation of a silicate ion in the surface of the anhydrous orthosilicate to form the tribasic orthosilicate ion, $HSiO_4^{-3}$, followed by 2) dissolution of the tribasic metallic orthosilicate from the surface. In the cases of the barium and strontium compounds the second of these steps was found to be rate-determining; for the two calcium compounds the rate-determining step was the first. It is further postulated that the dissolved silicate is very rapidly converted to the dibasic species in solution.

The measured activation energies were 4.82, 9.05, 11.4, and 16.6 Kcal/mole for Ba_2SiO_4, Sr_2SiO_4, β-Ca_2SiO_4, and γ-Ca_2SiO_4, respectively.

Study in various ways of the hydrated species collected by concentrating the reaction products showed them to be also orthosilicates, with molar metal to silica ratios of almost 1. The infrared spectra of the orthosilicates and their hydrates were similar except for slightly higher frequencies of the asymmetric stretching modes and slightly lower frequencies of the bending modes for the hydrates.

INTRODUCTION

One of the most important chemical reactions known to technology is that of water with compounds in the calcium orthosilicate system. This reaction is common and yet, despite an enormous amount of research, is one of the least understood. Methods for following heterogeneous reactions are few and complex and have not been applied fruitfully to the study of the calcium silicate hydration reactions. The purpose of this work was to make a systematic study of several important variables in the heterogeneous reactions of divalent alkaline-earth orthosilicates and water, and to compare their differences in order to elucidate the important parameters for the reactions.

There are four crystallographic modifications of dicalcium silicate, of which two are the gamma and beta forms. The crystallographic forms are orthorhombic and monoclinic respectively. It has been stated that the gamma form is unreactive (1)* while the beta form is known to react in pastes, i.e. when mixed with a small amount of water, giving products that harden to a hydraulic cement. Barium and strontium orthosilicates have been reported to be reactive

---

* Numbers in parentheses refer to the list of references at the end of the text.

with water (2), and barium silicate has been investigated as a possible cement (3).

The reactions of these orthosilicates are complicated, in paste form, by saturation or supersaturation of the solution phase with hydroxides formed as by products in the reaction, and, at least for the calcium salts, by precipitation of the insoluble hydrated silicate reaction products onto the anhydrous surfaces. It is thought that such coatings soon cause diffusion processes to become rate-controlling. The reactions in this study were carried out so as to eliminate saturation and any resultant difficulties. The study of dilute suspensions rather than pastes results in an unfortunate lack of correspondence with the system of technological importance, concrete. The justification for such a departure is that the aim was to investigate the early reaction processes, and an implied assumption is that the earliest chemical processes are similar in the two kinds of systems.

This study involved the hydration of a series of orthosilicates, the surface areas of which were determined by krypton adsorption. The hydration reactions were carried out in large excesses of water, and the rates of production of the hydroxides were measured conductimetrically. The effects of temperature, pH, and sample size were studied, and the stoichiometry of the products formed and their physical properties were also investigated.

A model of a reaction mechanism was fitted to the data obtained.

LITERATURE SURVEY

Orthosilicates are so-called because they contain the orthosilicate ion. The orthosilicate ion is tetrahedral and shares its corners with no other silicate ion (4). The alkaline-earth orthosilicates have many similarities, but also enough differences to warrant a discussion of each system separately.

Barium Silicates and Barium Silicate Hydrates

Two barium orthosilicates have been reported. Gallo (3) first reported Ba_3SiO_5, but offered little characterization. Toropov et al. (5) prepared and obtained x-ray diffraction data for Ba_3SiO_5. They postulated the same structure for Ba_3SiO_5 as that of its isotype Rb_3BeF_5. Glushkova and Keler (6) reported x-ray diffractions results that were indexed on the basis of a hexagonal unit cell. The lattice parameters are shown in Table 1. They reported a method of preparation of Ba_3SiO_5 in which the crucible was of Ba_3SiO_5 composition. Hanna (7) tried to prepare Ba_3SiO_5, but was unsuccessful. Eskola (8), one of the first investigators of the BaO-SiO_2 system, found the most basic phase to be Ba_2SiO_4 rather than Ba_3SiO_5.

Lehmann, Muller, and Wermbter (9) reported that Ba_3SiO_5

Table 1. Structural Data for Orthosilicates.

	Space Group	Unit Cell Pop.	Lattice Parameters, Å			Ref.
			a	b	c	
Ba_3SiO_5	(Hexagonal)	10	15.62		7.19	6
Ba_2SiO_4	Pmnb	4	7.56	10.17	5.76	11
Sr_3SiO_5	(Tetragonal)	4	6.934		10.72	15
Sr_2SiO_4	Pmnb	4	7.26	9.66	5.59	11
Ca_3SiO_5	$R\bar{3}m$	9	7.0		25.0	18
β Ca_2SiO_4	$P2_{1/n}$	4	5.48	6.76	9.28	21
γ Ca_2SiO_4	Pmnb	4	5.06	11.28	6.78	20
Cd_3SiO_5	(Orthogonal)	2	6.85	6.86	4.85	15
Cd_2SiO_4	Fddd	8	6.04	11.85	9.75	15

is unstable below 740°C with respect to disproportionation to BaO and Ba_2SiO_4.

Eskola (8) and Levin and Ugrinic (10) reported difficulties in preparing pure Ba_2SiO_4 because of the reactivity of BaO towards platinum, with which it forms barium platinates.

Hanna (7) prepared Ba_2SiO_4 and made an extensive study of its hydration reactions in paste form. He concluded that a crystalline hydrate was formed with composition BaH_2SiO_4. In an excess of water he found a BaO/SiO_2 ratio of the hydrate of 1:1, but in pastes the ratio was 1.4:1. His crystalline hydration product had a specific surface area from 3 to 35 m^2/g, with the compound with a high BaO/SiO_2 ratio being the more crystalline. He also found a linear relationship between the amount of $Ba(OH)_2$ formed and the non-evaporable water remaining in the hydrate. Non-evaporable water is defined as the water driven off by ignition to red heat, but not by a more gentle drying process, such as oven-drying or desiccation over magnesium perchlorate dihydrate or ice at the dry-ice temperature. It is, roughly speaking, the "combined" as opposed to the free or adsorbed water. Hanna interpreted his result as indicating that the same product was formed throughout the reaction.

Barium orthosilicate, Ba_2SiO_4, has been studied by Zhuravlev (2), Eskola (8), Levin and Ugrinic (10), and Glushkova and Keler (6). None of the above investigators

found evidence of polymorphism. O'Daniel and Tsheischwili (11) reported lattice parameters for Ba_2SiO_4 by analogy with its isotype Rb_2BeF_4; these are shown in Table 1.

Funk (12) made an extensive study of the hydrates of barium silicates. He prepared many of them by precipitation using solutions of sodium silicate and barium chloride or hydroxide. He reported that Ba_2SiO_4 reacted with $Ba(OH)_2$ solution at 100°C for 24 hours to form $BaO \cdot SiO_2 \cdot H_2O$. A barium silicate hydrate of composition $BaO \cdot SiO_2 \cdot 6H_2O$ was made by heating and shaking a 1 percent $Ba(OH)_2$ solution for several days at room temperature with $BaO \cdot SiO_2 \cdot H_2O$, or alternatively amorphous silicic acid was treated with a large amount of 1.0 percent $Ba(OH)_2$ solution. The concentration of $Ba(OH)_2$ was critical; if less than 0.5 percent, no $Ba(OH)_2$ was absorbed, if greater than 1.0 percent, $BaO \cdot SiO_2 \cdot H_2O$ was formed.

Another amorphous phase with the composition of $BaO \cdot 2SiO_2 \cdot H_2O$ was prepared by Funk (12) from $BaCl_2$ and NaH_3SiO_4 solutions. This hydrate was stable over the temperature range 0-100°C but was poorly crystalline.

Hohne and Dornberger-Shiff (13) were able to grow crystals of $BaO \cdot SiO_2 \cdot 6H_2O$ of about 0.1 mm in size and made a complete crystal structure analysis. The crystallographic data are given in Table 1. The crystal contains the orthosilicate group. The stoichiometry corresponds to the composition $BaH_2SiO_4 \cdot 5H_2O$. While the structure of $BaO \cdot SiO_2 \cdot H_2O$

is unknown, it is an orthosilicate in view of the fact that it is formed from the orthosilicate $BaH_2SiO_4 \cdot 5H_2O$ by loss of five moles of water at only 100°C.

Strontium Silicates and Strontium Silicate Hydrates

Nurse (14) reported the preparation of Sr_3SiO_5 by firing a 3:1 molar mixture of $SrCO_3$ and SiO_2 at 1500°C in a platinum boat. He reported that Sr_3SiO_5 did not resemble Ca_3SiO_5 structurally and did not react with water in the way that Ca_3SiO_5 does. Glasser and Glasser (15) reported a tetragonal structure with the parameters shown in Table 1. They also showed an analogy of the Sr_3SiO_5 structure to that of Ca_3SiO_5, in contradiction to the findings of Nurse.

Eskola (8) reported reaction conditions for the formation of Sr_2SiO_4. O'Daniel and Tscheischwili (11) reported a structure for Sr_2SiO_4 based on the analogy with its isotype K_2BeF_4. Their structural parameters are given in Table 1.

Carlson and Wells (16) made a study of the strontium silicate hydrates, several of which they prepared hydrothermally. One crystalline hydrate with a composition of $3SrO \cdot 2SiO_2 \cdot 3H_2O$ was prepared by adding 12 grams of $Na_2SiO_3 \cdot 9H_2O$ dissolved in a small amount of water to a boiling solution of strontium hydroxide (30 g of $Sr(OH)_2 \cdot 8H_2O$ in about 800 ml. of water). The precipitate was boiled for an hour and then kept at 100°C overnight. The crystals were small, lath shaped, and slightly birefringent with negative elongation. Differential thermal analysis of this phase

showed a large endotherm at 340°C and two smaller ones at 820° and 890°C.

The same preparation was carried out with silicic acid instead of $Na_2SiO_3 \cdot 9H_2O$, and dendritic crystals of the composition $3SrO \cdot 2SiO_2 \cdot 4H_2O$ were formed. Differential thermal analysis of this phase showed two large endotherms, one at 230°C and the other at 300°C. Carlson and Wells (17) interpreted the peak at 230°C as showing a conversion to $3SrO \cdot 2SiO_2 \cdot 3H_2O$. This interpretation was strengthened by further endothermic peaks at 800°C and 890°C, just as were obtained with the 3:2:3 hydrate. When a 3:1 molar mixture of $Sr(OH)_2 \cdot 8H_2O$ and silica gel were heated together for seven days at 158°C under hydrothermal conditions a compound of composition $3SrO \cdot SiO_2 \cdot 2H_2O$ was formed that crystallized in small needles or plates. No differential thermal analysis was run on this sample, but if the reaction was carried out above 183°C only $Sr(OH)_2 \cdot 8H_2O$ and Sr_2SiO_4 were formed.

Carlson and Wells (16) treated a 2:1 molar ratio mixture of $Sr(OH)_2 \cdot 8H_2O$ and silicic acid at 138°C for 13 days and obtained needle-shaped crystals of a product of composition $2SrO \cdot SiO_2 \cdot H_2O$. Above 156°C in a bomb $2SrO \cdot SiO_2 \cdot H_2O$ decomposed to Sr_2SiO_4 irreversibly. When a 1:1 molar mixture of $Sr(OH)_2 \cdot 8H_2O$ and silicic acid was treated hydrothermally at 135°C for 7 days a phase was formed with the composition $SrO \cdot SiO_2 \cdot H_2O$. This phase appeared as minute flakes with a refractive index of 1.604, and it was always

contaminated.

When a 1:2 molar ratio mixture of $Sr(OH)_2 \cdot 8H_2O$ to silicic acid was reacted at 200°C for 7 days a contaminated mixture of $SrO \cdot SiO_2$ and $SrO \cdot 2SiO_2 \cdot H_2O$ was obtained. All attempts to prepare pure $SrO \cdot 2SiO_2 \cdot H_2O$ failed. Sr_2SiO_4 did not react with water hydrothermally.

Calcium Silicates and Calcium Silicate Hydrates

Tricalcium silicate was first stated to be the principle component of portland cement by Tornebohm (17). Jeffery (18) made a systematic study of the structures of the crystallographic modifications of Ca_3SiO_5. Single crystals of pure Ca_3SiO_5 were grown by Nurse and Jeffery (18), who determined their structure. The structural parameters are given in Table 1.

Alite is essentially Ca_3SiO_5 modified by solid solution of Al_2O_3 and MgO, with a stoichiometry of $54CaO \cdot 16SiO_2 \cdot Al_2O_3 \cdot MgO$ (18). It is the substance found in portland cement, rather than tricalcium silicate, which it closely resembles.

A third polymorph of Ca_3SiO_5 contains small quantities of FeO, Fe_2O_3, MnO and P_2O_5 as well as MgO and Al_2O_3 and is similar to alite.

Four crystallographic polymorphs of Ca_2SiO_4, α, α', β and γ have been reported (19).

The beta form is stable only above 450°C but can be stabilized at room temperature by the addition of 0.5 weight percent B_2O_3 (18) at 1000°C and then rapid cooling. Other

substances can also be used as stabilizers. In the absence of such a stabilizer the beta form spontaneously converts to the gamma with a large increase in volume of the unit cell (20). This process is called dusting, and it destroys large crystals of β- and γ-Ca_2SiO_4. Until recently, there were no crystals large enough to make a single crystal structure study. Smith, Majumdar, and Ordway (20) prepared a large crystal of γ-Ca_2SiO_4 by refluxing ethyl orthosilicate with $Ca(NO_3)_2$, firing at 400°C, then at 1000°C, and finally at 1500°C. Most of the crystals were destroyed upon cooling, but a few large crystals of pure γ-Ca_2SiO_4 were salvaged. The structure that had been postulated by O'Daniel and Tscheischwili (11), which is orthorhombic (as shown in Table 1), was verified.

The structure of β-Ca_2SiO_4 was determined by Midgely (21). It is monoclinic with the cell constants and space group shown in Table 1.

The properties and preparation of the calcium silicate hydrates have been reviewed many times; see Taylor (23, 24).

When β-Ca_2SiO_4 is reacted with water it forms one of several closely related calcium silicate hydrates, depending on reaction conditions. One of these, C-S-H(I) exhibits CaO/SiO_2 molar ratios of 0.8 to 1.5; the H_2O/SiO_2 ratio vary from 2.5 to 0.5 (22). Another, C-S-H(II) has a CaO/SiO_2 ratio varying from 1.5 to about 2. The microscopical appearance of calcium silicate hydrate (I) is described as an

amorphous, gelatinous material with a flaky habit. The specific surface area of this material is very high, of the order of 300 m^2/g.

Greenberg and Chang (25) studied the solubility characteristics of calcium silicate hydrates. They analyzed the solutions and the solids and calculated the solubility product for the compound CaH_2SiO_4. The pK_{sp} was + 7.0. They prepared calcium silicate hydrates with compositions varying from CaO/SiO_2 ratios of 0.8 to 1.5 by precipitation, and also hydrothermally, and then determined their solubilities in water at 25°C. The conclusions they drew were that the $H_2SiO_4^{-2}$ ion forms an insoluble product by reaction with Ca^{+2} ions.

Thorvaldson et al. (26) used radioactive calcium-45 solutions to measure the exchange rate between calcium hydroxide solutions made with calcium-45 and calcium silicate hydrates of composition $CaO \cdot SiO_2 \cdot XH_2O\text{-}Ca(OH)_2$. They discovered that two separate processes were taking place, one of which was rapid and the other much slower. They also calculated the CaO/SiO_2 mole ratio of the portion of the system that exchanged only slowly and found it to be essentially one.

Roller and Erwin (27) prepared calcium silicate hydrates with composition varying from CaO/SiO_2 ratios of 0.8 to 1.5. These hydrates were then placed either in water or calcium hydroxide solution where they dissolved to form calcium and

silicate ions, or adsorbed calcium hydroxide, depending on the molar CaO/SiO_2 ratio in the solid. If the equilibrium was attained by liberating ions from the solid to the solution, Roller and Erwin called the process the D approach. If, however, the solid adsorbed lime from solution they called the process the S approach. The equilibrium data for concentration of calcium and silica in solution as obtained from S and D approaches were plotted as the log of the CaO/SiO_2 molar ratio in the solid versus the log of the Ca^{+2} ion concentration in the solution. These data are shown in Figure 1. The breaks and level portions of the curve show the special stability of 1:1 calcium to silica molar ratio in the solid.

Roller and Erwin (27) assumed the composition of the solid to have a 1:1 CaO/SiO_2 molar ratio. They assumed that the excess $Ca(OH)_2$ over a mole ratio of 1:1 was adsorbed on the substrate of composition CaH_2SiO_4, and they were able to fit the adsorption data to a Freundlich isotherm. They also found that the adsorption of lime in region I in Figure 1 was rapid.

The nature of the surface area of calcium silicate hydrates has been studied by Kantro, Brunauer, and Weise (28). They discussed the calcium silicate hydrate formed from Ca_3SiO_5 from the point of view of the composition $Ca_3Si_2O_7 \cdot 3H_2O$.

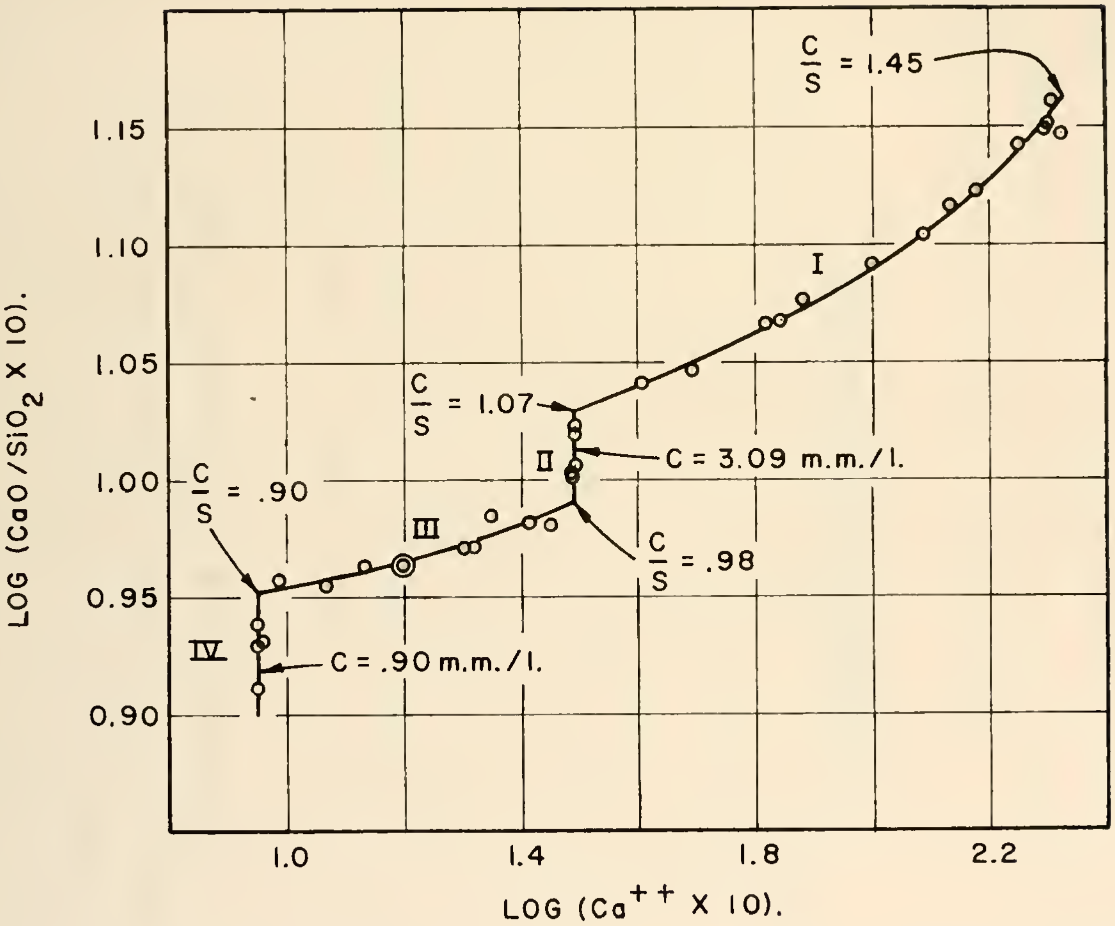

FIGURE 1. MOLE RATIO OF CaO TO SiO$_2$ IN SOLID AGAINST CONCENTRATION OF CALCIUM ION IN SOLUTION (MILLIMOLES/LITER).

Cadmium Silicates and Cadmium Silicate Hydrates

The $CdO-SiO_2$ system has been studied by Glasser and Glasser (18). They reported preparative techniques and x-ray diffraction data for Cd_3SiO_5, Cd_2SiO_4 and $CdSiO_3$. The lattice parameters and crystallographic data for Cd_2SiO_4 and Cd_3SiO_5 are shown in Table 1. The hydrates of these systems have not previously been studied.

Infrared Studies on Orthosilicates and Some Silicate Hydrates

The infrared adsorption spectra of orthosilicates have been studied by Tarte (29). He used the method of isomorphic substitution with solid solutions of the type $X_2(Si,Ge)O_4$, $(X,Y)_2SiO_4$, and $(X,Y)_2GeO_4$ where X and Y are divalent cations. By using the method of diluted solid solutions he was able to assign fundamental modes to spectral contributions from X-O and Si-O bands (29). Tarte studied the following divalent cations: X,Y = Mg, Ni, Co, Fe, Mn, and Ca.

Theoretical justification for the differences in molecular vibrations with varying lattices has been provided by Halford (30). He stated that the maximum symmetry a polyhedron can exhibit while confined to a crystallographic site is the symmetry of the site. If the crystal symmetry is known, to the extent of the space group, then the treatment of Halford can be used to predict the maximum number of spectral lines. Halford's method does not predict the intensity of the bands, but it can be used to rationalize the

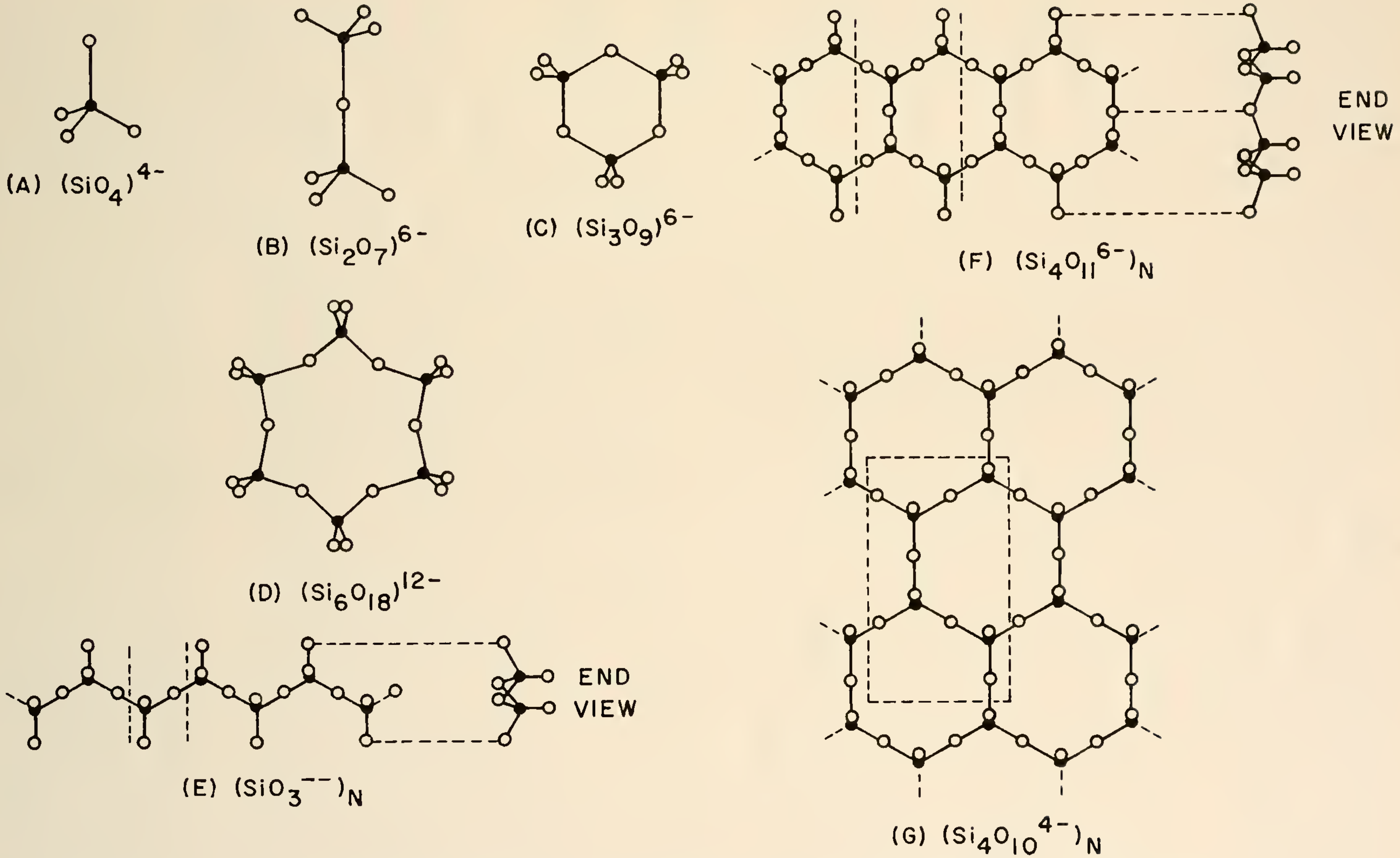
(A) $(SiO_4)^{4-}$
(B) $(Si_2O_7)^{6-}$
(C) $(Si_3O_9)^{6-}$
(F) $(Si_4O_{11}{}^{6-})_N$
END VIEW
(D) $(Si_6O_{18})^{12-}$
(E) $(SiO_3{}^{--})_N$
END VIEW
(G) $(Si_4O_{10}{}^{4-})_N$

FIGURE 2. SILICATE GROUPINGS: (A) ISOLATED UNIT; (B) DIMER; (C,D) RINGS; (E) INFINITE CHAIN; (F) INFINITE BAND; (G) INFINITE SHEET.

splitting of certain degenerate modes of vibrations in an assymmetric crystalline environment. Matossi (31) calculated the force constants and infrared frequencies for several silicate ions. His results are given in Table 2.

Saksena (32) calculated theoretical frequencies for silicate structural units. The units were isolated silicate tetrahedra, a sheet structure of the composition Si_4O_{10}, a chain structure of the composition SiO_3, and the dimer group Si_2O_7. The structures are shown in Figure 2. Saksena's conclusions about the distinguishing characteristics of the spectra for these structures are as follows:

(a) Sheet structures show one strong absorption band close to 1000 cm^{-1}.

(b) Orthosilicates show two strong bands, one about 1000 cm^{-1} and the other about 893 cm^{-1}.

(c) Chain structures show a strong band at 1111 cm^{-1}.

Hunt (33) made a study of the infrared spectra of some compounds in the CaO-SiO_2-H_2O system. The compounds he studied were natural minerals of the stoichiometry $CaO \cdot 2SiO_2 \cdot 2H_2O$ (Okenite), $CaO \cdot 2SiO_2 \cdot \frac{1}{2}H_2O$ (Truscottite), $2CaO \cdot 3SiO_2 \cdot 2H_2O$ (Gyrolite), $Ca_3(HOSiO_3)_2 \cdot 2H_2O$ (Afwillite), and $2CaO \cdot SiO_2 \cdot H_2O$ (Hillebrandite).

Hunt also studied the spectra of β-Ca_2SiO_4, γ-Ca_2SiO_4, and Ca_3SiO_5. He applied Halford's rules (30) to the analyses of the spectra of these anhydrous orthosilicates. His conclusions were that lattice modes, combination modes, and

Table 2. Calculated and Observed Frequencies for Silicate Ions (31)*.

Ion	Frequency, (cm^{-1})				
$SiO_4^{=}$	observed	944- 894	770	455 (440)	300 (360)
($ZrSiO_4$)	calculated	924	770	450	260
$Si_2O_7^{-6}$	observed	980- 860	587	486	435
(Thortvetite)	calculated	915	610	490	---
$Si_3O_9^{-6}$	observed	1065- 930	768	500- 462	385
(Benitoite)	calculated	1000	740	535	340
$SiO_3^{=}$	observed	1120	970- 930	565	520
(Clinoenstatite)	calculated	1050	1000- 920- 870	600	520

---

*Data in parenthesis derived from Raman spectra.

overtones make the spectra so complex a strict interpretation by means of Halford's rules is difficult.

The band assignments, according to Matossi (31) and Landolt-Bornstein (34), for the tetrahedral SiO_4^{-4} ion are shown in Table 3.

Table 3. Fundamental Vibrations of the Tetrahedral Ion (34).

Vibrational Species	Number of Vibrations	Approximate Frequency, cm^{-1}
A_1, non-degenerate	1	800 Raman, active
E, doubly degenerate	1	500 Raman, active
T_2, triply degenerate	2	625, 1050 Raman and I. R., active

Pepperhoff (35) measured the spectra of β- and γ-Ca_2SiO_4 and determined that they were similar but that the frequencies of the absorption bands were higher for β-Ca_2SiO_4.

Hunt (33) also investigated the state of the water in the hydrates by observing the OH stretching bands in the region of 3600 cm^{-1}. He found strong peaks in the OH stretching region of afwillite ($Ca_3(SiO_3H)_2 \cdot H_2O$) that led him to believe there was strong hydrogen bonding present.

Petch, Sheppard, and Megaw (36) studied afwillite in the range 2000 to 3600 cm^{-1}. They measured the spectra of powder and of oriented single crystals in order to determine the direction of O-H vibrations. They used crystal structure information to predict six hydrogen bond positions

per unit cell where hydrogen bonds occur. Three of these have O-H-O distances of 2.7Å, and three have O-H-O distances of 2.5Å. The bonds at 2.7Å correspond to absorption at approximately 3000 cm^{-1}. The 2.5Å hydrogen bonds absorb at lower frequencies. The observed spectra consisted of three bands at 2800, 3130, and 3340 cm^{-1}, corresponding to 2.7Å bands, and a band at 2400 cm^{-1} and two others at lower frequencies that were difficult to resolve.

Measurements made by Hunt (33) on the other calcium silicate hydrates showed that none of them possessed strong hydrogen bonding similar to that found in afwillite. He found no water deformation bands in truscottite ($CaO \cdot 2SiO_2 \cdot \frac{1}{2}H_2O$) or hillebrandite $2CaO \cdot SiO_2 \cdot H_2O$. The spectrum of afwillite, $Ca_3(SiO_3OH)_2 \cdot 2H_2O$, showed a weak band at 1650 cm^{-1}.

Tri-calcium silicate, Ca_3SiO_5, hydrated in a ball mill showed a sharp absorption at 3620 cm^{-1} owing to $Ca(OH)_2$ and broad absorption at longer wavelengths due to the presence of hydrogen bonds of moderate strength.

The water contained in a crystal as H_2O may be "lattice water" or "complex water" (37). In general, lattice water, actually -OH groups attached to the silicate framework, absorbs at 3550-3200 cm^{-1} (antisymmetric and symmetric OH stretching modes). Much fine structure can be observed, depending on the crystalline environment. Lattice water absorbs in the low frequency infrared region (600-300 cm^{-1})

owing to librational modes. Librational modes are due to crystal lattice restricted rotational motions because of hydrogen bonding to neighboring atoms. The molecular motion is a rotational oscillation (37).

"Complex water" can be thought of as being strongly bound to some other atom, and as such it takes on new molecular symmetry and selection rules. The frequencies of complex water absorption modes are sensitive to the coordinating atoms, and consequently general interpretations of spectra are dangerous (37). There have been several studies of coordinated water (38, 39, 40).

Hydroxyl groups in complexes may give rise to O-H stretching bands in the 3600-3000 cm^{-1} region. Hunt (33) used the lack of H-OH deformation at 1630 cm^{-1} to indicate the lack of water. Nevertheless, MOH bonds exhibit deformation modes if the M-OH bond is covalent. Scargill (41) studied ruthenium - hydroxo complexes and observed bands at 3500-3200 cm^{-1} and MOH bending bands at 1000-970 cm^{-1}.

Heterogeneous Kinetics

Some examples of heterogeneous kinetics have been studied in connection with catalysis and are described in references (49) and (50).

O'Conner and Greenberg (44) measured the kinetics for the dissolution of silica in aqueous solutions. In the rate equation used by them it was assumed that the stirring was not rate-determining as long as the suspension was well

stirred. They also assumed the rate of dissolution of SiO_2 was first order with respect to the surface area and that the reversible reaction rate was proportional to the concentration of monomeric silica and to the surface area of undissolved silica.

If the silica particles were assumed to be spherical, the concentration would be related to the surface area of the particle by

$$C_p = \frac{4}{3} \pi r^3 \times \frac{\rho n}{60.08}$$

where C_p is the "concentration" of the undissolved silica particles, r is their radius, ρ is their density, and n is the number of particles in a gram of silica.

This rate equation, which assumed spherical particles, fit the data well (44). It should be noted that the ratio of the volume of any particle to its surface area is proportional to a mean dimension of the particle.

The integrated equation of O'Conner and Greenberg is

$$C_p^{1/3} = C_{po}^{1/3} - kt$$

O'Conner and Greenberg's conclusions were as follows:

1) Their rate equation holds well for solution in alkaline media.

2) The reaction for solution in water holds only if the silica is well dispersed.

3) In alkaline solution a negative surface charge prevents flocculation and aids dispersion.

4) Quartz is covered by an amorphous layer of silica.

5) The activation energy for solution of silica in water is about 18 Kcal/mole.

Spring (50) studied the rate of decomposition of calcium carbonate single crystals. He worked with parallelepipeds of marble that were waxed on all faces but one. This face was exposed to a five percent hydrochloric acid solution. From studies on various sizes of parallelepipeds and various concentrations of hydrochloric acids, he found that the rate of production of CO_2 was proportional to the hydrogen ion concentration and to the surface area of the carbonate mineral, by the equation

$$\frac{d\,[CO_2]}{dt} = k\,[S]\,[H^+]$$

From temperature versus rate data Spring measured an activation energy of 6,350 cal/mole over a temperature range from 15-55°C. On the basis of molecular collision with the surface, Moelwyn-Hughes (51) calculated that one out of every 42 ions that strike the surface of the carbonate mineral forms an HCO_3^- ion, which decomposes to CO_2 and OH^- in acid solution. Diffusion is not a rate determining step.

Special heterogeneous kinetics examples can be found in Moelwyn-Hughes (51), Glasstone (52), and Benson (53).

Aqueous Silicate Ions

Roller and Erwin (27), Greenberg (25), and Iler (46) discussed the aqueous chemistry of the silicate ion. In acid solution and slightly alkaline solutions of pH as high as 7.7 the major species is the unionized orthosilicic acid (H_4SiO_4). Between pH 7.7 and 10.5 the stable species is the ion $H_3SiO_4^-$. At pH above 10.5 the dominant silicate ion is $H_2SiO_4^=$. Greenberg (25) pointed out that, when dissolving C-S-H(I), after 20 minutes the silicate ion is still that produced by the calcium silicate hydrate solid phase ($H_2SiO_4^=$) even though the $H_3SiO_4^-$ ion should be a major component. Roller and Erwin (27) determined the polymerization equilibrium constant for dimerization of the $H_3SiO_4^-$ ion to be 2200 (i.e. $\frac{H_4Si_2O_7^=}{{H_3SiO_4^-}^2} = 2200$). The rate of dimerization is not known, but one would expect the rate to be slow, since the reaction would involve the interaction of two negatively charged species.

The rate of polymerization of the $H_2SiO_4^=$ ion has not been measured, but one would expect that it would be even slower than that of the $H_3SiO_4^-$ ion, because of the higher charge.

The coordination state of the hydrated silicate ion has been a subject of some controversy. Weyl (46) argues that, because silicon shows a coordination of 6 in ions with fluorine ($SiF_6^=$) and also because the water molecule is

similar in size to the fluoride ion, that the hydrated silicate ion should be octahedrally coordinated ($(H_2O)_2SiO_4H_2^{=}$). Fortnum (48) measured the Raman spectra of the $H_2SiO_4^{=}$ ion in solution and, by analogy with the spectra of octahedrally coordinated hydrated titanate ion, he eliminated the possibility of an octahedrally coordinated silicate ion, in contradiction to the speculation by Weyl.

Frydrych (49) measured the relative rate of reaction of silicate ions with molybdic acid to form a silicomolybdic acid that is colored and has long been used as a colorometric method for analysis of silica (57). Frydrych (49) showed that the dimeric silicate ion does not react with molybdic acid at an appreciable rate, so that the colorometric analysis is sensitive only to monomeric silicate species.

EXPERIMENTAL

Preparation of Compounds

The anhydrous orthosilicates were made from reagent grade carbonates and ignited silicic acid. The carbonates and silica were mixed in a water slurry in a two to one molar ratio of carbonate to silica. The slurry was oven dried at 105°C in a 150 ml beaker. The oven dry charge was placed in a 100 ml platinum dish and ignited at 1000°C to 1500°C with intermittent grinding and mixing until the x-ray diffraction pattern showed no unreacted carbonate, oxide, or crystalline silica or metasilicate. In the case of Ba_2SiO_4 and Sr_2SiO_4, where the alkaline earth oxides were reactive toward the platinum, the charge was sintered at 850°C for 24 hours before ignition at 1000 - 1200°C. The Ba_2SiO_4 and Sr_2SiO_4 were slightly discolored owing to the formation of alkaline earth platinates.

The anhydrous orthosilicates were then stored in oven-dry glass vials with plastic friction caps.

The preparation of Ba_2SiO_4 and Sr_2SiO_4 presented no special problems with the exception of the platinate contamination. Special care had to be taken, on the other hand, to prevent the formation of mixtures of the polymorphs of

Ca_2SiO_4. Incomplete conversion of the β form to the γ form occurs unless the charge is heated above 1460°C. Furthermore, the β form must be stabilized. The β form of Ca_2SiO_4 was prepared by adding 0.5% of B_2O_3 (as H_3BO_3) to the pure γ-Ca_2SiO_4 and heating to 1000°C for 12 hours, followed by air quenching.

Mg_2SiO_4 is difficult to prepare because of the slow reaction between MgO and SiO_2. After four weeks at 1400°C there were still traces of MgO and $MgSiO_3$ in the charge.

All the orthosilicates were separated into size fractions by sedimentation in absolute ethanol. The orthosilicates were ground slightly to remove large lumps. Then they were sieved through a number 200 sieve. The sieved powders were placed in a 250 ml ground-glass-stoppered reagent bottle and were covered with 200 cc of absolute ethanol. The mixture was shaken and then allowed to settle for one minute. The suspended silicate was poured off into another 250 ml bottle, and the residue was oven dried at 105°C for 1 hour. The procedure was repeated successively with 2, 3, and 4 minutes sedimentation times. The four resulting size fractions were oven dried at 105°C for 2 hours. Even after drying at 105°C a faint odor of ethanol was distinguishable, and further removal of ethanol was accomplished by heating at 150°C at 10^{-4} mm of mercury pressure for 1 hour.

The surface areas of the orthosilicates were measured according to the Brunauer, Emmett, and Teller procedure

described by Faeth and Willingham (55) using the apparatus described in Appendix A. The adsorbed gas was krypton, which was used because it has a low vapor pressure at the temperature of liquid nitrogen and is, therefore, useful for measurement of small surface areas.

Silicate hydrates of the alkaline earth metals were prepared by two procedures. The first was a precipitation from mixed solutions of alkaline earth nitrates and sodium metasilicate of varying molar proportions. The precipitates were collected, washed, and dried in an oven at 105°C. The second method was reaction of the anhydrous silicate with water in dilute suspension and collection of the product.

These two methods will be described in detail. The precipitation reaction was carried out in a three-necked flask into which a Friedrichs condenser with an ascarite drying tube, a thermometer, and a ground glass standard-taper stirring paddle were inserted.

The solution of $Na_2SiO_3 \cdot 9H_2O$ was made by adding 0.1 mole of the compound to 400 ml of carbon dioxide-free, deionized water. The proper amount of alkaline earth nitrate was dissolved in 400 ml of water. Ratios of 1, 2, and 3 moles of alkaline earth metal to silica were used. The silicate and the nitrates were mixed quickly in a one-liter beaker containing 200 ml of deionized water. The resulting slurry was then poured into the aforementioned flask and was stirred under an atmosphere of high purity nitrogen 24

hours, either at 25°C or under refluxing conditions (100°C).

The precipitate was filtered on a Buchner funnel, washed with two 100-ml portions of deionized water, and rinsed with ethanol; then it was oven dried at 105°C for 20 minutes.

In the second method of preparation a charge of anhydrous orthosilicate was placed in an extraction thimble, which was put in a Soxhlet apparatus and extracted for 12 hours. After extraction was ended the flask contained a clear solution until it was cooled to room temperature. Then, in all instances, a finely divided solid precipitated from the solution and adhered to the flask. The solution was poured off, and the flask was rinsed with ethanol, dried at 105°C for an hour, and the solid was scraped off the wall and bottled.

Characterization of Compounds

The anhydrous orthosilicates were subjected to microscopic examination to observe homogeneity and to x-ray diffraction to determine the crystalline composition.

X-ray diffraction patterns were obtained with a General Electric XRD-5 diffractometer using nickel-filtered CuK-radiation at 50 KV and 16 ma. The sample was prepared for x-ray analysis essentially according to the method of McCreary, as described in Klug and Alexander (54).

The infrared spectra were determined with a Beckman IR-10 double beam grating spectrophotometer. The samples were

run in the form of Nujol mulls. The powders were ground in an agate mortar with a few drops of high purity mineral oil (Nujol). The mull was then thinly spread over a CsBr plate and placed in a sample holder. Another CsBr plate was covered with a Nujol film and placed in the reference beam. The amount of Nujol in the reference beam was adjusted exactly to compensate for the Nujol in the sample so that no Nujol bands appear in the spectra. The spectra were obtained in the slow-scan mode, in which a scan of the 4000-300 cm^{-1} region required about 30 minutes. Nujol absorption occurs at 3.40, 3.55, 6.85 and 7.30 and 13.90 μ. If these bands interfered with bands of interest of the compound, the spectra were rerun using a completely halogenated mineral oil (perfluorolube). The halocarbon and Nujol mulls offer advantages over KBr pellets in that there is usually no interaction between the compounds and the matrix.

Differential thermal analysis was applied to the hydrates. The instrument was a Fisher Model 260, and platinum-platinum rhodium thermocouples were used. The output of the thermocouples was recorded on a Sargent SR recorder at a 1.0 mv full scale range. The instrument was programmed at a 10°C/min heating rate. Approximately 100 mg of sample were weighed into a fused silica tube, and the sample thermocouple was inserted. The reference thermocouple was inserted into a similar tube containing anhydrous Al_2O_3.

The hydrate crystallites were also examined with a

Siemans Elmiskop I electron microscope, at 47,000X magnification.

Measurement of Kinetics of Reaction of Anhydrous Compounds

The reactions of the anhydrous materials with water were measured by monitoring the ionic species produced by means of continuous measurement of conductivity and by chemical analysis of aliquot portions removed at closely-spaced intervals.

The reaction flask was a three-necked Morton stirring flask fitted with a stirring paddle. A second neck of the flask was connected to a high purity nitrogen tank, and a nitrogen flow was maintained. The stirring motor was kept at constant speed for all runs. The third neck contained a Beckman conductivity cell with a cell constant of 2.02 cm^{-1}. It was inserted so that it rested between two baffles of the reaction vessel. The entire flask and its contents were contained in a constant temperature bath. Measurements were made at three temperatures in order to obtain values of activation energies. For the rapidly reacting compounds these temperatures were 0.4, 18, and 25°C; for the slowly reacting ones they were 18, 25 and 35°C.

The water used in the reaction was deionized, boiled, and stored in a five gallon polyethylene bottle, which was protected from exposure to the air.

The resistance of the solution was measured with a Wheatstone bridge, which is described in Appendix B. The

bridge was made with resistance units such that the output from the rectifier circuit was between 0 and 120 millivolts when the resistance range was between 20,000 and 50 ohms.

The samples were weighed, then rapidly washed into the reaction vessel containing 1000 g of deionized water, and simultaneously the recorder was turned on. The resistances were recorded graphically as soon as they reached 20,000 ohms.

Samples were taken from the reaction vessel with an inverted 5 ml pipette. The samples were quickly filtered with suction through a sintered glass Buchner funnel into a six-inch test tube. From the filtered solution, a 3 ml sample was rapidly withdrawn and placed into a 100 ml volumetric flask. The silicomolybdate blue complex was developed according to the procedure of Kilmar (58). The transmittances of the solutions were measured with a Beckman Model B spectrophotometer and compared to a calibration curve made from solutions of Ottawa Silica of 99.99% purity, fused in Na_2CO_3 and dissolved in dilute HCl.

The Wheatstone bridge was powered by a two-volt signal of 1000 cps generated by a Hewlett-Packard Model 200 AB audio oscillator. Output voltage variations were small. The bridge could have been adjusted to any of a large number of resistance ranges simply by nulling the desired maximum resistance and adjusting the resistance at the output to achieve the minimum desired resistance at 120 mv output.

The diode rectifier and filter produced full wave rectified d.c. with a maximum ripple amplitude of one tenth of a millivolt at 1000 cps. The ripple was so fast that the recorder could not respond to it. The 0.05 μfd capacitor in the circuit between the rectifier and the output of the bridge is to prevent d.c. feedback from the rectifier circuit, which would polarize the cell.

After the run was finished, the final measurement of conductivity and determination of silica and calcium concentration was made.

The apparatus for measuring the reaction kinetics is shown in Figure 3.

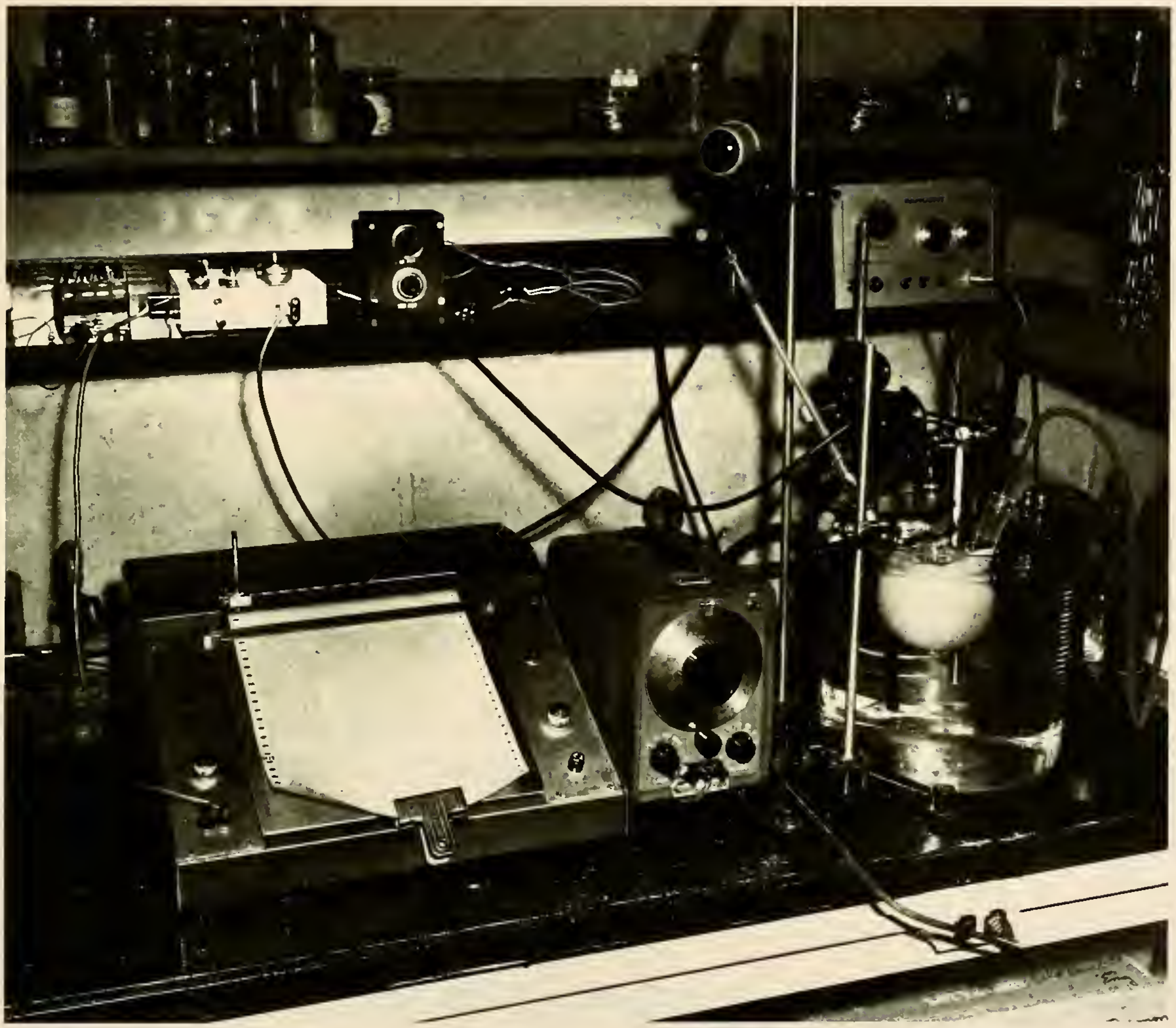

FIGURE 3. APPARATUS FOR MEASURING REACTION KINETICS

DATA

X-Ray Diffraction

The "d"-values and values of the relative intensities of each peak for the anhydrous orthosilicates studied are shown in Table 4. The x-ray diffraction data for the hydrates are shown in Table 5.

Infrared Spectra

The infrared absorption spectra for the anhydrous orthosilicates and the hydrates derived therefrom are shown in Figures 4 to 8.

Differential Thermal Analysis

The results for the differential thermal analyses of the hydrates and anhydrous silicates are shown in Figures 9 and 10.

Electron Micrographs

The electron micrographs of the barium-, strontium, β-calcium; γ-calcium-, and cadmium silicate hydrates are shown in Figures 11 to 15.

Adsorption Data on Anhydrous Silicates

The BET plots of selected, typical krypton adsorption data for the anhydrous silicates are shown in Appendix A.

Table 4. X-Ray Diffraction Data

(A) Ba_2SiO_4		(B) Sr_2SiO_4		(C) β-Ca_2SiO_4		(D) γ-Ca_2SiO_4		(E) Ca_2SiO_4	
d, Å	I/I_o	d, Å	I/I_o	d, Å	I/I_o	d, Å	I/I_o	d, Å	I/I_o
4.22	30	4.37	25	4.66	10	5.63	40	4.71	10
3.43	60	4.03	50	3.83	5	4.33	60	3.78	40
3.13	20	3.61	10	3.80	5	4.06	40	2.95	65
3.11	20	3.22	70	3.39	10	3.82	60	2.79	100
3.04	100	2.97	50	3.25	10	3.77	40	2.68	75
2.96	90	2.81	100	3.13	5	3.33	50	2.56	30
2.94	30	2.55	40	3.06	10	3.25	10	2.45	5
2.68	20	2.37	50	2.88	30	3.03	70	2.35	10
2.53	10	2.29	30	2.81	35	2.91	50	2.32	30
2.44	20	2.20	40	2.79	100	2.82	20	2.15	10
2.40	20	2.17	60	2.75	70	2.76	60	1.94	25
2.31	10	2.04	40	2.73	30	2.73	100	1.84	40
2.25	30	2.01	50	2.72	40	2.59	35	1.82	45
2.12	20	1.90	10	2.61	60	2.54	20	1.69	30
2.10	30	1.87	20	2.55	10	2.50	35	1.68	10
2.02	10	1.83	40	2.45	10	2.47	30	1.65	25
1.98	20	1.78	30	2.33	10	2.45	50	1.63	10
1.91	20	1.71	20	2.32	5	2.33	20	1.57	15
1.87	20			2.28	30			1.50	10
1.79	10			2.20	25			1.48	10
1.76	30			2.19	45			1.46	10

Table 5. X-Ray Diffraction Data for the Hydrates of the Orthosilicates

(A) $BaH_2SiO_4 \cdot aq$		(B) $SrH_2SiO_4 \cdot aq$		(C) $CaH_2SiO_4 \cdot aq$		(D) $CdH_2SiO_4 \cdot aq$	
d, Å	I/I_o	d, Å	I/I_o	d, Å	I/I_o	d, Å	I/I_o
3.71	100	10.6	50	3.04	100	2.94 very broad	
2.29	20	9.1	5	2.79	10		
3.22	20	4.37	10	1.83	10		
2.78	20	3.70	20				
2.60	10	3.50	20				
2.26	10	3.20	100				
2.14	20	3.05	60				
1.79	5	2.94	70				
		2.75	30				
		1.96	10				
		1.90	10				

Figure 4.

Infrared Spectra of A) Ba_2SiO_4 and B) $BaH_2SiO_4 \cdot aq$.

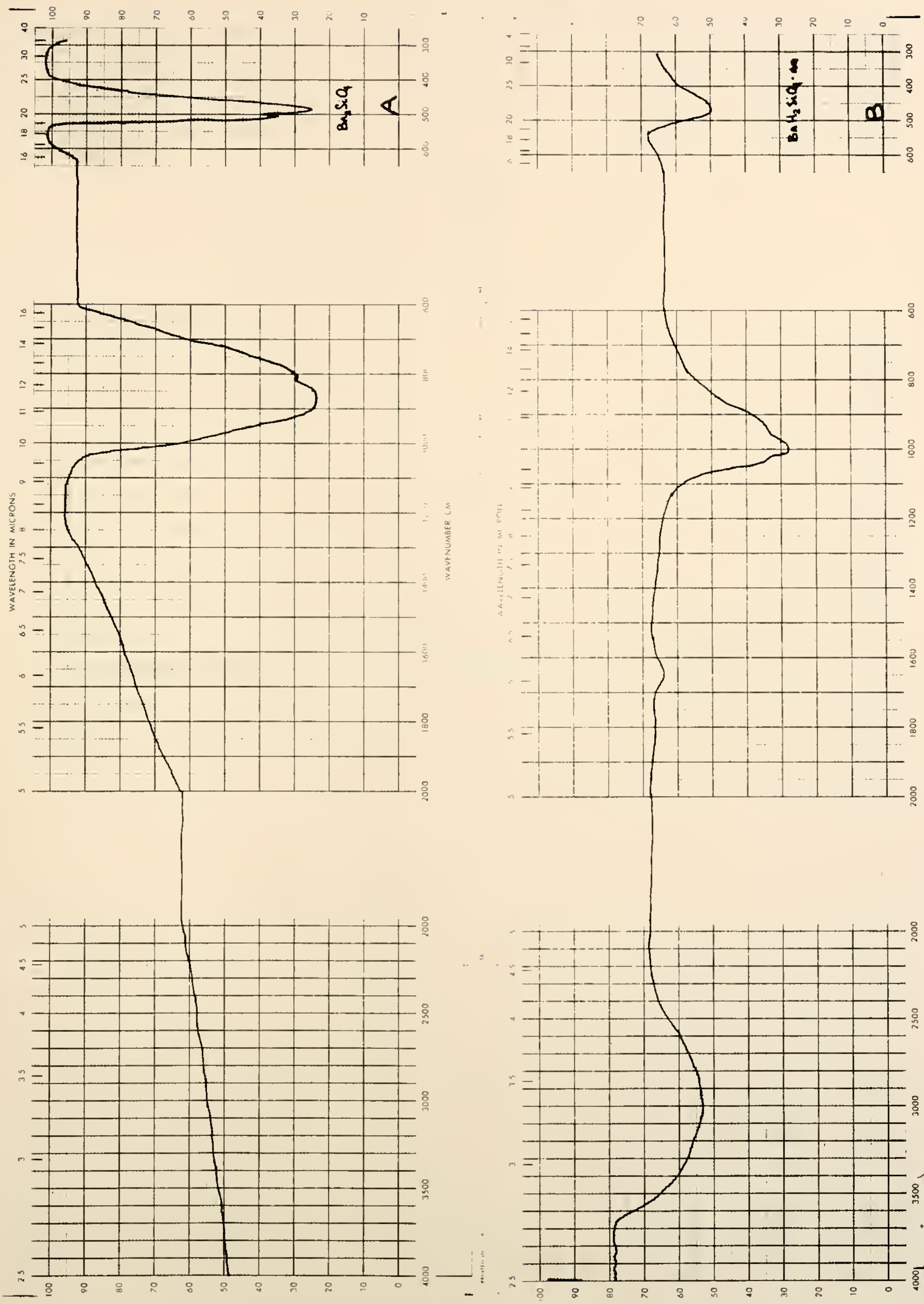
WAVELENGTH IN MICRONS
2.5
3
3.5
4
4.5
5
5.5
6
6.5
7
7.5
8
9
10
11
12
14
16
18
20
25
30
40
WAVENUMBER CM
4000
3500
3000
2500
2000
1800
1600
1400
1200
1000
800
600
500
400
300
100
90
80
70
60
50
40
30
20
10
0
Ba_2SiO_4
A
$BaH_2SiO_4 \cdot aq$
B

Figure 4.

Figure 5.

Infrared Spectra of A) Sr_2SiO_4 and B) $SrH_2SiO_4 \cdot aq$.

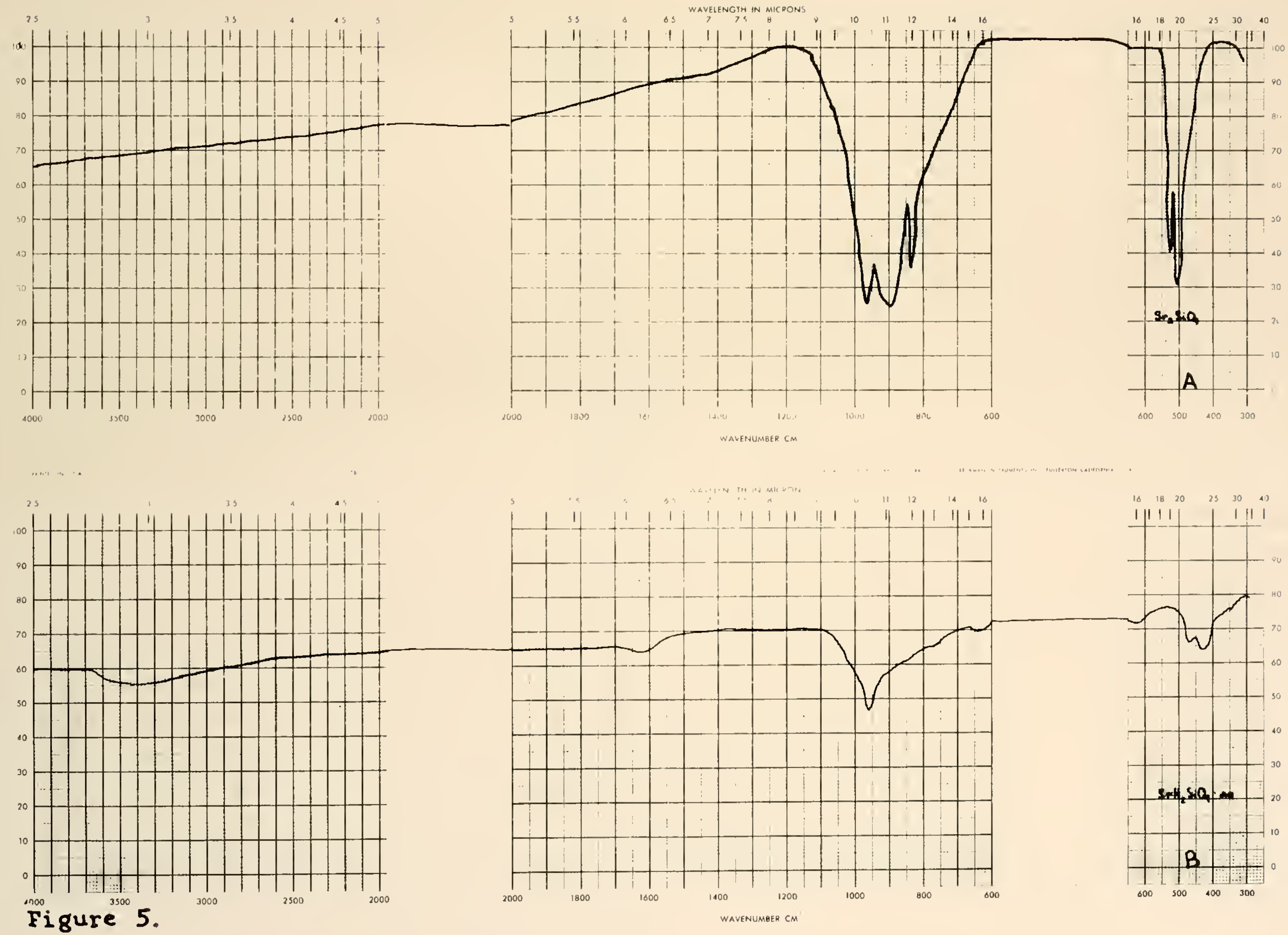
WAVELENGTH IN MICRONS
WAVENUMBER CM
Sr_2SiO_4
A
$SrH_2SiO_4 \cdot aq$
B
2.5
3
3.5
4
4.5
5
5.5
6
6.5
7
7.5
8
9
10
11
12
14
16
18
20
25
30
40
4000
3500
3000
2500
2000
1800
1600
1400
1200
1000
800
600
500
400
300
0
10
20
30
40
50
60
70
80
90
100

Figure 5.

Figure 6.

Infrared Spectra of A) β-Ca_2SiO_4 and B) $CaH_2SiO_4 \cdot aq.$

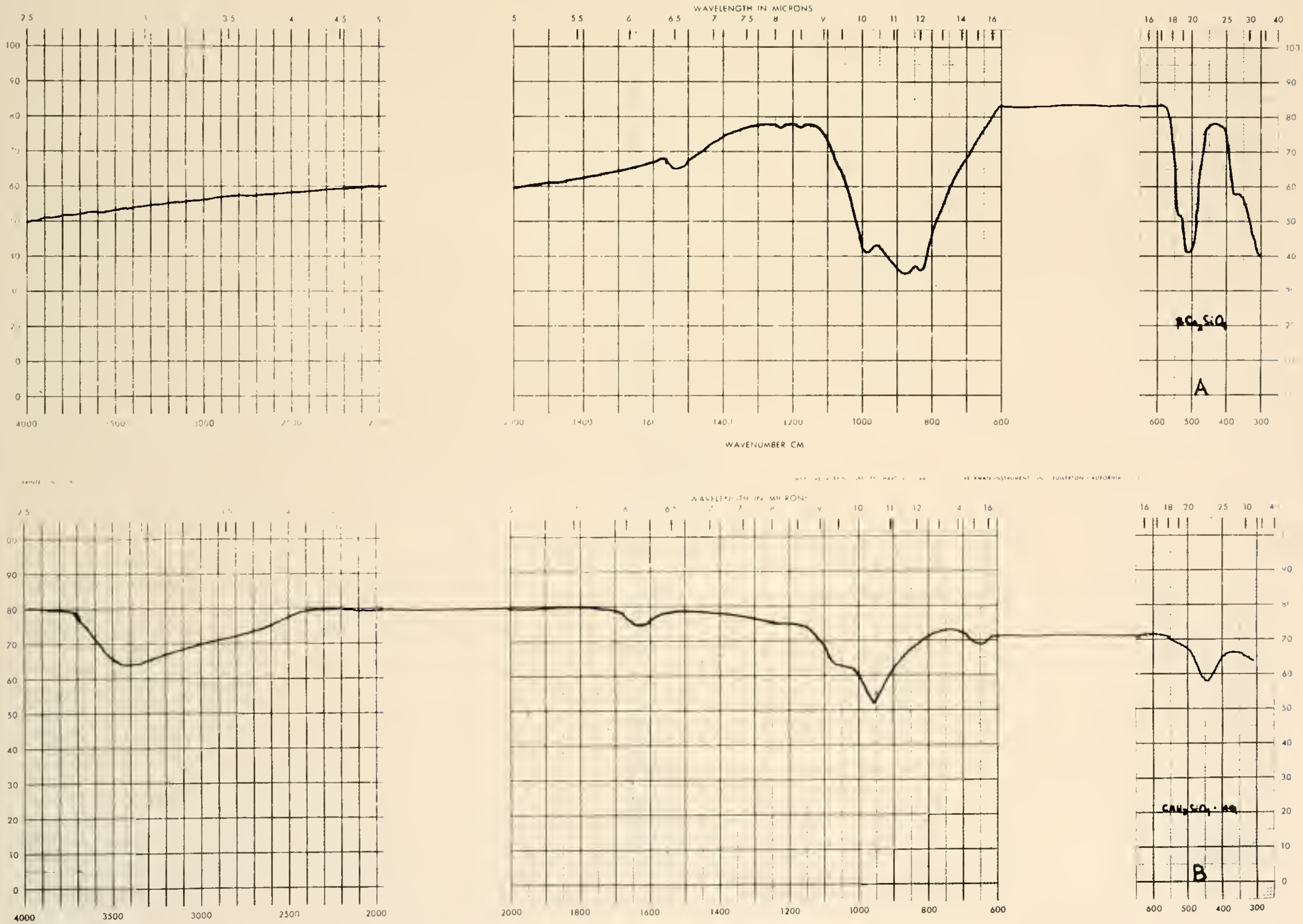
WAVELENGTH IN MICRONS
WAVENUMBER CM
βCa₂SiO₄
A
CaH₂SiO₄ · aq
B
WAVENUMBER CM⁻¹

Figure 6.

Figure 7.

Infrared Spectra of A) γ-Ca_2SiO_4 and B) $CaH_2SiO_4 \cdot aq$.

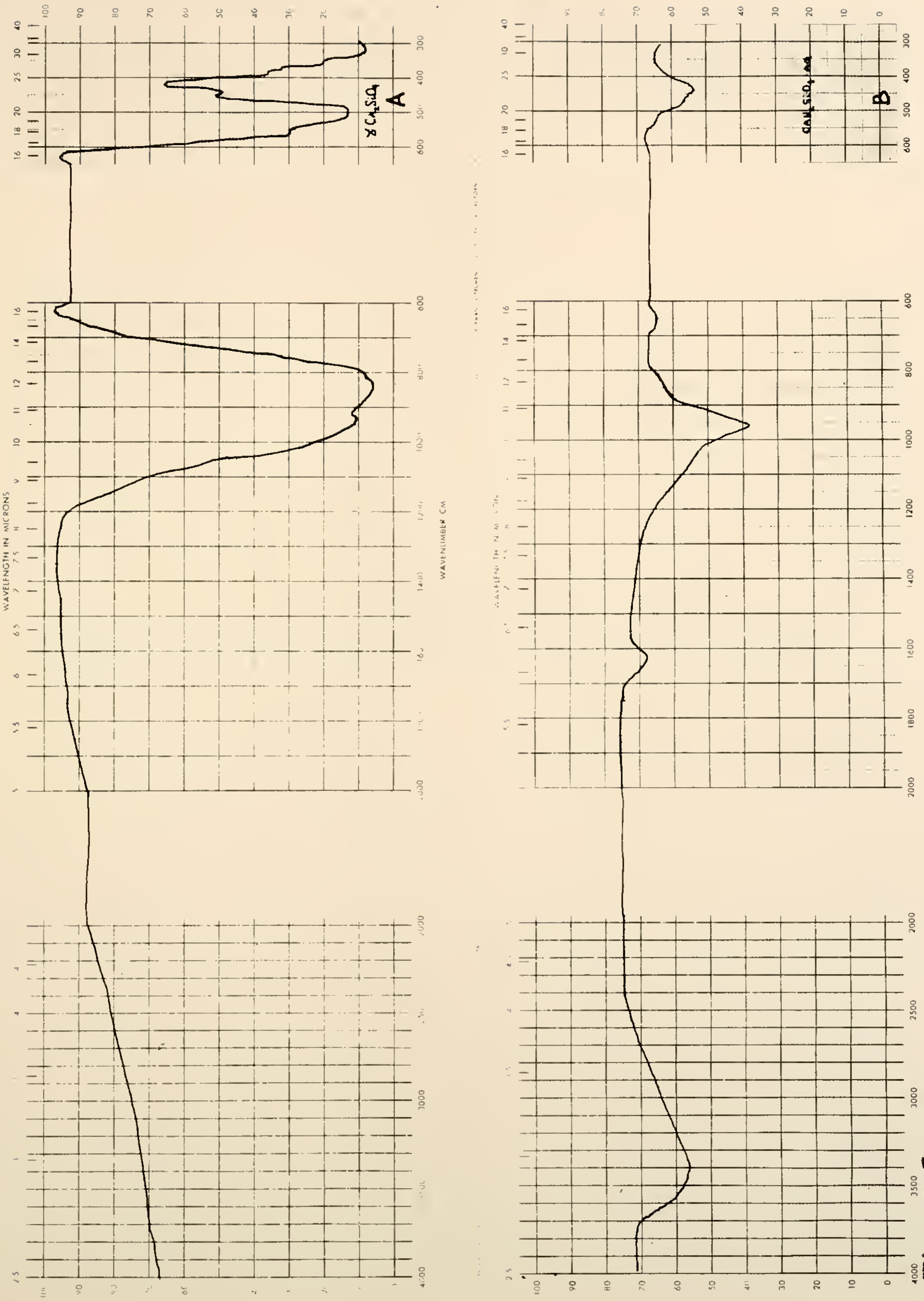
WAVELENGTH IN MICRONS
WAVENUMBER CM⁻¹
4000
3500
3000
2500
2000
1800
1600
1400
1200
1000
800
600
500
400
300
0
10
20
30
40
50
60
70
80
90
100
γ Ca₂SiO₄
A
αCa₂SiO₄, aq
B

Figure 7.

Figure 8.

Infrared Spectra of A) Cd_2SiO_4 and B) $CdH_2SiO_4 \cdot aq$.

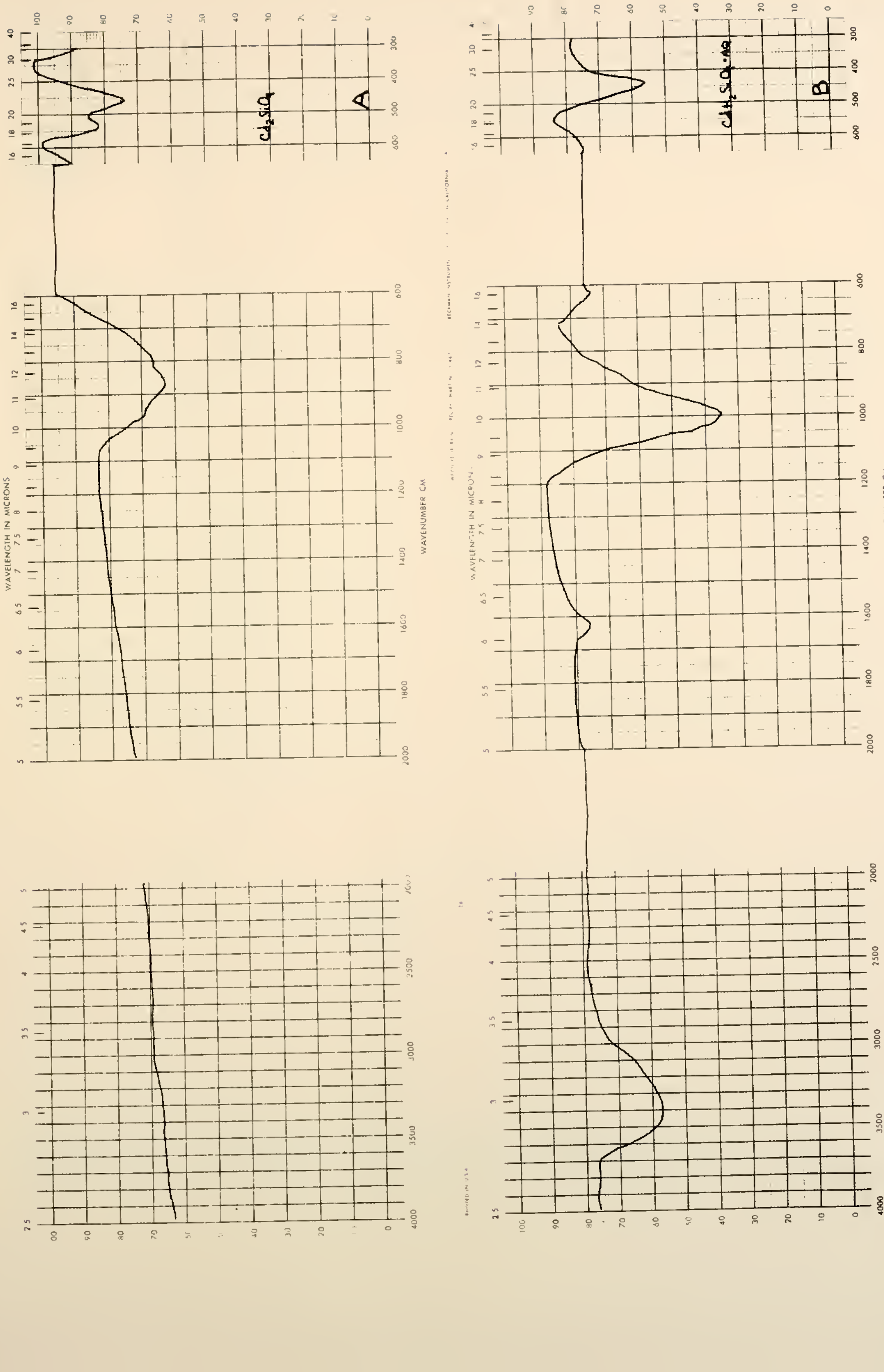
WAVELENGTH IN MICRONS
WAVENUMBER CM
Cd_2SiO_4
A
$CdH_2SiO_4 \cdot aq$
B

Figure 8.

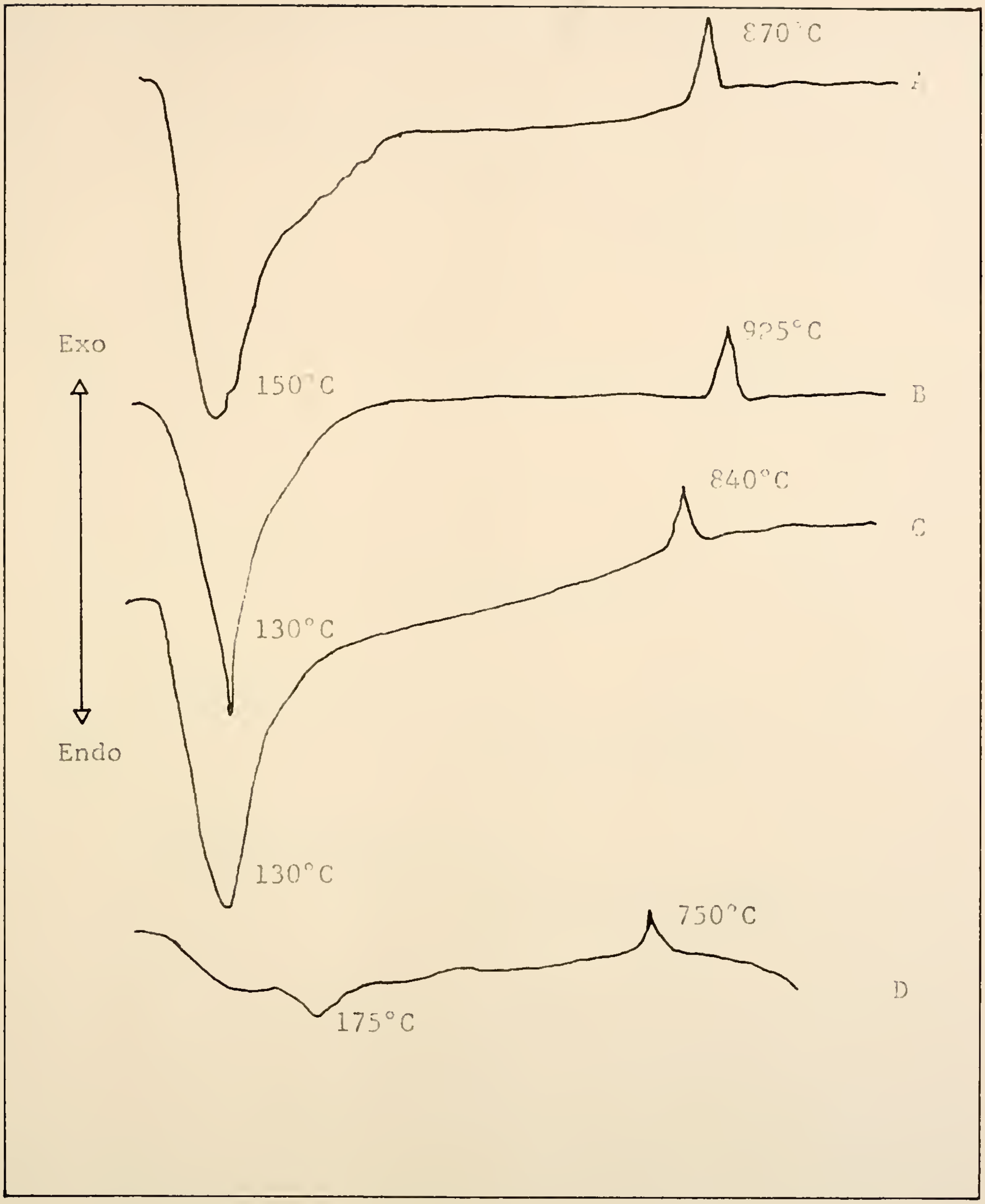

Figure 9. Differential Thermal Analysis Results (A) Hydrate of Sr_2SiO_4, (B) Hydrate of β-Ca_2SiO_4 and γ-Ca_2SiO_4, (C) Hydrate of Ba_2SiO_4, (D) Hydrate, CdH_2SiO_4

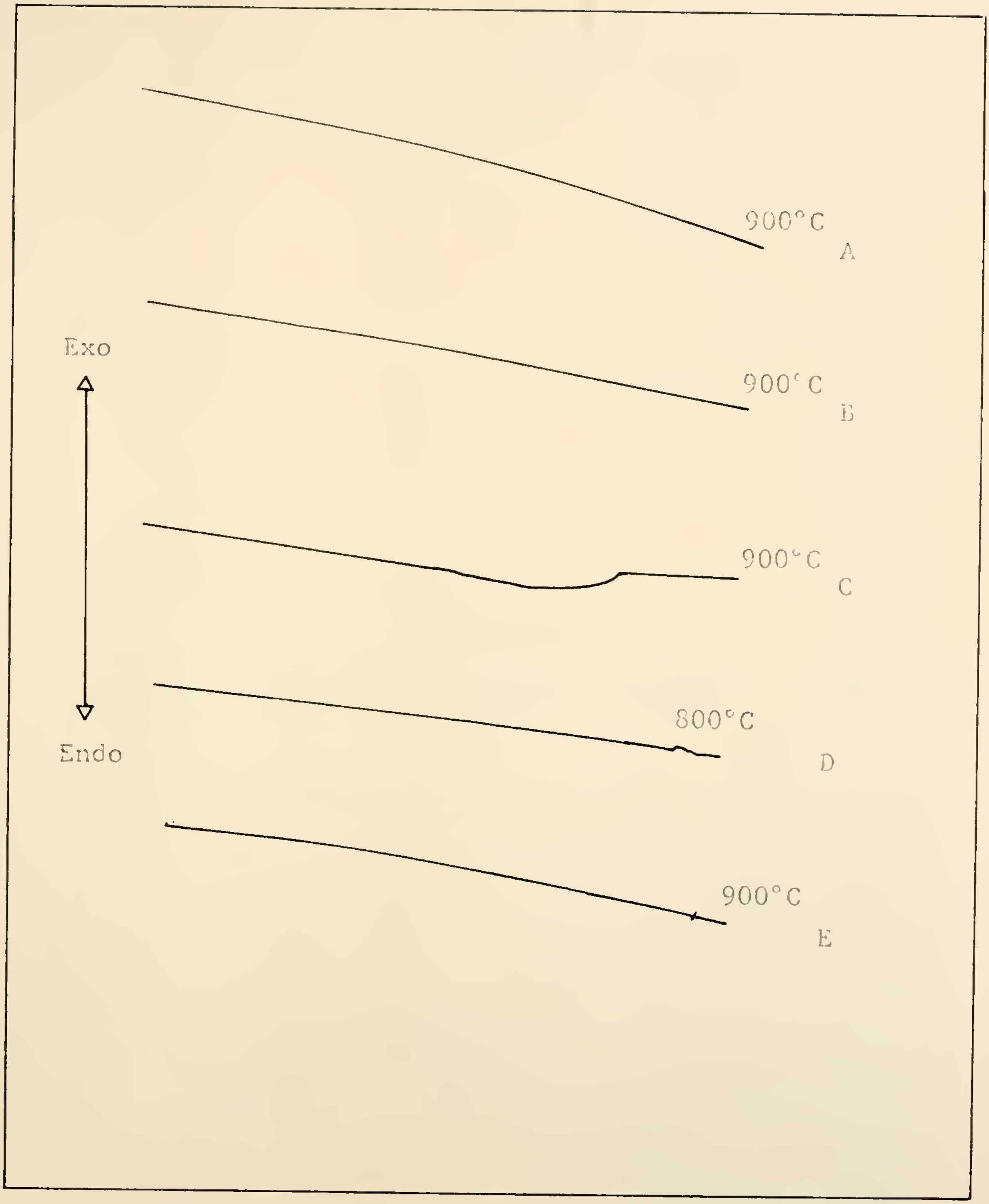

Figure 10. Differential Thermal Analysis Results (A) Ba_2SiO_4, (B) Sr_2SiO_4, (C) Cd_2SiO_4, (D) γ-Ca_2SiO_4, (E) β-Ca_2SiO_4

Figure 11.

Electron Micrograph of Hydrate of Ba_2SiO_4 (47000X).

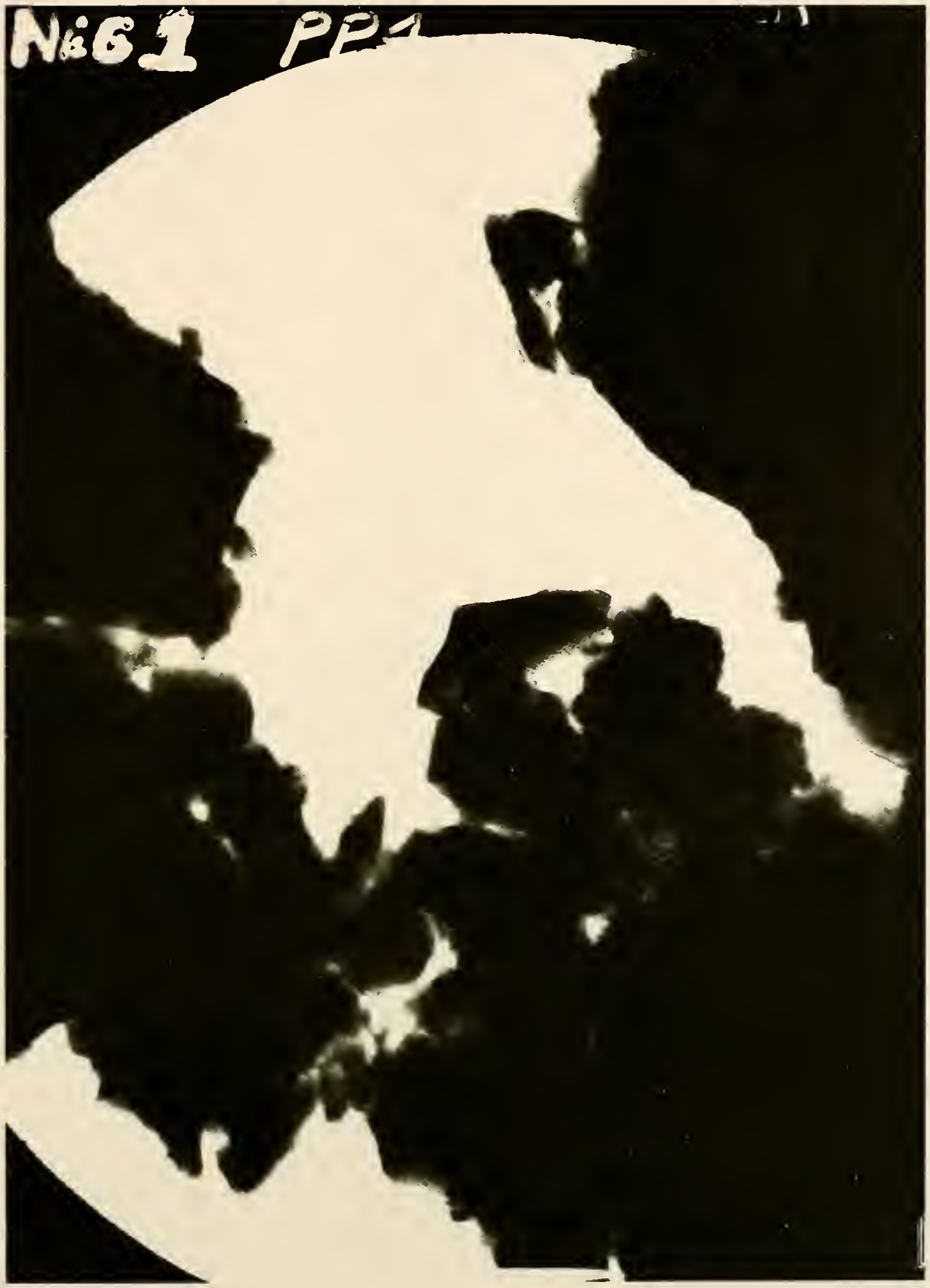

Figure 11.

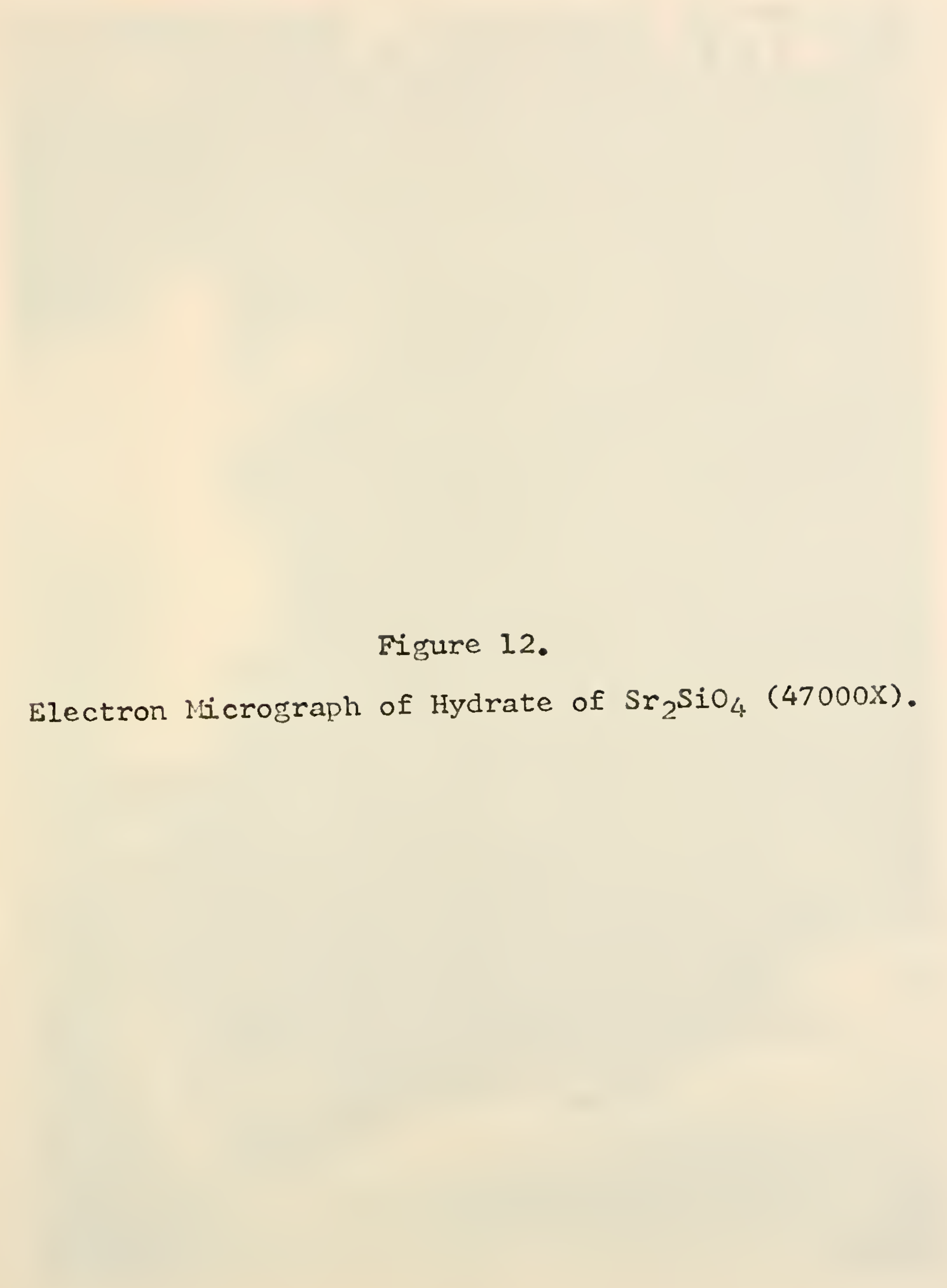

Figure 12.

Electron Micrograph of Hydrate of Sr_2SiO_4 (47000X).

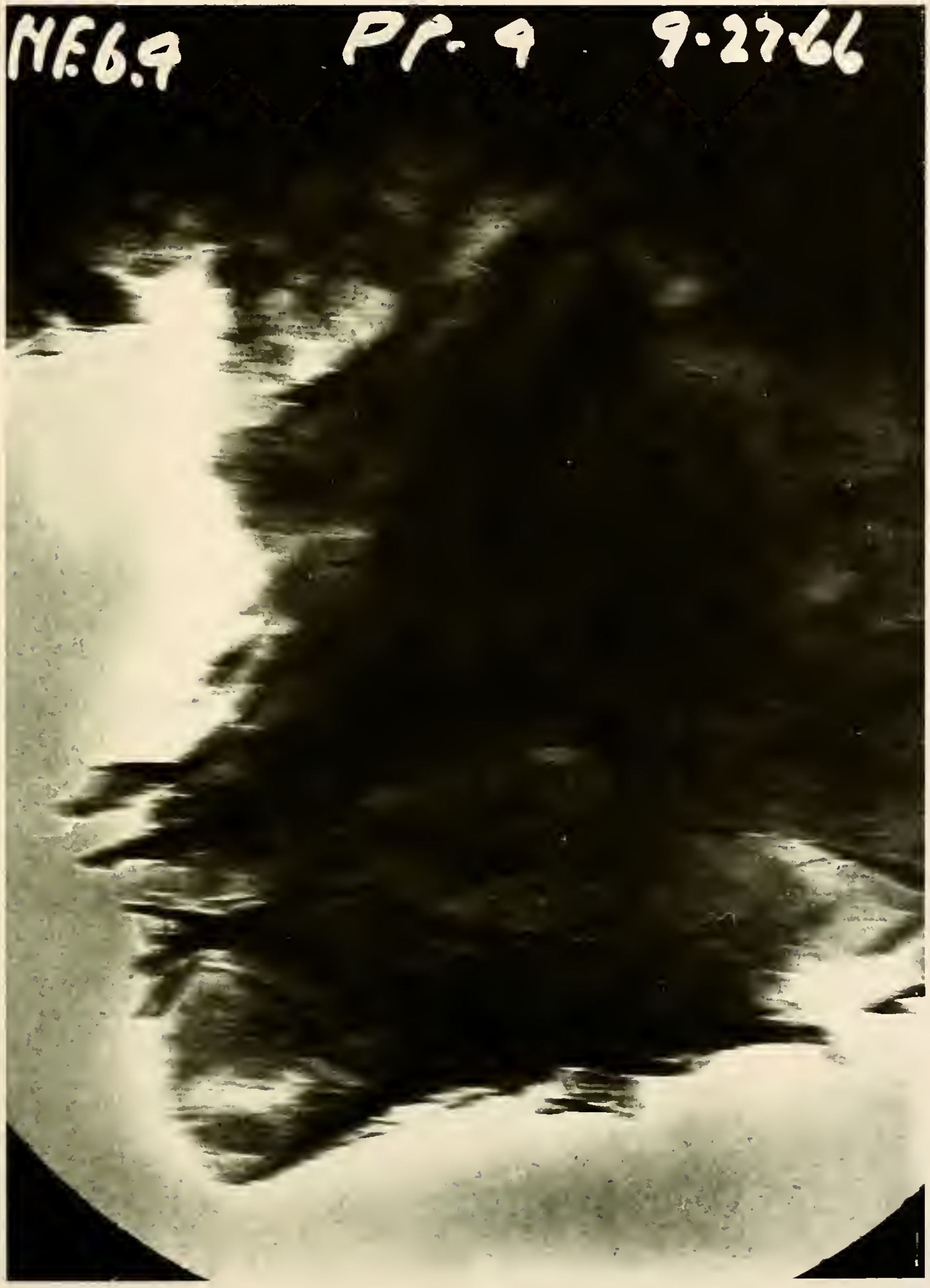
NE6.9
PP-9
9-27-66

Figure 12.

Figure 13.

Electron Micrograph of Hydrate of β-Ca_2SiO_4 (47000X).

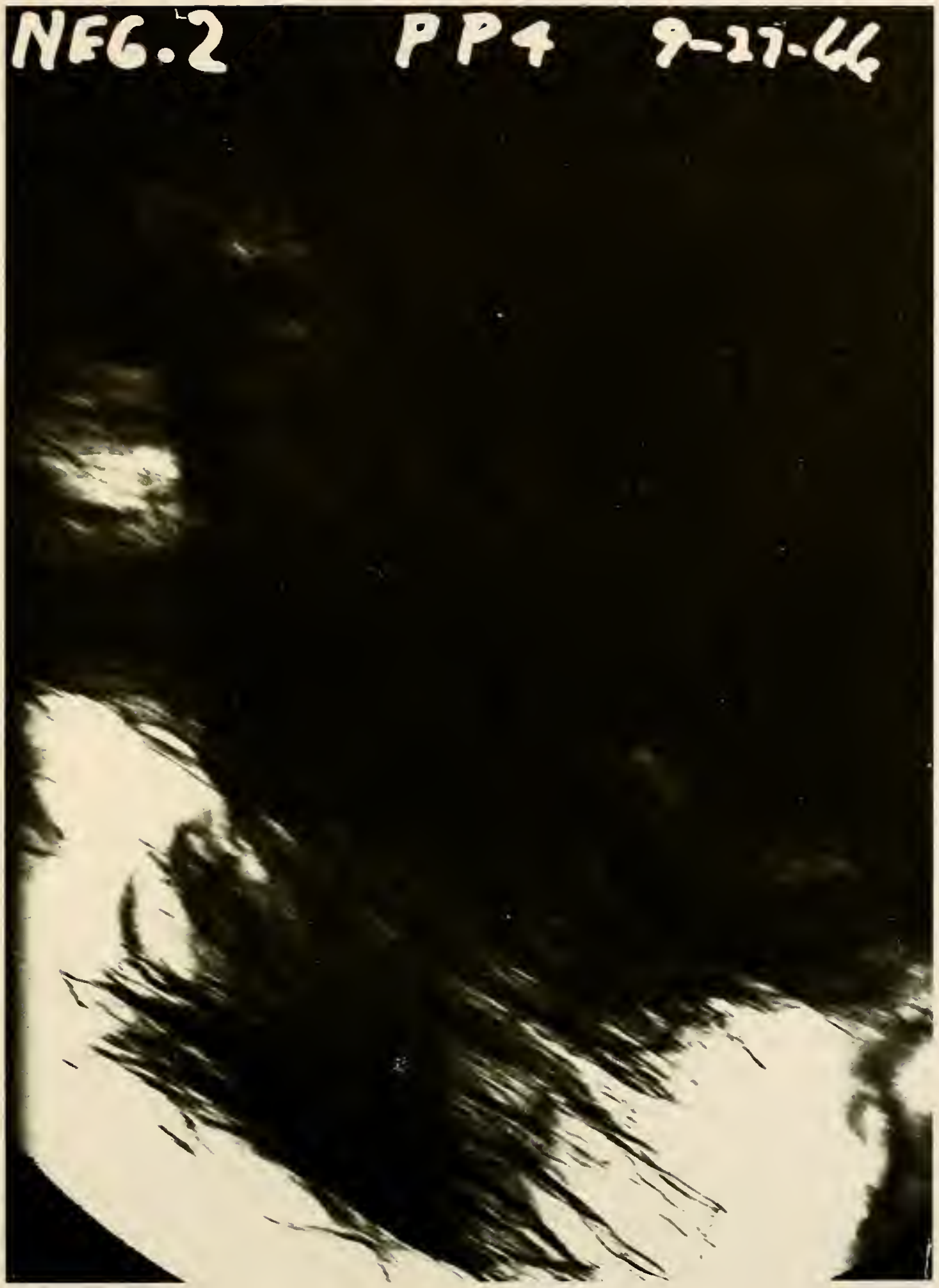
NEG.2
PP4
9-27-66

Figure 13.

Figure 14.

Electron Micrograph of Hydrate of γ-Ca_2SiO_4 (47000X).

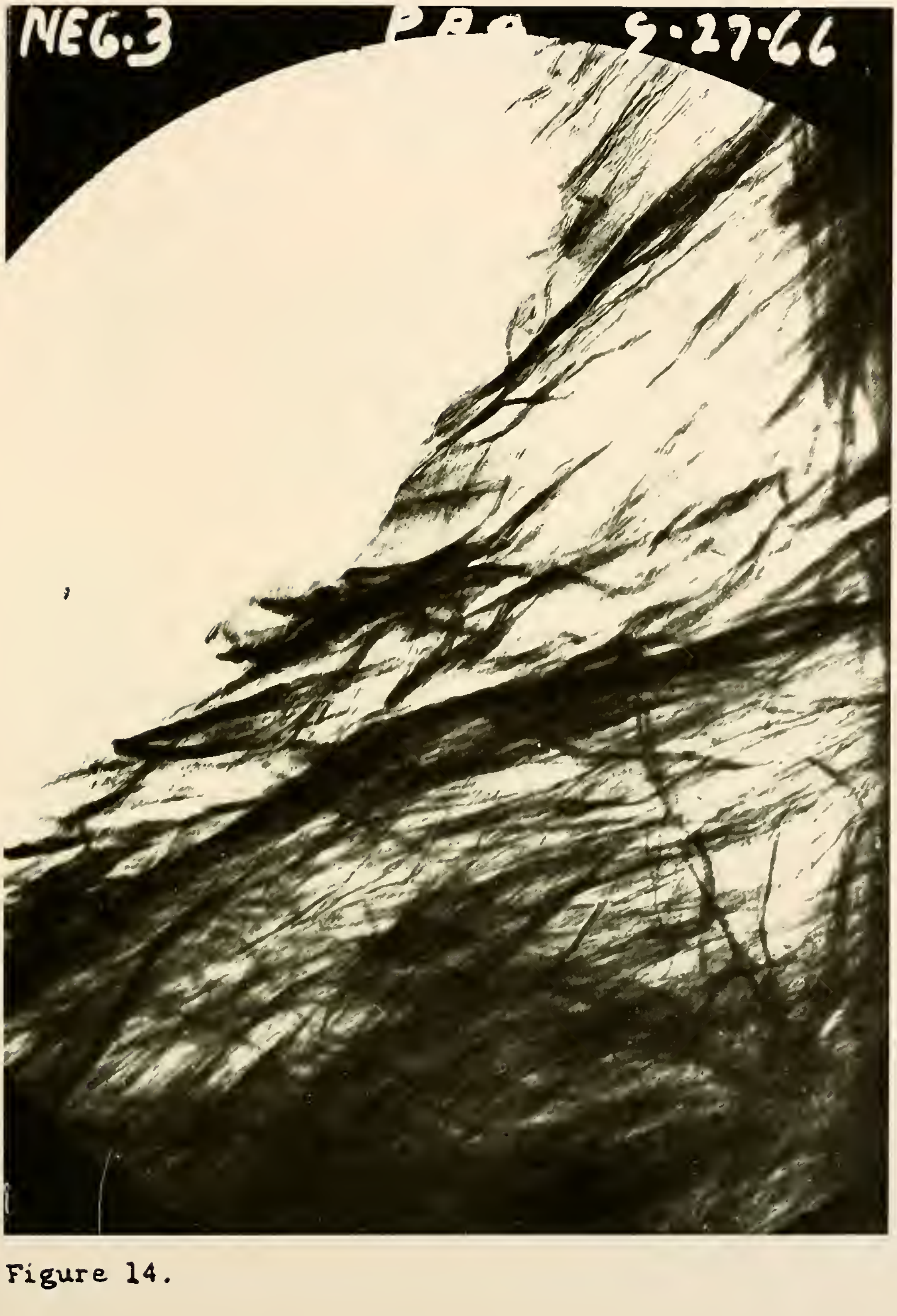
NEG.3
PRO
9.27.66

Figure 14.

Figure 15.

Electron Micrograph of $CdH_2SiO_4 \cdot aq.$ (47000X).

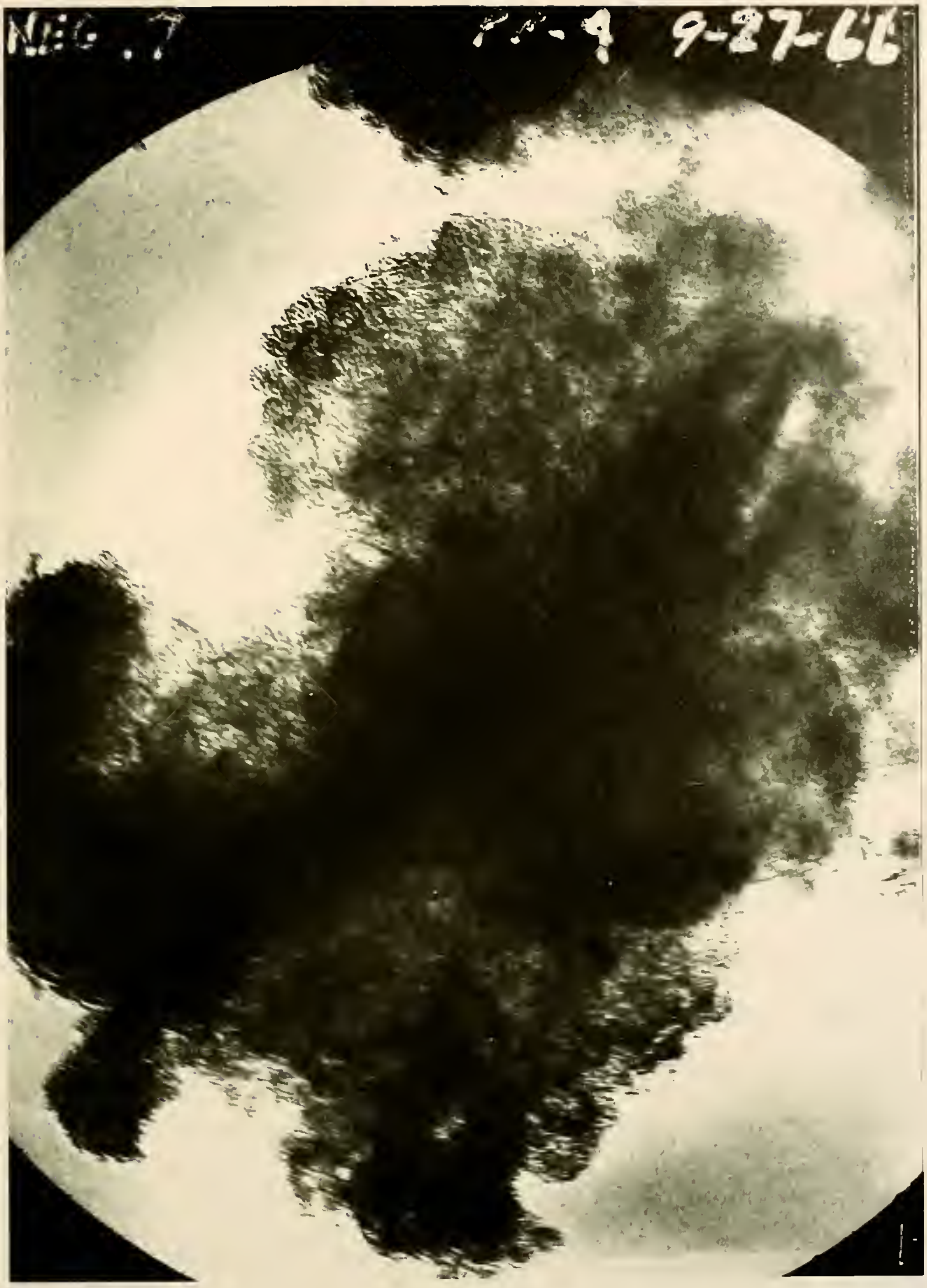
NEG .7
PP-9
9-27-66

Figure 15.

Kinetic Measurements

The data for the kinetic measurements are presented as the fraction of the anhydrous orthosilicate reacted, α , as a function of time. This fraction, α , was determined, for the cases of Ba_2SiO_4 and Sr_2SiO_4 by measuring the concentration of silica in solution. This was interpreted as indicating the concentration of MH_2SiO_4, assuming that the reaction is of the form:

$$M_2SiO_4 + 2H_2O \rightarrow M(OH)_2 + MH_2SiO_4$$

and that the concentration of the silicate hydrate is less than saturated. The basis for assuming the correctness of this reaction is given in the Discussion section.

In the case of the calcium silicates the partial insolubility of the hydrate made a determination of α by means of a determination of the dissolved silica not possible. It was, therefore, necessary to determine the hydroxide content of the solution, but this could not be done both directly and accurately in such dilute solutions. Therefore an indirect determination was made as follows: The dissolved silicate, assumed again to be CaH_2SiO_4, was determined by determining soluble silica in solution. The total calcium concentration was determined complexometrically. The concentration of $Ca(OH)_2$ in solution was then calculated as the difference between these molal values and was taken to be the amount of anhydrous material reacted, according to

the assumed stoichiometry.

The data for the hydration of Ba_2SiO_4, showing the effects of varying sample size, initial pH, specific surface area of the sample, and temperature are shown in Figures 16 to 19 respectively. Corresponding data for the hydration of Sr_2SiO_4 are shown in Figures 20 to 23. In these data plots and the analyses thereof the term "concentration" is used in two senses: c_o refers to the moles of solid sample used per unit volume of reaction system; c_i, on the other hand, refers to the moles of dissolved alkaline-earth hydroxide in homogeneous solution.

Figure 24 is a plot of individual concentrations of $Ca(OH)_2$ and of CaH_2SiO_4 produced in solution as the result of the hydration of β-Ca_2SiO_4, for three different sample sizes (c_o) as functions of time. It was assumed that the analyzable silica in solution is $H_2SiO_4^{-2}$, as was previously mentioned.

Figures 25 to 28 show the effects of varying sample size, initial pH, specific surface area, and temperature on the reaction rate of β-Ca_2SiO_4.

Figure 29 shows the deviation of the silica concentration from that of the $Ca(OH)_2$ in solution for γ-Ca_2SiO_4. This figure is analogous to Figure 24 for the β-Ca_2SiO_4, and the same comments apply. Figures 30 to 33 show the effects of varying sample size, initial pH, specific surface area of the sample, and temperature on the reaction rate of

γ-Ca_2SiO_4.

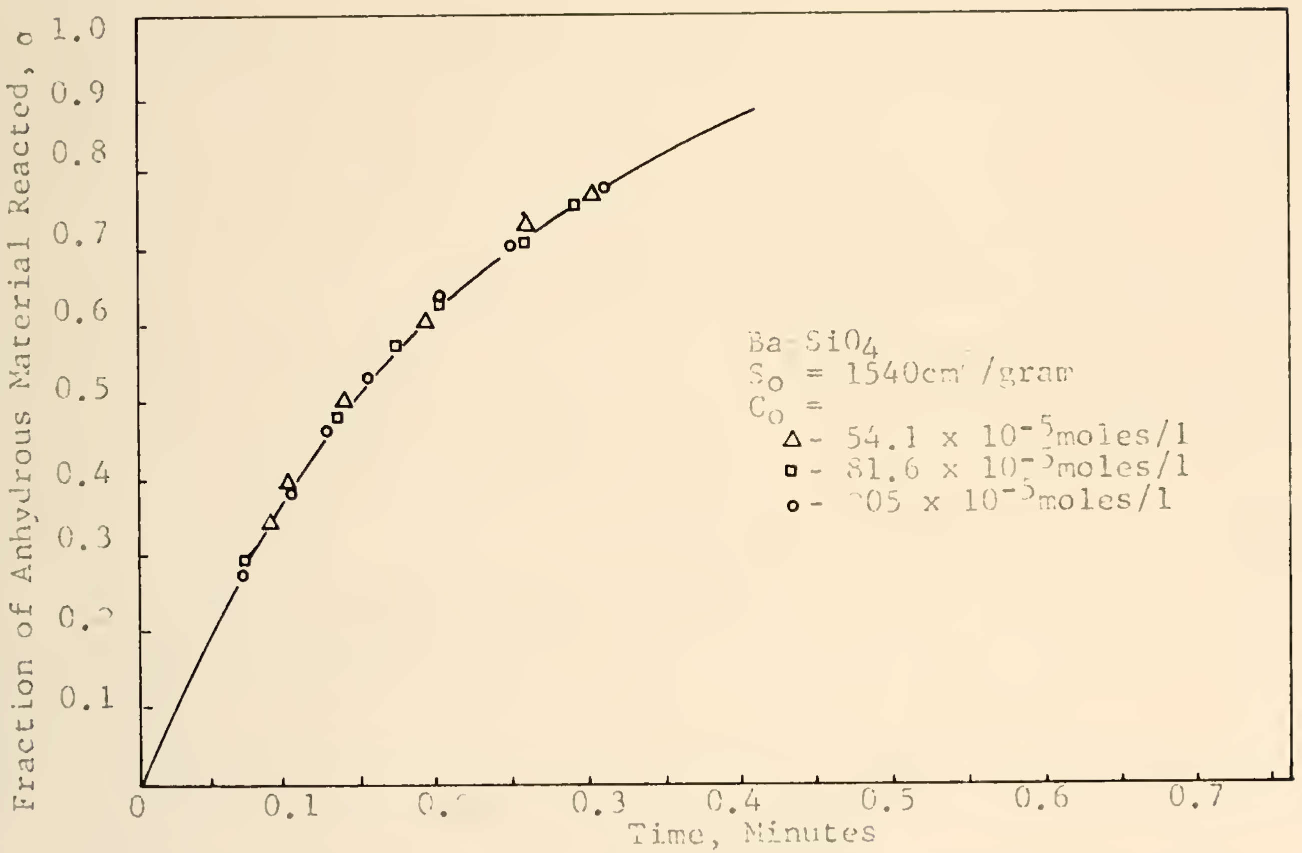

Figure 16. Fraction Reacted of Ba$_2$SiO$_4$ vs. Time for Several Values of Sample Sizes (C$_o$)

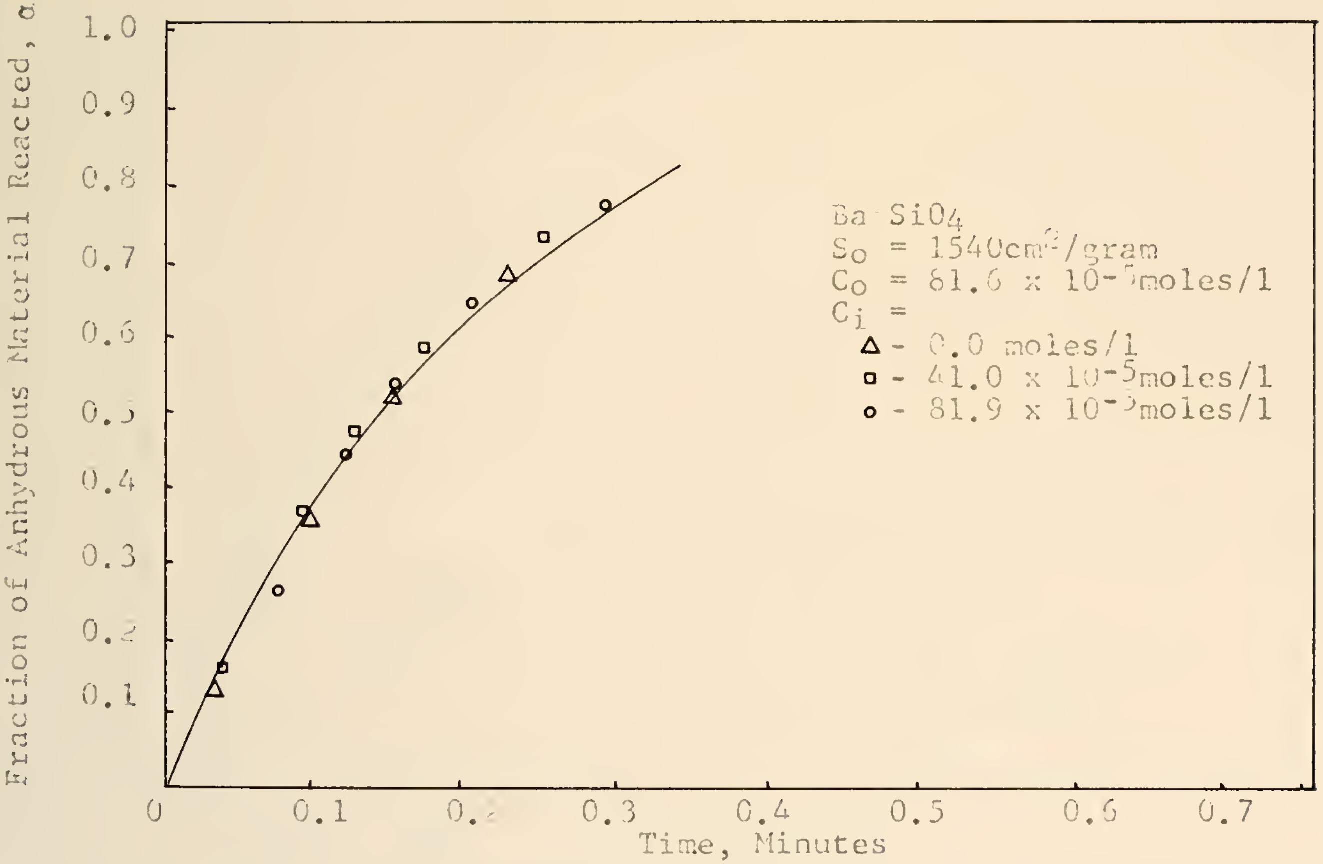

Figure 17. Fraction Reacted of Ba_2SiO_4 vs. Time for Several Values of Initial $Ba(OH)_2$ Concentration (C_i)

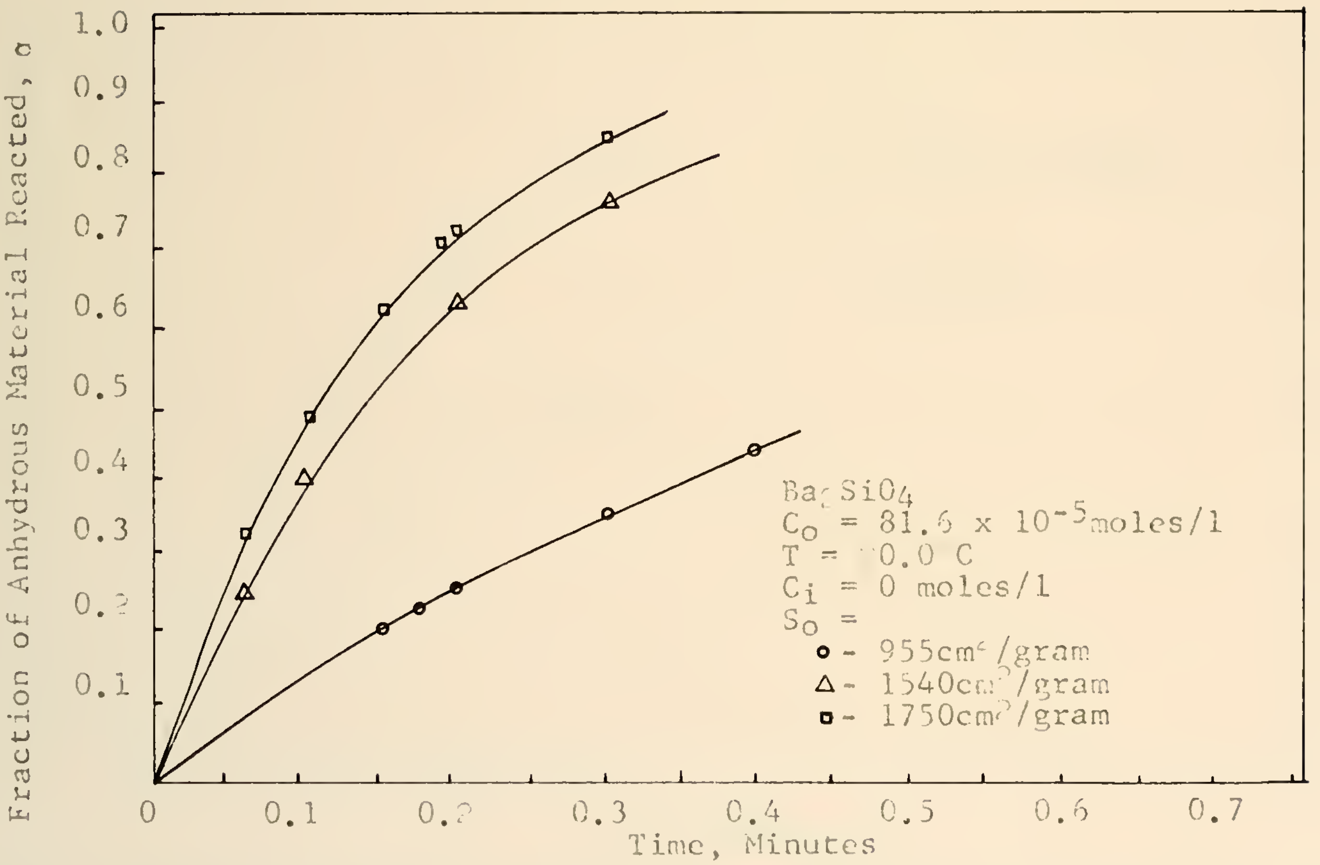

Figure 18. Fraction Reacted of Ba_2SiO_4 vs. Time for Several Values of Sample Specific Surface Areas (S_o) but Constant Amount (C_o)

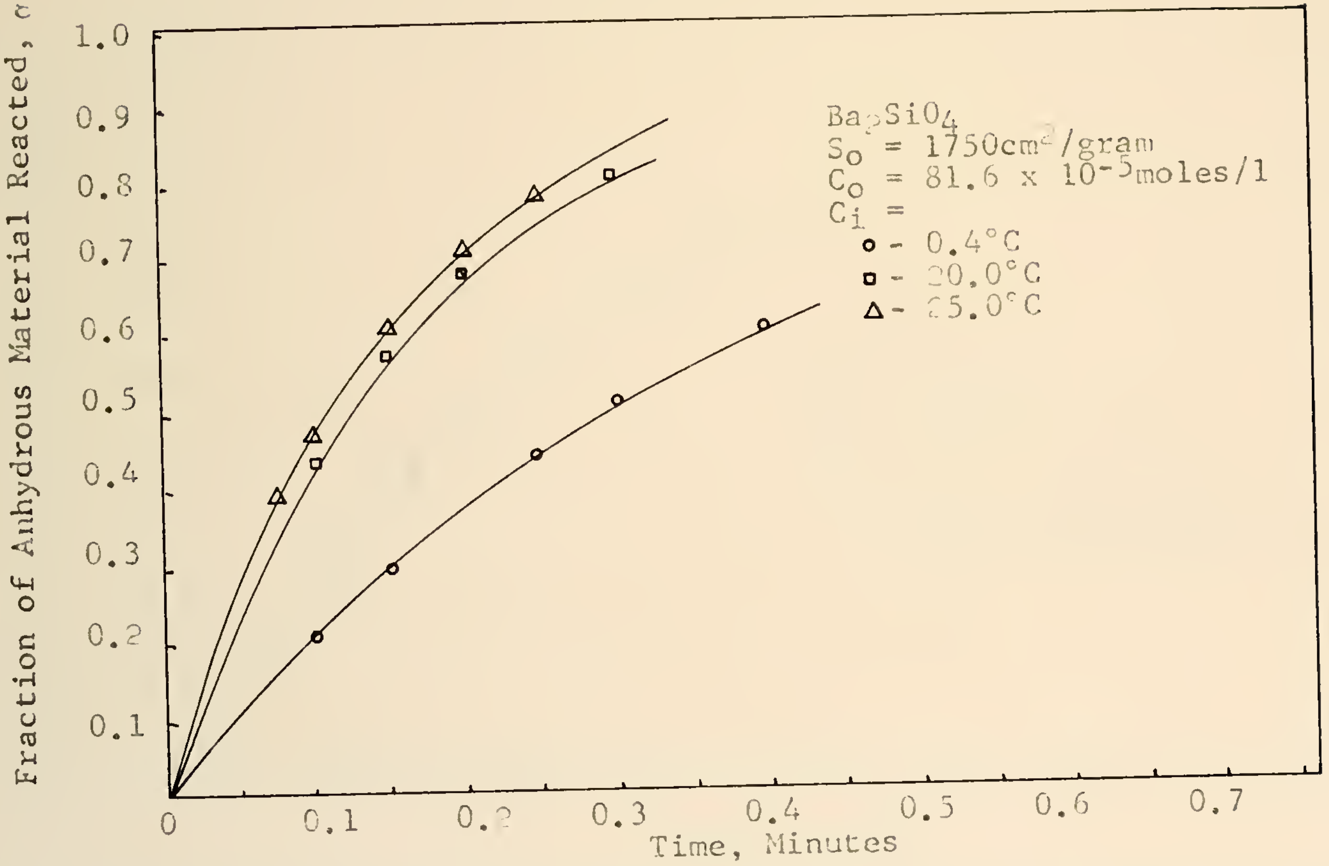

Figure 19. Fraction Reacted of Ba_2SiO_4 vs. Time for Various Temperatures but Constant Sample Size and Surface Areas

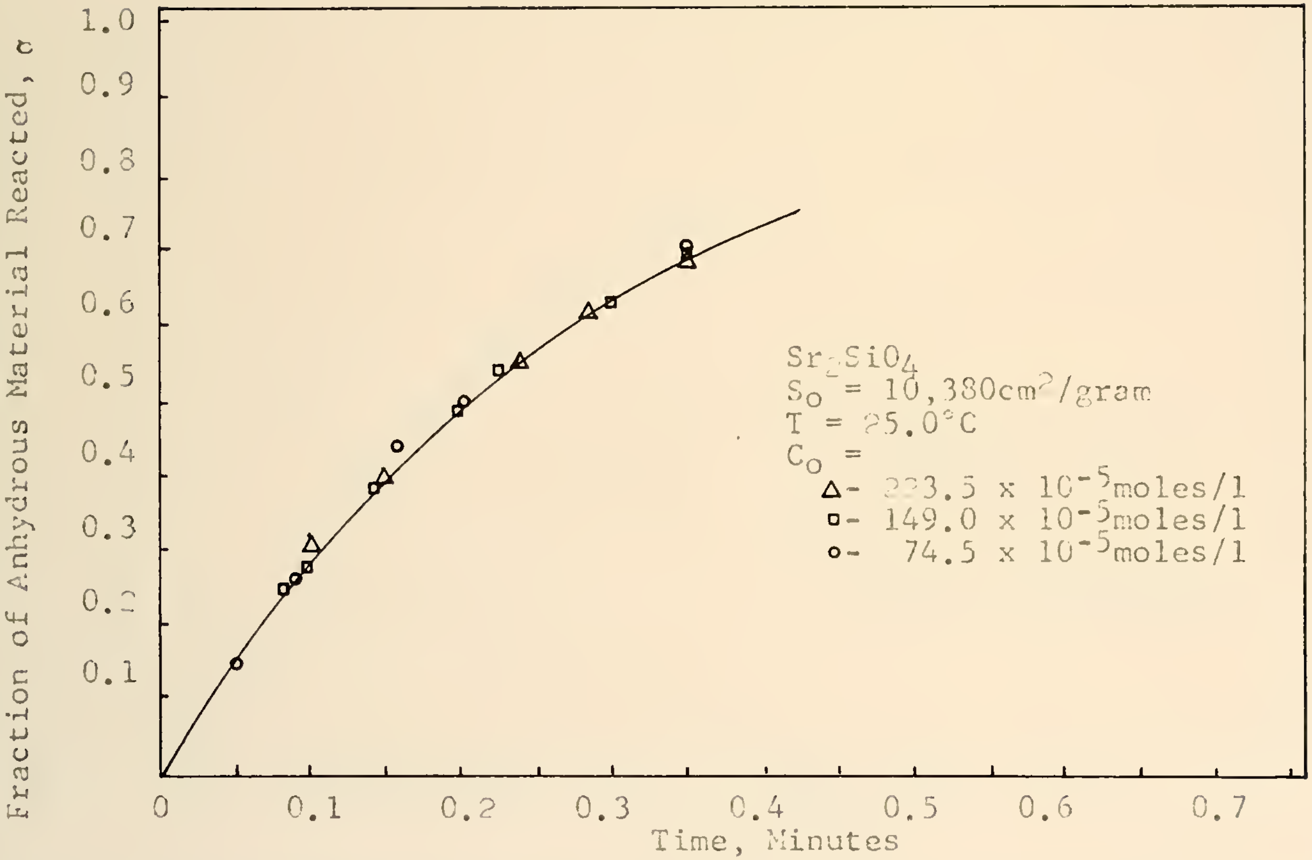

Figure 20. Fraction Reacted of Sr_2SiO_4 vs. Time for Several Values of Sample Sizes (C_o)

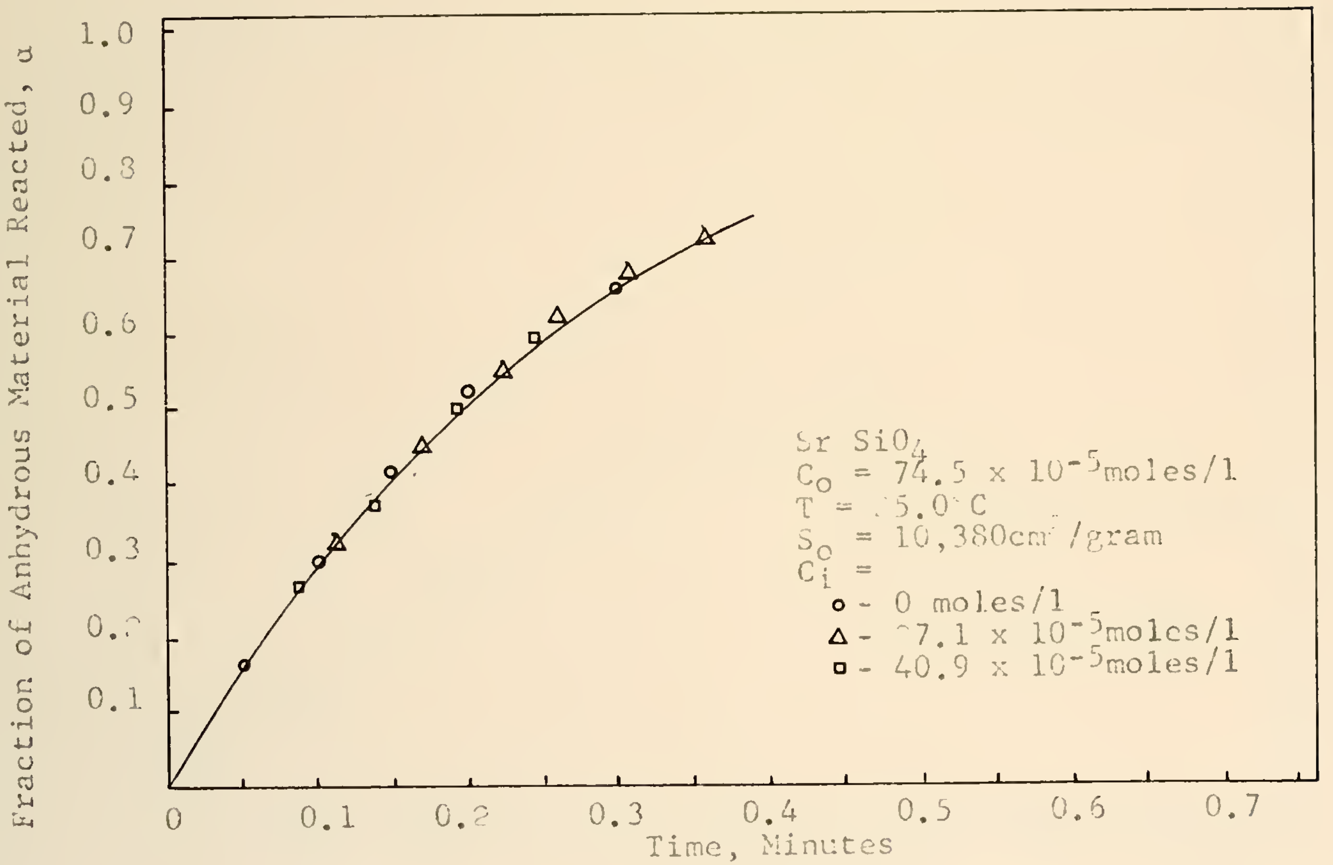

Figure 21. Fraction Reacted of Sr_2SiO_4 for Several Values of Initial $Sr(OH)_2$ Showing α vs. Time for Concentration (C_i)

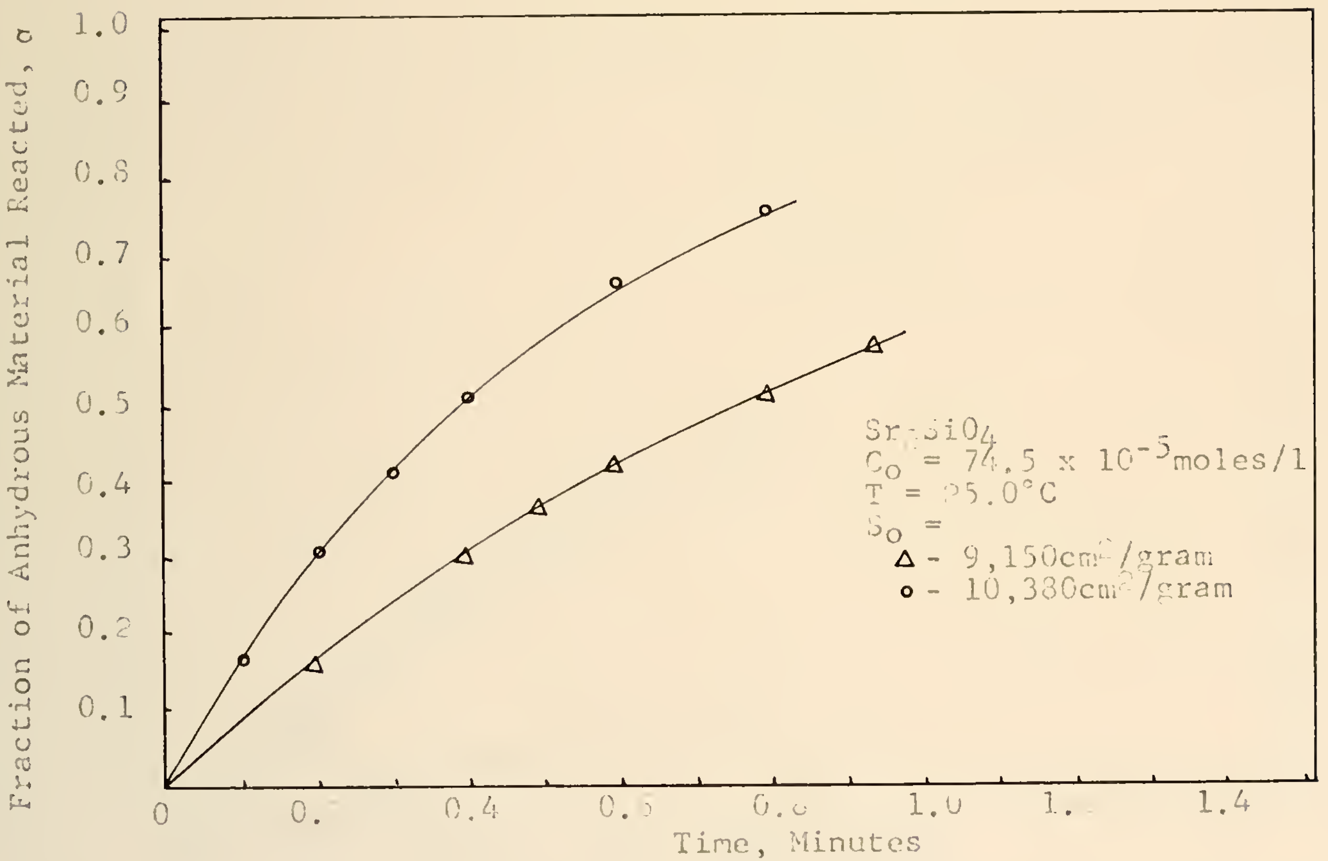

Figure [illegible]. Fraction Reacted of Sr_2SiO_4 vs. Time for Different Surface Areas (S_o)

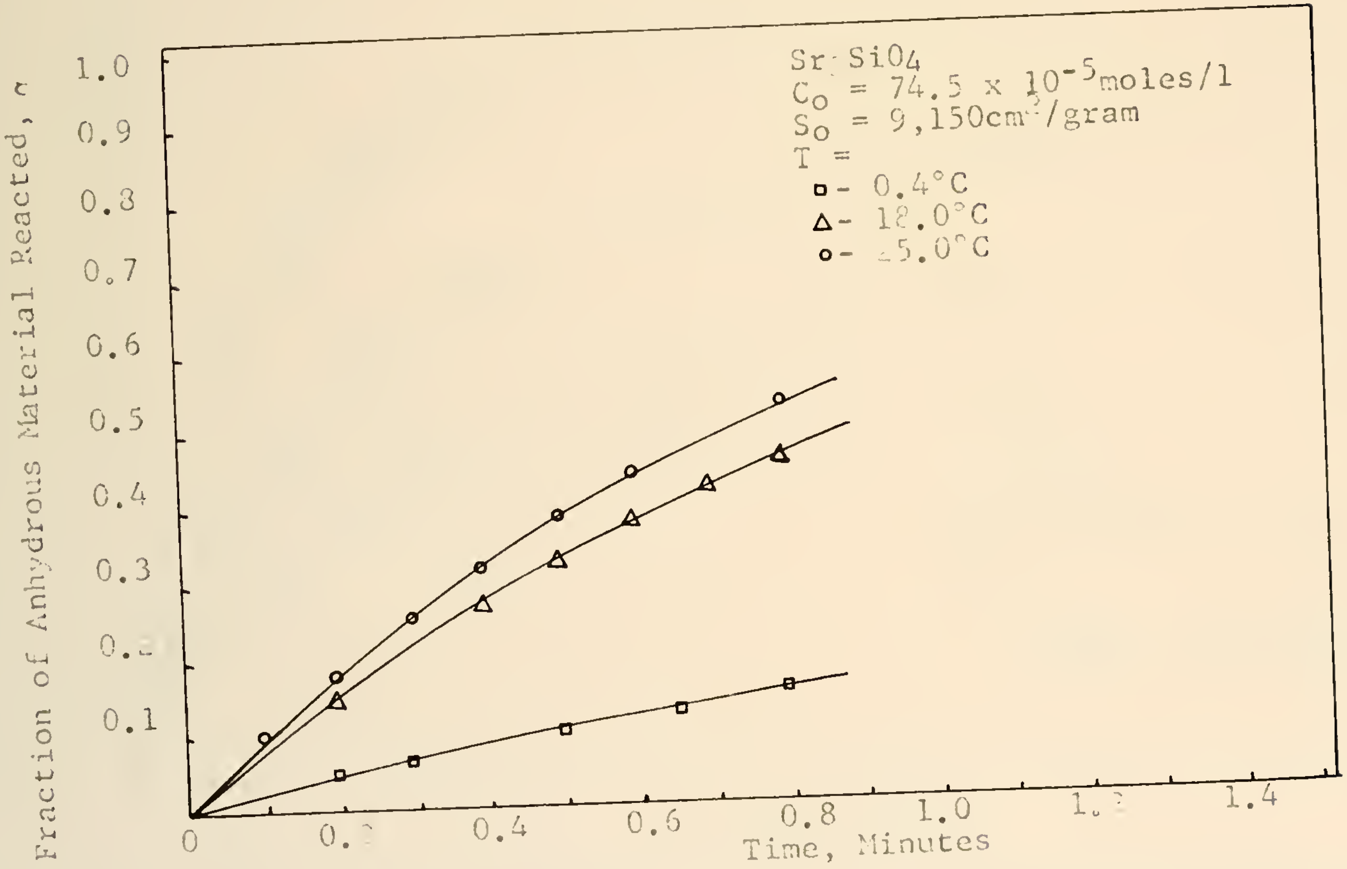

Figure 23. Fraction Reacted of Sr_2SiO_4 vs. Time for Several Values of Temperature (T)

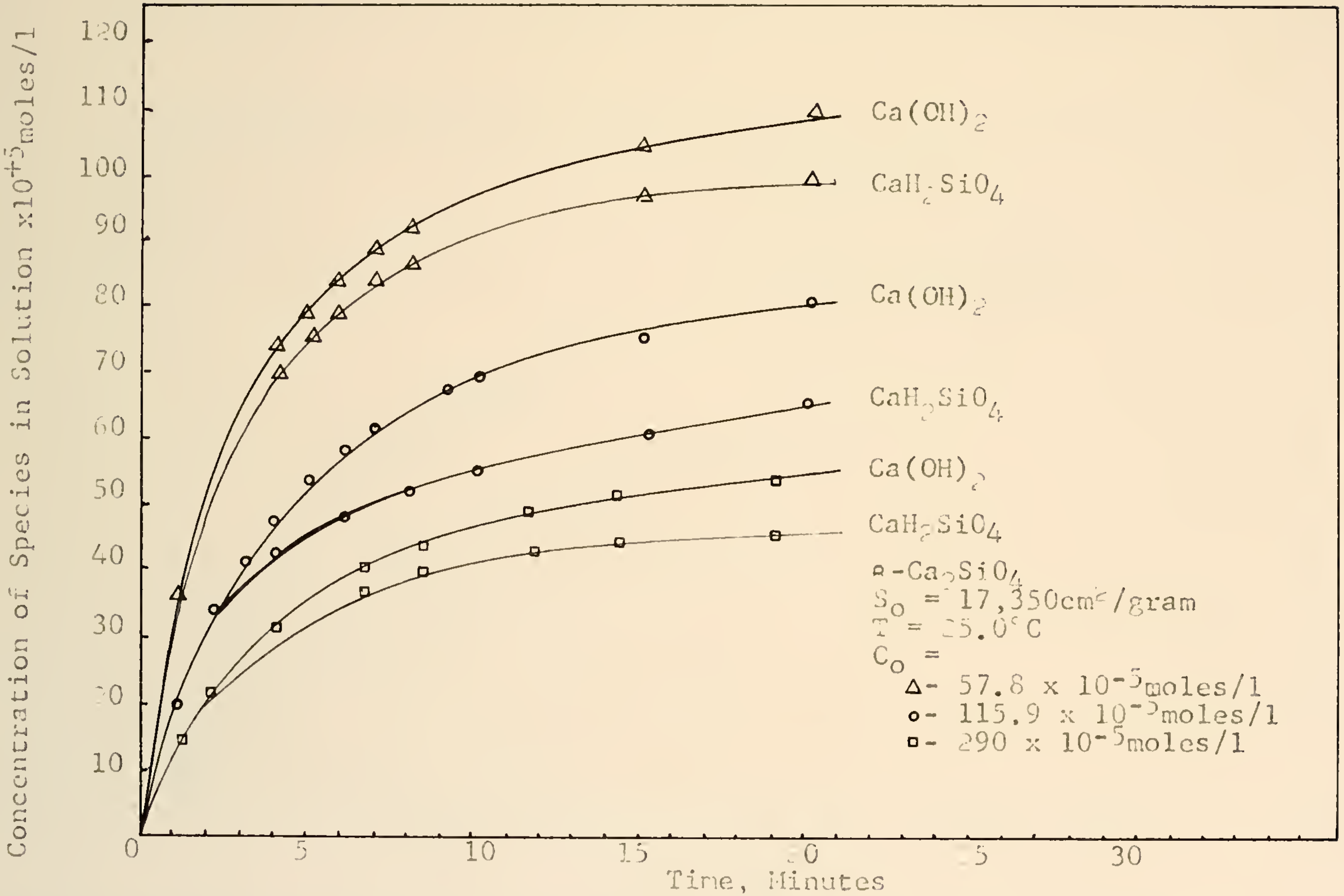

Figure 24. Concentration of $Ca(OH)_2$ and CaH_2SiO_4 in Solution as Function of Time for the Reaction of β-Ca_2SiO_4

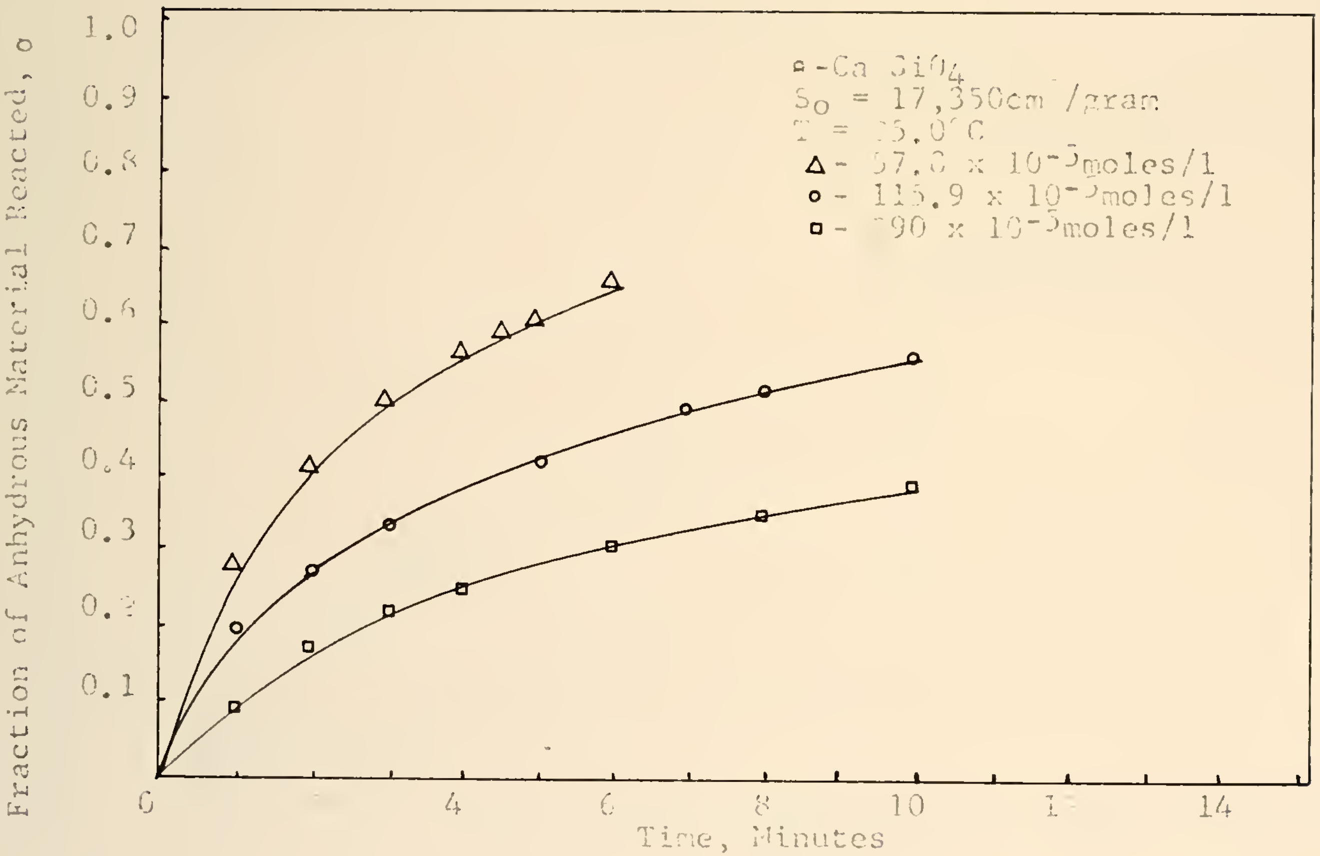

Figure 25. Fraction Reacted of β-Ca SiO$_4$ vs. Time for Several Values of Sample Sizes (C_o)

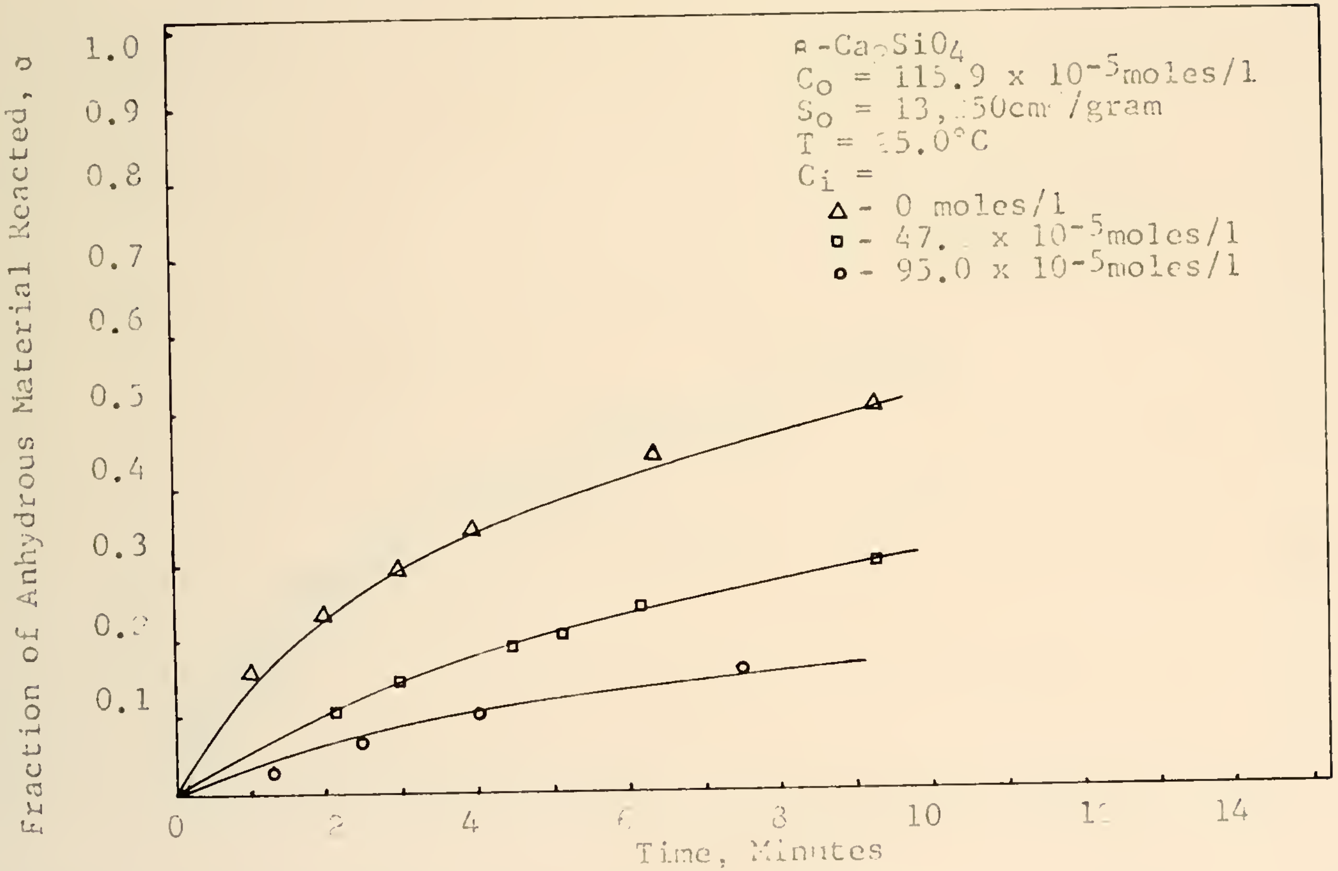

Figure [illegible]. Fraction Reacted of β-Ca$_2$SiO$_4$ vs. Time for Several Values of Initial Ca(OH)$_2$ Concentration (C_i)

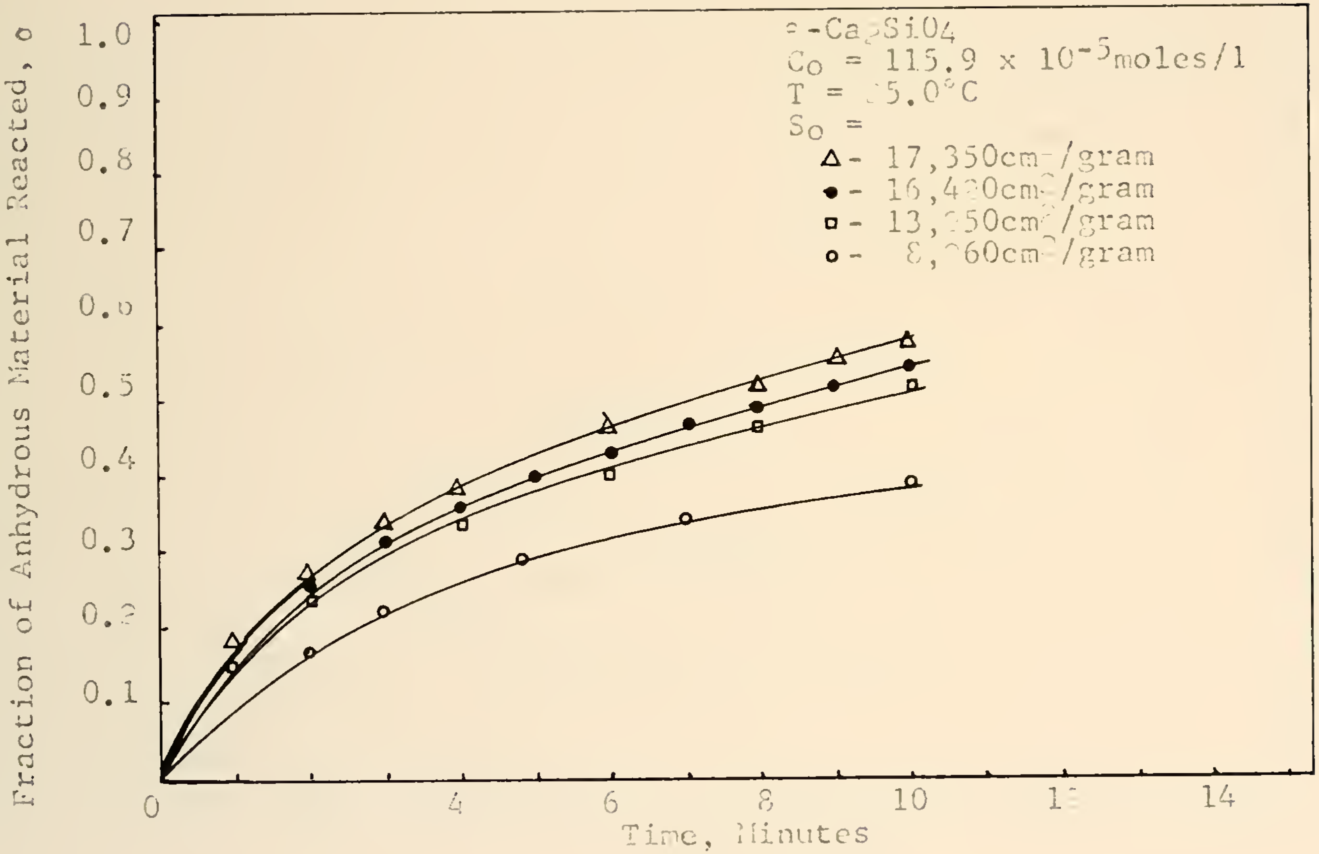

Figure 27. Fraction of β-Ca_2SiO_4 vs. Time for Several Values of Specific Surface Areas (S_o)

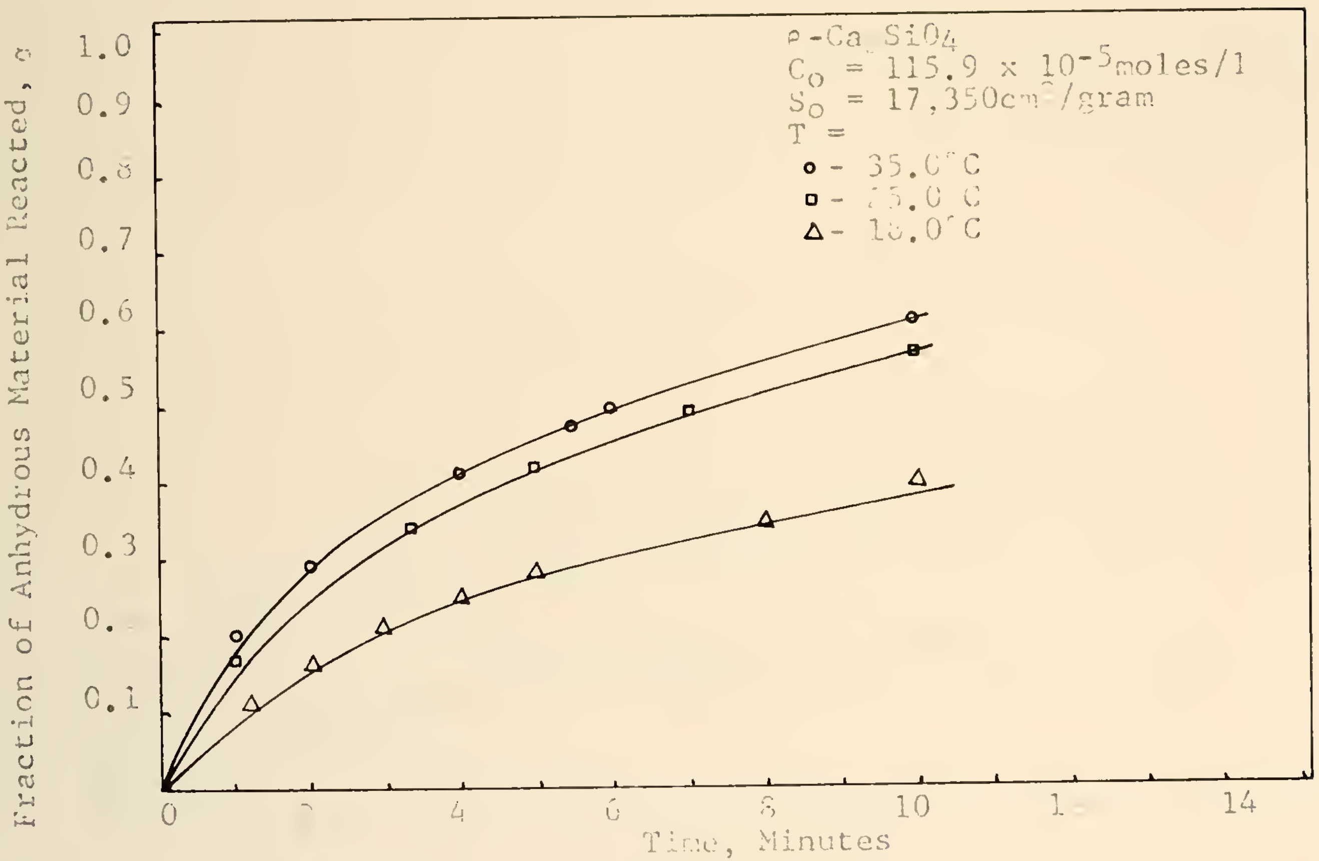

Figure 28. Fraction Reacted of β-Ca_2SiO_4 vs. Time for Several Values of Temperature (T)

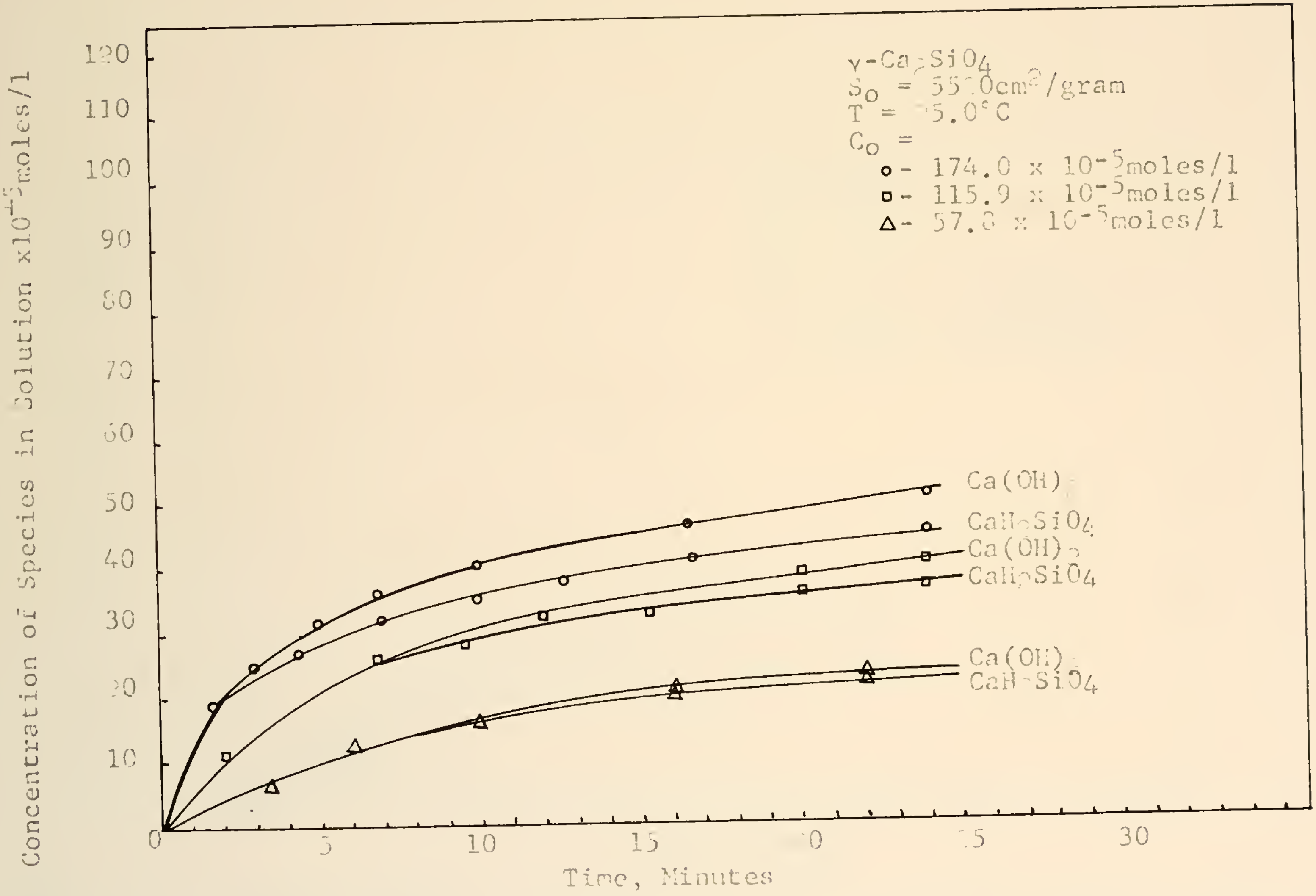

Figure 29 . Data for γ-Ca_2SiO_4 Showing Concentration of Species in Solution vs. Time for Various Values of (C_o)

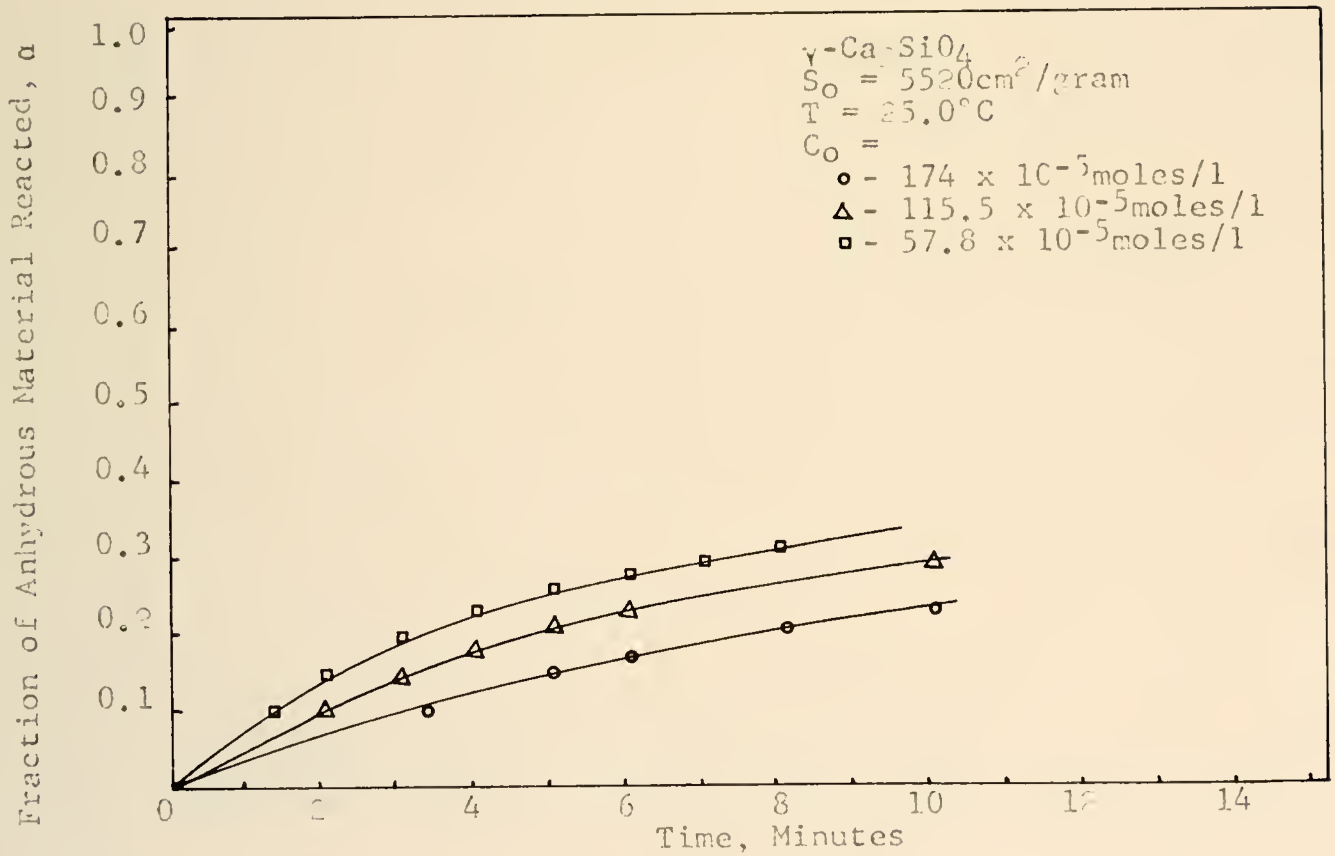

Figure 30. Fraction Reacted of γ-Ca_2SiO_4 vs. Time for Several Values of Sample Sizes (C_o)

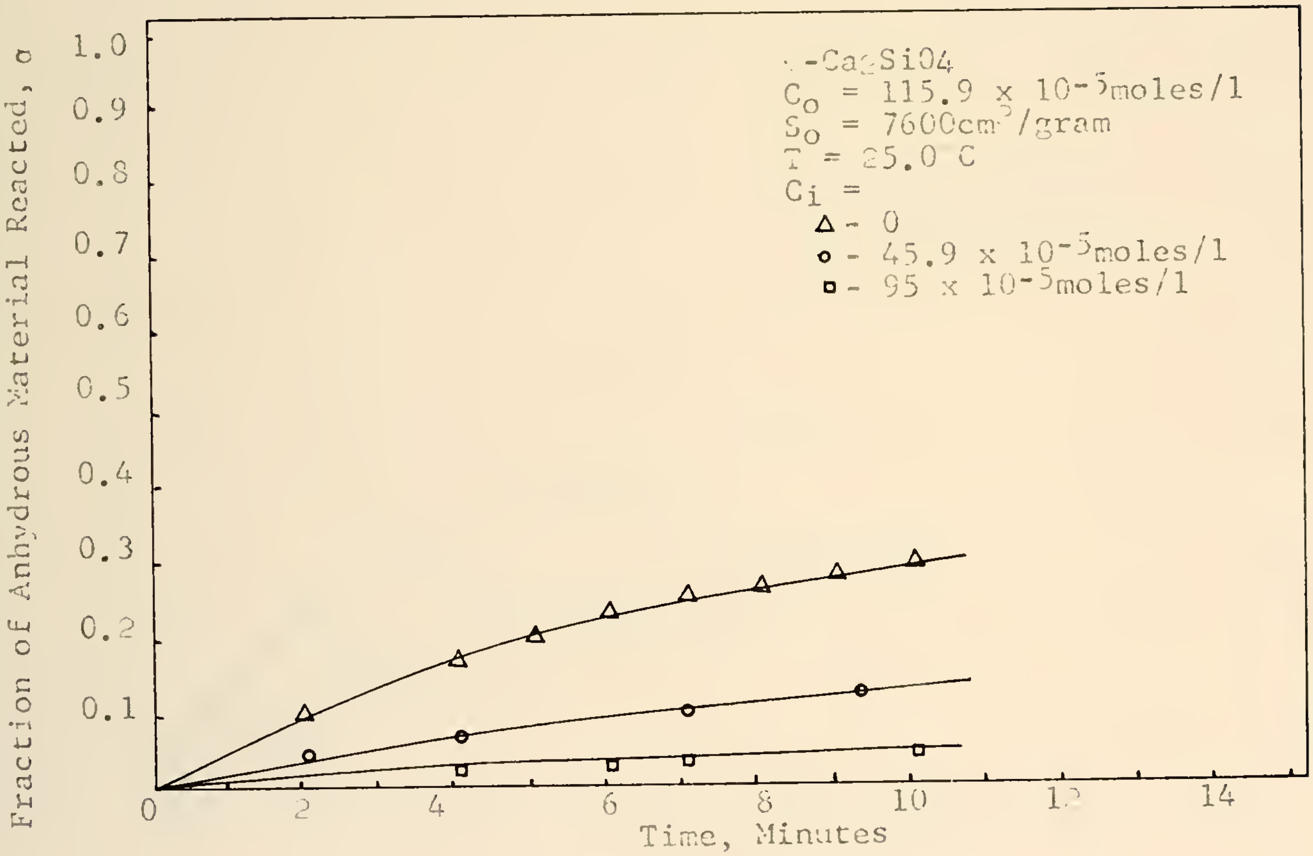

Figure 31. Fraction Reacted of γ-Ca$_2$SiO$_4$ vs. Time for Several Values of Initial Ca(OH)$_2$ Concentration (C_i)

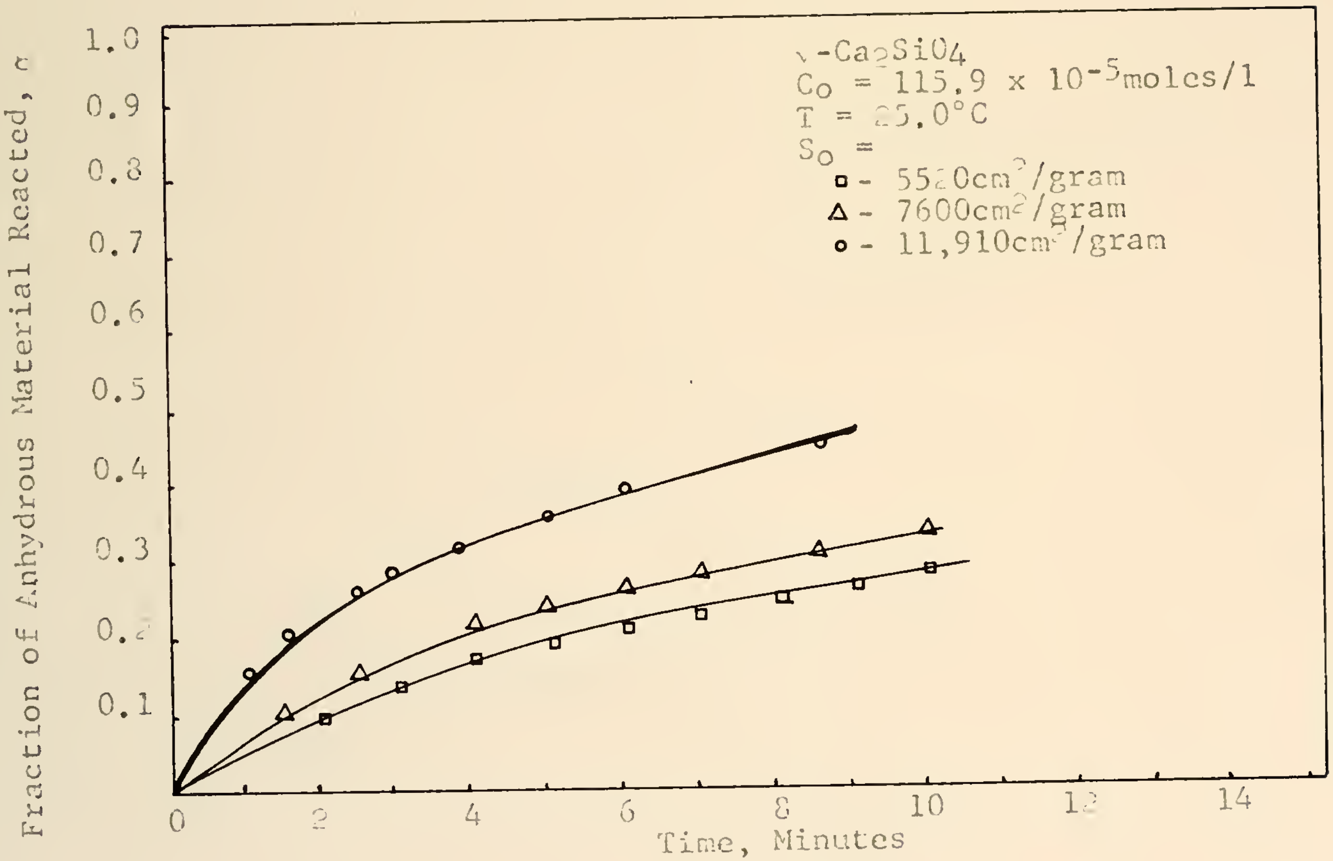

Figure 32. Fraction Reacted of γ-Ca$_2$SiO$_4$ vs. Time for Several Values of Specific Surface Areas (S_o)

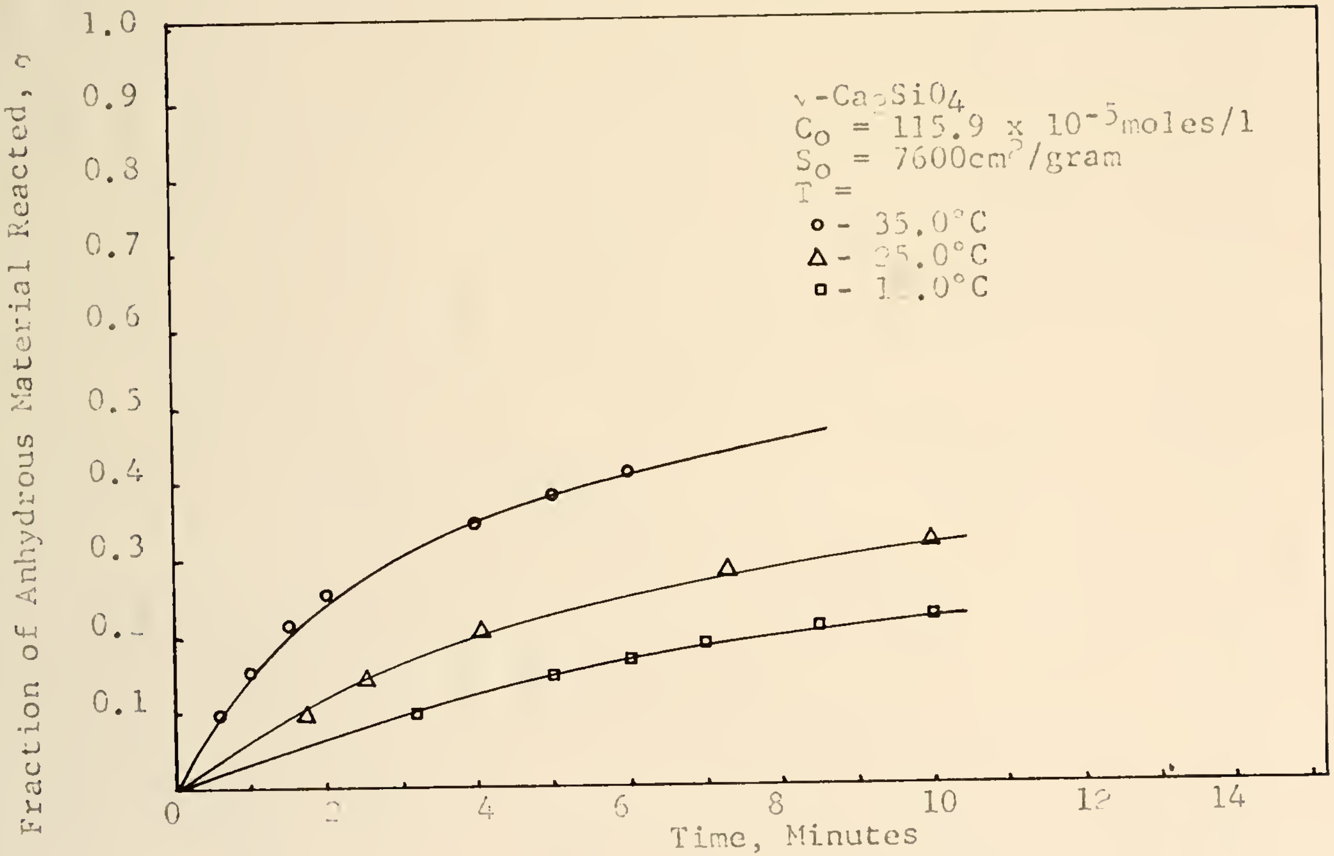

Figure 33. Fraction Reacted of γ-Ca$_2$SiO$_4$ vs. Time for Several Values of Temperature (T)

DISCUSSION OF RESULTS

The x-ray diffraction patterns secured for the anhydrous materials match corresponding patterns in the literature (11, 20, 21). The x-ray data indicate that the hydrate of Ba_2SiO_4 is a poorly crystallized version of the low $BaO:SiO_2$ ratio hydrate found by Hanna (7). The hydrates of β- and γ-Ca_2SiO_4 are very poorly crystalline and have only three poorly-defined peaks. These peaks are identical with those generally found for poorly crystallized calcium silicate hydrates. The peaks found for $SrH_2SiO_4 \cdot 0.8H_2O$ do not match any reported by Carlson and Wells (16) or those of $SrCO_3$ or $Sr(OH)_2 \cdot 8H_2O$. The $CdH_2SiO_4 \cdot 0.20H_2O$ pattern consisted of one broad peak. The author is aware of no reported x-ray data for any cadmium silicate hydrate.

The infrared spectrum of Ba_2SiO_4 has two regions of absorption. One occurs at approximately 870 cm^{-1} and the other at approximately 485 cm^{-1}. The spectrum expected for an isolated tetrahedron contains two infrared active vibrational modes each of which is triply degenerate (29). Triply degenerate means that there are three energetically equivalent vibrational modes which therefore absorb at the same frequency. When the tetrahedral ion is perturbed by an

asymmetric field, such as that generated by nearby ions, the modes will be changed to an extent that depends on the symmetry of the perturbing field. If two of the modes are perturbed to the same extent but the third to a different extent, then the absorption band would split into two bands of a relative intensity of 2:1. If all the modes are perturbed to a different extent, then the band would split into three equally intense bands. There are two absorption bands in the approximately 800 cm^{-1} region of the spectrum of Ba_2SiO_4. One is a broad band centered at 870 cm^{-1} and the other a smaller band at 800 cm^{-1}. Halford's analysis (30), as applied to this spectrum, is shown in Appendix C.

Halford's analysis predicts four bands in the 800 cm^{-1} region. The three-fold degenerate mode should be completely split, and the infrared inactive symmetric stretching mode should become infrared active. The observed spectrum can be explained in two different ways. The small band at 800 cm^{-1} could be a splitting of the triply degenerate mode or the infrared forbidden symmetric stretching mode. If it is the split triply degenerate mode, then the band at 870 cm^{-1} should be slightly less than twice as intense as the 800 cm^{-1} band. It is more likely that the band at 800 cm^{-1} is the symmetric A_1 stretching mode and the band at 870 cm^{-1} is the unresolved triply split T_2 asymmetric stretching mode. The bands at 510 cm^{-1} and 480 cm^{-1} are not as ambiguous. The band at 510 cm^{-1} is approximately half as intense as the

band at 480 cm^{-1}, and they are probably both splittings of the triply degenerate deformation mode. The infrared forbidden deformation is either very weakly absorbing, or it is overlapped by the 480 cm^{-1} band.

The spectrum of BaH_2SiO_4 is similar to that of the anhydrous compound, but the stretching modes are shifted to higher frequencies, and the deformation is shifted to lower frequencies. The band corresponding to the symmetric stretching mode is shifted from 800 cm^{-1} in Ba_2SiO_4 to 930 cm^{-1} in BaH_2SiO_4. In the spectrum of BaH_2SiO_4 the band corresponding to the asymmetric stretching mode is split into two bands of 2:1 relative intensity at 1000 cm^{-1} and 1040 cm^{-1}. The bands corresponding to the split infrared active T_2 deformation mode in Ba_2SiO_4 are shifted to 470 cm^{-1} and the splittings become unresolved. The very weak band at 1650 cm^{-1} comes from the H_2O deformation mode and is probably due to the presence of adsorbed water. The broad band from 3650 cm^{-1} to 2400 cm^{-1} comes from hydrogen bonding that causes broadening of the OH stretching mode.

The spectrum of Sr_2SiO_4 is similar to that of Ba_2SiO_4. There are two areas of absorption. The sharp band at 810 cm^{-1} is probably the symmetric stretching mode. The bands at 900 cm^{-1} and 970 cm^{-1}, which have intensity ratios of 2:1 correspond to the asymmetric stretching mode, which is a doubly split, triply degenerate, T_2 mode. The resolution for the symmetric mode absorption is better than in the Ba_2SiO_4

spectrum, because there is less overlap due to a shift to higher frequencies for the asymmetric mode absorption in Sr_2SiO_4. The bands at 510 cm^{-1} and 540 cm^{-1} are approximately 2:1 in relative intensity and are probably the absorption bands for the infrared active T_2 deformation bands.

The spectrum of SrH_2SiO_4 is similar to that of Sr_2SiO_4. It has a broad, poorly-resolved peak at 960 cm^{-1}. The 960 cm^{-1} band trails off slowly on the low frequency edge, and there is a slight bulge at approximately 1010 cm^{-1}. The deformation mode absorbs at 425 cm^{-1} and 470 cm^{-1} in a 2:1 intensity ratio, respectively. There is a small band from 1630 cm^{-1} attributable to the free water deformation. The broad band from 3650 cm^{-1} to 2800 cm^{-1} is due to the hydrogen bonded OH stretching vibration.

The spectrum of β-Ca_2SiO_4 is composed of the doubly split asymmetric mode which absorbs in a 2:1 intensity ratio at 880 cm^{-1} and 990 cm^{-1}, respectively. The infrared inactive mode becomes active and absorbs at 820 cm^{-1}. The deformation mode is doubly split and absorbs in a 2:1 intensity ratio at 510 cm^{-1} and 540 cm^{-1}, respectively. The small band at 1530 cm^{-1} is probably due to the small amount of B_2O_3 used to stabilize the β-Ca_2SiO_4 structure (33). The band at 380 cm^{-1} could be the infrared inactive E deformation, but it could just as well be a lattice absorption.

The spectrum of the hydrate of β-Ca_2SiO_4 shows a broad band in the region of the asymmetric stretch with a shoulder

at 1060 cm^{-1} and the main band centered at 960 cm^{-1}.

The deformation band at 440 cm^{-1} is unsplit. The small band at 650 cm^{-1} could be a combination of the band at 440 cm^{-1} and a lattice mode at 210 cm^{-1}.

The spectrum γ-Ca_2SiO_4 consists of the symmetric stretching band, which appears as a weak shoulder at 800 cm^{-1}, and the asymmetric stretching mode with bands at 850 cm^{-1} and 940 cm^{-1}. The deformation mode T_2 is multiply split into 2:1 intensity ratio bands at 500 cm^{-1} and 560 cm^{-1}, with a shoulder at 440 cm^{-1}, which is probably the infrared inactive deformation mode. Additional bands between 400 cm^{-1} and 300 cm^{-1} are due to lattice modes. The spectrum of the hydrate of γ-Ca_2SiO_4 is identical to that of the hydrate of β-Ca_2SiO_4.

The spectrum of Cd_2SiO_4 has a very broad band, which is split into 2:1 intensity ratio bands centered at 870 cm^{-1} and 960 cm^{-1}, respectively, and the symmetric stretching mode at 800 cm^{-1}. The split triply degenerate T_2 deformation bands absorb in 2:1 intensity ratio at 440 cm^{-1} and 540 cm^{-1}, respectively. In the spectrum of the hydrate of composition CdH_2SiO_4 there is no resolution in the asymmetric stretch region; rather there is a single band centered at 1000 cm^{-1}. The band at 440 cm^{-1} has no splittings, but it is probably the T_2 deformation. There is a very small band at 620 cm^{-1} and the usual water deformation and stretching vibrational modes.

The results of the differential thermal analysis for the anhydrous materials shows no apparent phase transformations for Ba_2SiO_4, Sr_2SiO_4 or Cd_2SiO_4 between 50°C and 950°C. The data for γ-Ca_2SiO_4 show a small exothermic effect at 800°C, which corresponds to a phase transformation to the α^1 crystallographic form. β-Ca_2SiO_4 shows no phase transformation in the region 50°C to 950°C.

The differential thermal analysis of BaH_2SiO_4 shows a large, broad, endothermic effect at 150°C and a small, exothermic effect at 840°C. The broad, endothermic effect at 150°C has a rounded shoulder to 380°C and probably masks the small, broad, endothermic effect found at 340°C by Hanna (7).

The differential thermal analysis of $SrH_2SiO_4 \cdot 0.8H\ O$ also shows a broad, endothermic effect at 150°C but also shows a series of shoulders at temperatures up to 340°C. There is also the small, exothermic effect for $SrH_2SiO_4 \cdot 0.8H_2O$ that occurs at 870°C.

The hydrates of β- and γ-Ca_2SiO_4 have identical differential thermal responses. The broad, endothermic effect is maximum at 130°C, but it also trails off to 350°C. The calcium silicate hydrate also shows an exothermic effect at 925°C.

The endothermic effect for CdH_2SiO_4 is much smaller and broader than for the barium, strontium, or calcium systems. The small exothermic effect occurs at 750°C.

The results of the chemical analyses in Table 6 show that the predominant mole ratio of $MO:SiO_2$ is 1:1. This finding is consistant with Greenberg's statement (25) that the CaH_2SiO_4 is made of Ca^{+2} and $H_2SiO_4^{=}$ ion. The results of the chemical analyses, combined with the infrared spectra for the hydrates, offer evidence that they are orthosilicates.

The results of measurements of the surface area for the anhydrous orthosilicates is shown in Table 7. The only unexpected result is the values of the specific surface areas of fineness fractions number three and four for γ-Ca_2SiO_4.

The electron micrographs show the general character of the hydrates formed. The micrograph of BaH_2SiO_4 is not representative of the hydrate because the electron beam tends to "fry" the conglomerated lath shaped particles. To obtain a good micrograph, replicas should have been made, but the facilities were not available. The micrograph for $SrH_2SiO_4 \cdot 0.8H_2O$ shows the general, needle-like character of the hydrate.

The hydrates of β- and γ-Ca_2SiO_4 were identical and the pictures show the characteristic, fibrous bundles for calcium silicate hydrates.

The micrograph of the $CdH_2SiO_4 \cdot 0.2H_2O$ shows no fibrous structure. There seems to be little structure at all, but there might be some platy characteristics.

Table 6. Chemical Analysis of the Silicate Hydrates.

Cation	Molar Ratios $MO:SiO_2:H_2O$
Ba^{+2}	0.95:1.00:1.54
Sr^{+2}	0.99:1.00:1.80
Ca^{+2}	0.94:1.00:2.85
Cd^{+2}	1.01:1.00:1.20

Table 7. Results of Krypton Adsorption Specific Surface Area Measurements.

Fineness Fraction	1	2	3	4	5
			Surface area, cm^2/g		
Ba_2SiO_4	5,820	1,750	1,540	955	
Sr_2SiO_4	15,750		10,380		9,150
β -Ca_2SiO_4	17,350	16,420	13,250	8,260	
γ -Ca_2SiO_4	11,910	7,600	5,520	5,540	

An important aspect is the nature of the chemical species present in the reaction mixture. This question was attacked using data on chemical composition and conductivity of the mixture after the reaction had subsided substantially.

The resistance of a solution is a function of the concentrations of the ionic species present. For the ionic species produced by the reaction of interest the following equation holds:

$$\frac{1000J}{2R} = C_{M(OH)_2} \Lambda_{M(OH)_2} + C_{M\text{-}S\text{-}H} \Lambda_{M\text{-}S\text{-}H} \quad (1)$$

where J is the cell constant of the dipping conductivity cell, R is the resistance of the solution, C refers to concentration, Λ is the equivalent conductance, and M-S-H refers to the as yet undefined silicate hydrate produced by the reaction. For the cell used, J was determined by standard methods to be 2.020 cm^{-1} with no appreciable temperature variation over the range 0°C to 35°C.

Tables 8 and 9 show the results of chemical and conductometric analyses on suspensions of the hydrated silicates at 25.0°C. The equivalent conductances shown are those of the alkaline earth silicate hydrates if it is assumed that the reaction produced only $M(OH)_2$ and MH_2SiO_4 according to

$$M_2SiO_4 + 2H_2O \rightarrow M(OH)_2 + MH_2SiO_4$$

Table 8. Results of Chemical Analyses of Solutions After Reaction at 25.0°C.

	c_o, molar x 10^5	Cation conc., molar x 10^5	SiO_2 conc., molar x 10^5
Ba_2SiO_4	54.1	110.0	54.7
	81.6	159.0	80.0
	205.0	407.0	199.8
Sr_2SiO_4	74.5	148.0	72.0
	149.0	303.0	144.0
	223.5	251.0	220.3
β-Ca_2SiO_4	57.8	108.0	49.0
	115.9	162.0	72.0
	290.0	230.0	112.0
γ-Ca_2SiO_4	57.8	49.2	23.0
	115.9	86.8	40.8
	174.0	111.4	52.0
	290.0	120.0	53.0

Table 9. Measured Values of Equivalent Conductance of Silicate Hydrates.

	T, °C	Conc. of MH_2SO_4 molar x 10^5	Equivalent Conductance, cm^2 mho	
			M-S-H	M_2SO_4
β-Ca_2SiO_4	25.0	80.0	143	138
		54.7	125	138
		105.0	140	138
γ-Ca_2SiO_4	35.0	70.0	185	189
γ-Ca_2SiO_4	25.0	40.0	141	138
	35.0	52.0	146	138
Sr_2SiO_4	25.0	74.5	138	140
Sr_2SiO_4	18.0	75.0	115	120
Ba_2SiO_4	25.0	80.0	135	145
Ba_2SiO_4	0.4	78.0	68	74

If, on the other hand, the reaction of, for example, the Sr_2SiO_4 is assumed to produce $Sr(H_3SiO_4)_2$ the equivalent conductance would be about 8 cm^2/ohm, and if it produced $Sr_3(HSiO_4)_2$ the value would be over 300 in the same units.

In Table 9 are given also the handbook values of the equivalent conductances of the sulfates of the same cations. Since the sulfate and dibasic orthosilicate ions have the same charge, symmetry, and mass it is reasonable to expect their conduction behavior to be similar. If this is true, it is readily seen that the only assumption that is reasonable is that the species MH_2SiO_4 was the one produced. This is the basis for the assumption of the validity of the above-given reaction stoichiometry.

The importance of the correctness of this assumption has been discussed in the data section.

Next, an attempt was made to fit an appropriate model to the kinetic data in order to elucidate the mechanisms of the reactions taking place.

If c_o is the number of moles of the anhydrous M_2SiO_4 placed into the reaction vessel containing a liter of water and c is the amount reacted at any time, then c_o-c is the amount of anhydrous material remaining, and $\alpha = c/c_o$, the fraction reacted; $1-\alpha$ is the fraction unreacted.

It was discovered, by trial and error, that the kinetic data for the reaction of Ba_2SiO_4 and Sr_2SiO_4 were linear

when the logarithm of 1-α was plotted vs. time. Such plots are given in Figures 34-36 for the Ba_2SiO_4 reactions and in Figures 37-39 for the Sr_2SiO_4 and are essentially re-plots of the data presented earlier and show the same dependences on sample size, temperature, and sample surface area. The plots showing the influence of pH (or c_i) are not given because the results (see Figures 17 and 21) show that over a range of pH of 7 to 11 the rates of the reactions are independent of the ionic species in solution.

If the reaction occurs at the surface of a grain the rate law should be some order of the surface area of the material. If S is the surface area of an (assumed) spherical particle exposed to the reaction at time t and r is its radius, then

$$S = n\,4\pi r^2 \tag{2}$$

where n is the number of particles. If the weight of particles is w, $S_o = S/w$, where S_o is the specific surface area.

If c is the amount, in moles, of the anhydrous material that has reacted at time t and c_o is the initial amount, then c_o-c is the amount remaining.

The rate of the reaction can be written

$$\frac{dc}{dt} = k\,S^x \tag{3}$$

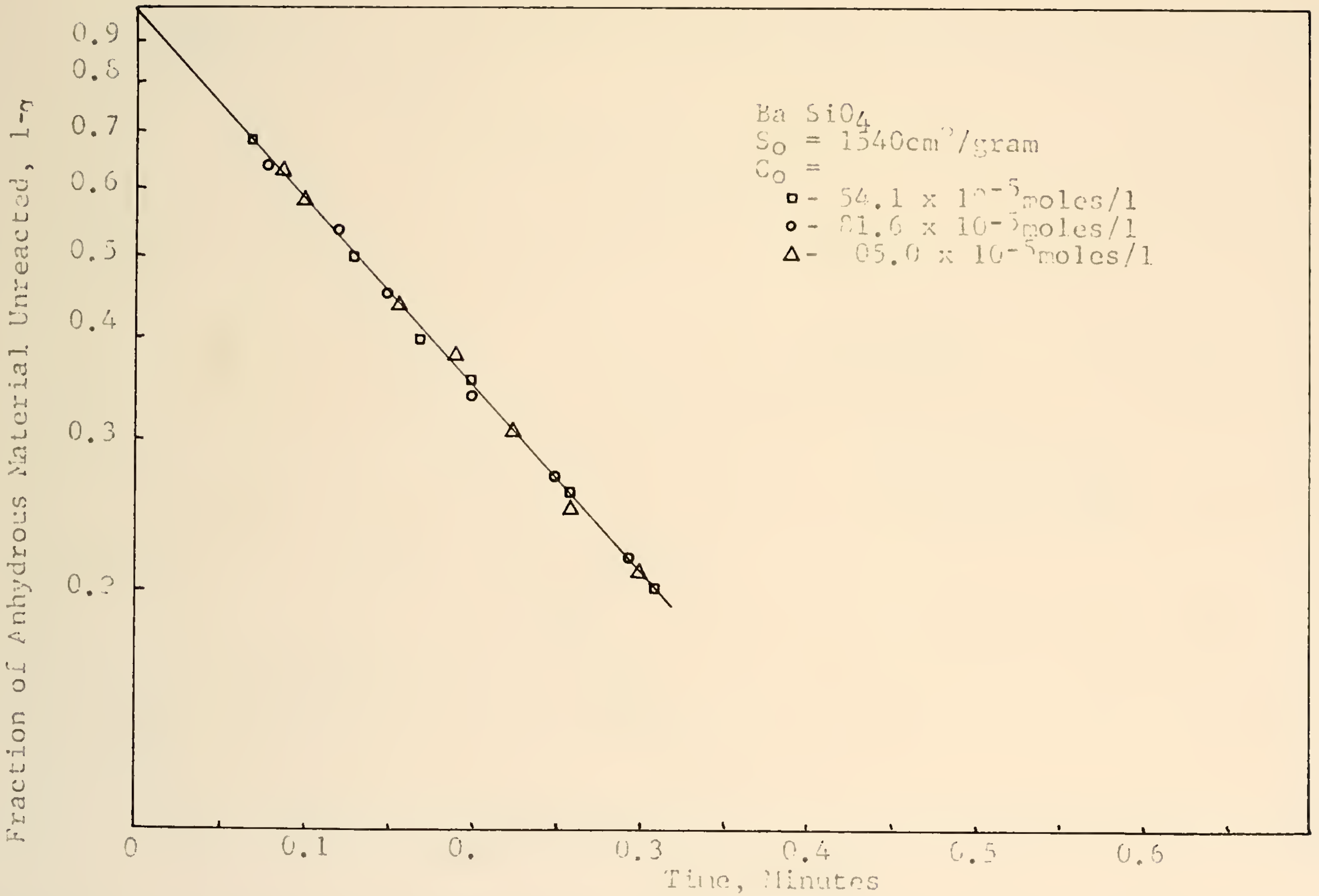

Figure 34. Fraction of Anhydrous Ba$_2$SiO$_4$ Remaining as a Function of Time for Varying Sample Sizes (C$_o$)

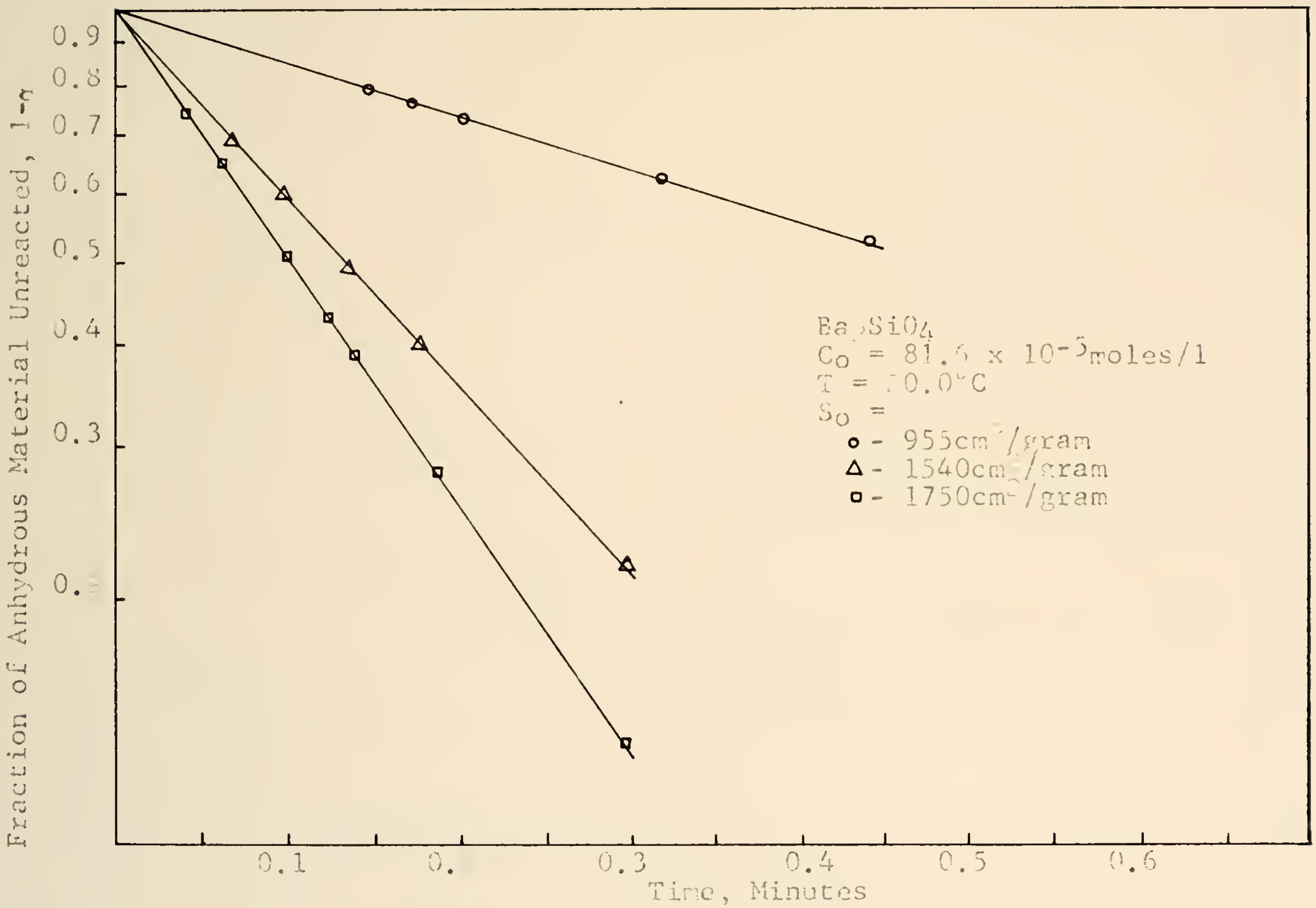

Figure 35 . Fraction of Anhydrous Ba_2SiO_4 Remaining as a Function of Time for Various Values of Specific Surface Area (S_o)

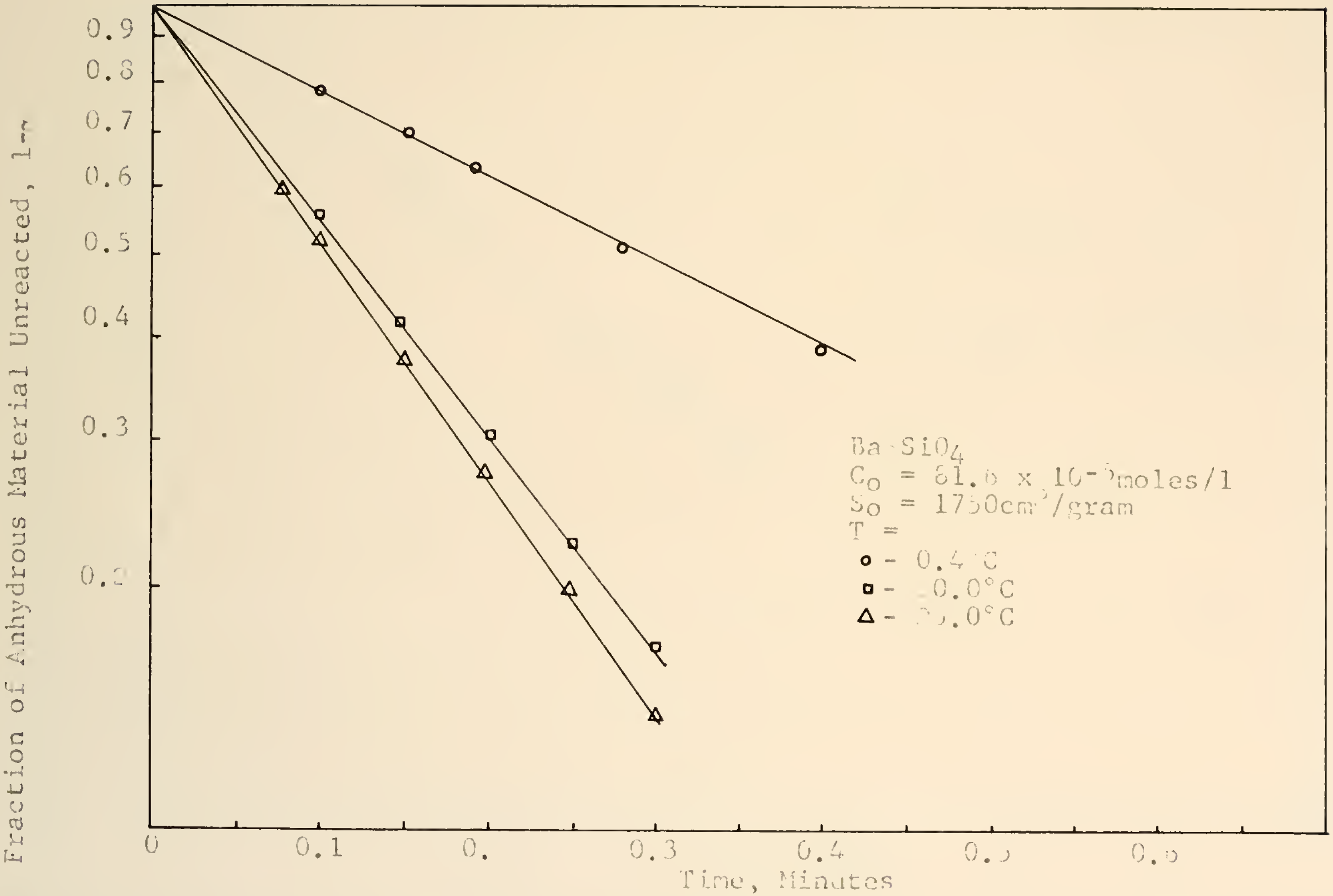

Figure 36. Fraction of Anhydrous Ba SiO_4 Remaining as a Function of Time for Varying Temperatures

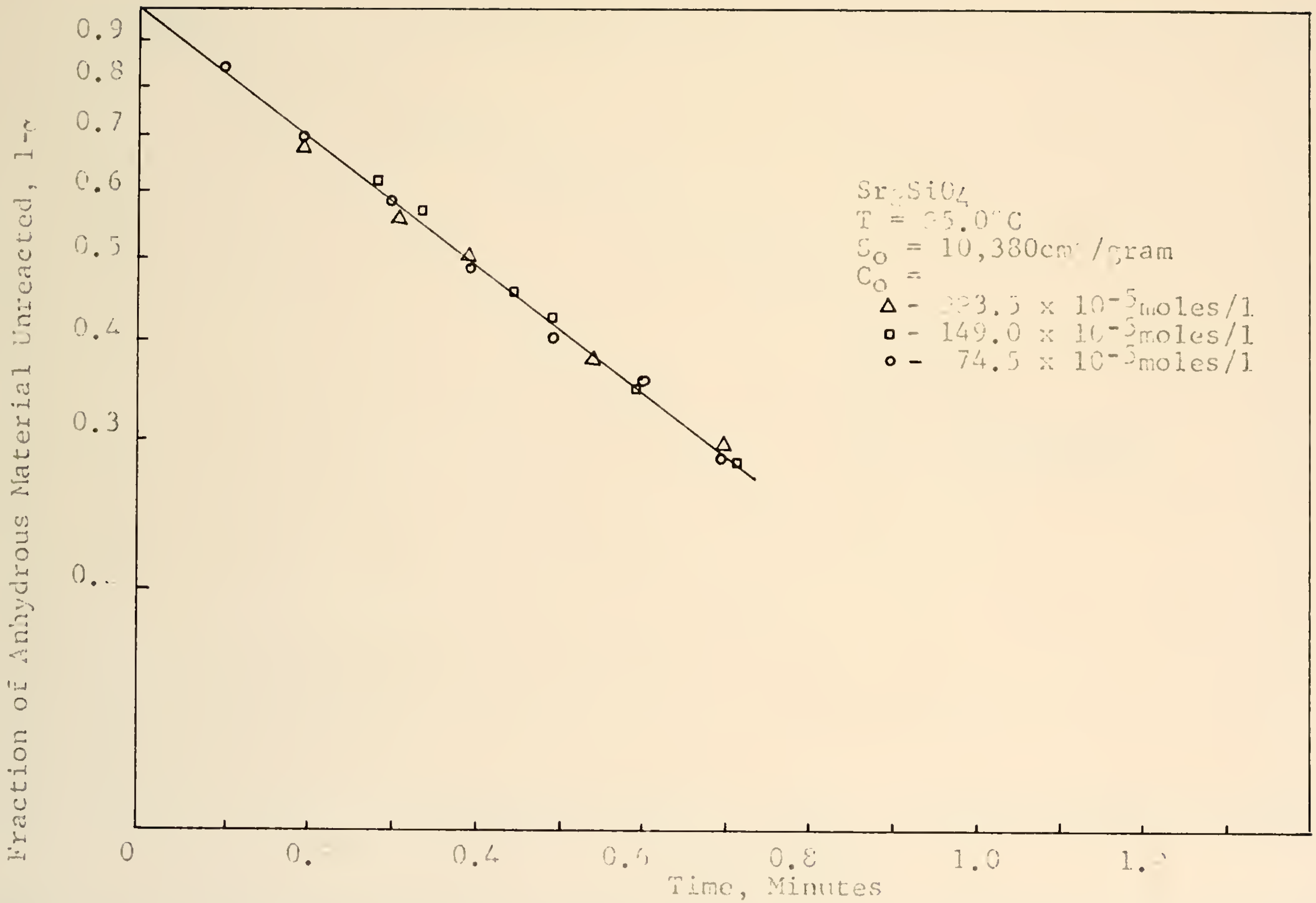

Figure 37. Fraction of Anhydrous Sr_2SiO_4 Remaining as a Function of Time for Various Sample Sizes (C_o)

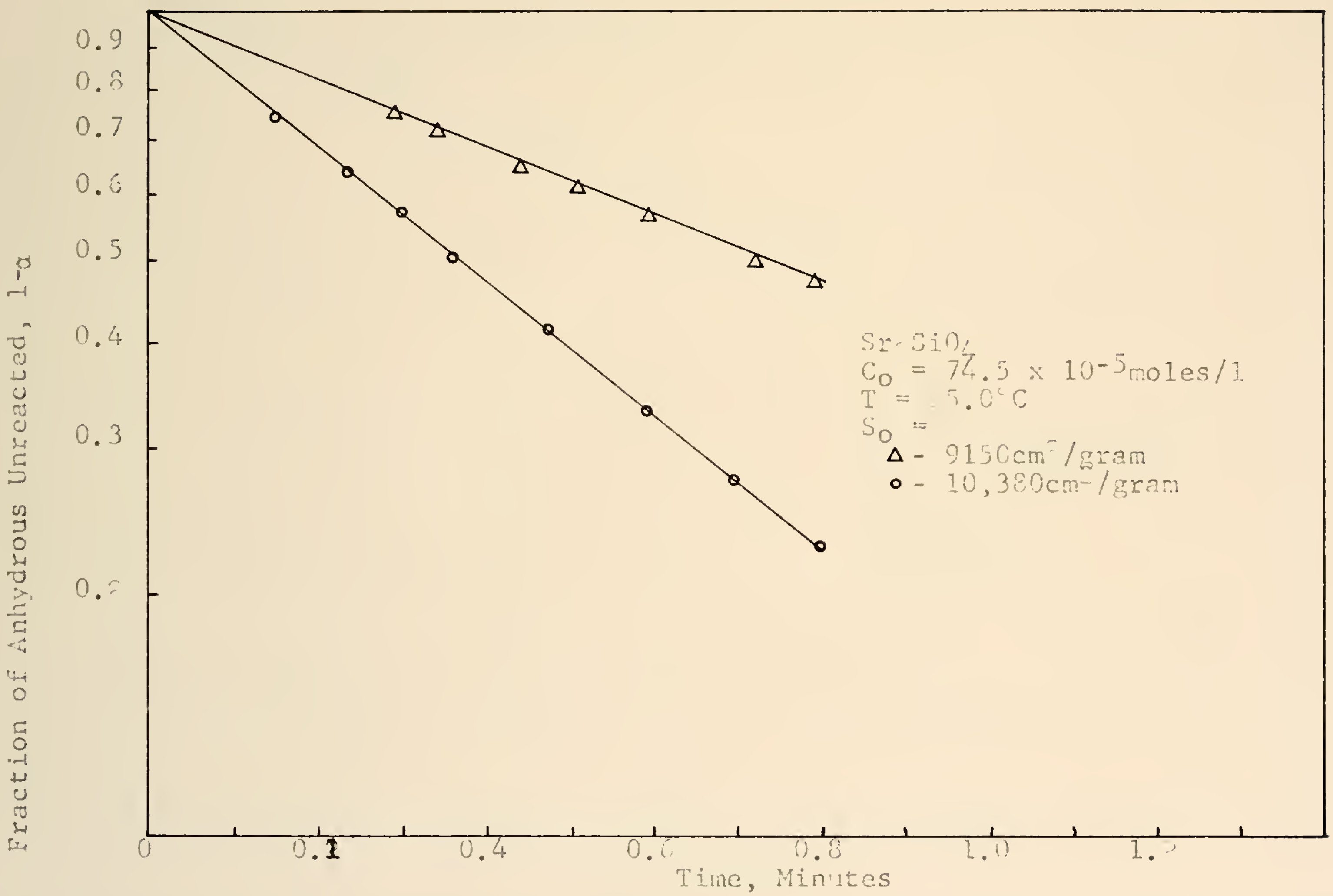

Figure 38. Fraction of Anhydrous Sr_2SiO_4 Remaining as a Function of Time for Various Specific Surface Area

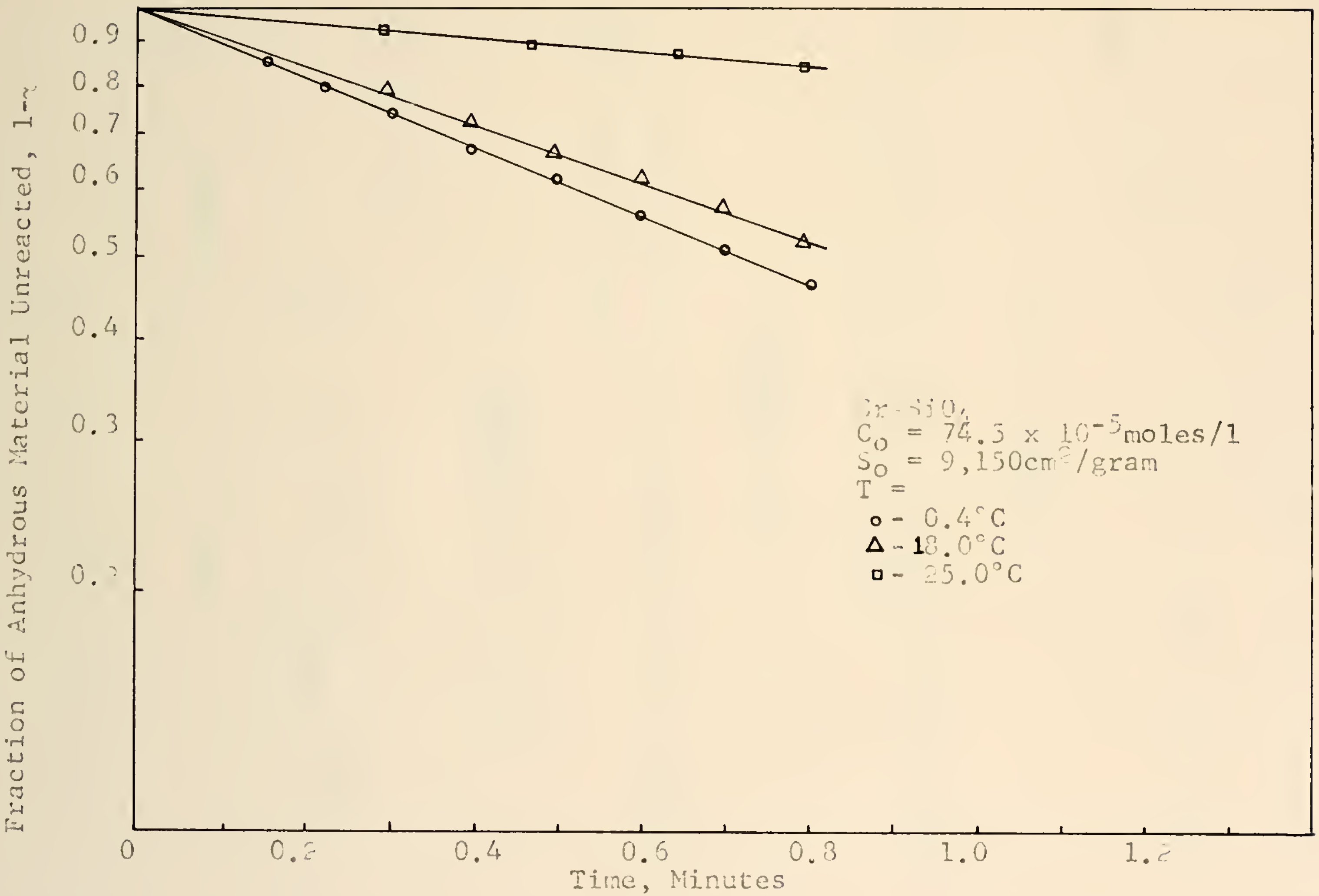

Figure 39 Fraction of Anhydrous Sr_2SiO_4 Remaining as a Function of Time for Various Temperatures

where x is the order of the reaction with respect to surface area. Then

$$\frac{dc}{dt} = k(4\pi nr^2)^x \qquad (4)$$

The radius of the grain is related to the number of moles present by

$$(c_o-c) = \frac{n4\pi r^3}{3}\frac{\rho}{M} \qquad (5)$$

where ρ is the density and M is the molecular weight.

Solving equation (5) for r gives

$$r = \frac{3M\ (c_o-c)^{1/3}}{4n\pi\rho} \qquad (6)$$

If this value of r is substituted into equation (4) the rate equation becomes

$$\frac{dc}{dt} = k\left[\left(\frac{3M(c_o-c)}{4\pi n\rho}\right)^{2/3} 4\pi n\right]^x \qquad (7)$$

or, rewriting

$$\frac{dc}{dt} = k\left[(4\pi n)^{1/3}\left(\frac{3M(c_o-c)}{\rho}\right)^{2/3}\right]^x \qquad (8)$$

This equation, with the introduction of $\alpha = c/c_o$, is then rewritten to obtain

$$\frac{d\alpha}{dt} = kk'n^{\frac{x}{3}}\ (1-\alpha)^{\frac{2x}{3}}\ c_o^{\left(\frac{2x}{3}-1\right)} \qquad (9)$$

where

$$k' = (4\pi)^{\frac{x}{3}} \left(\frac{3M}{\rho}\right)^{\frac{2x}{3}} \qquad (10)$$

If x is taken, provisionally, to be 3/2 then equation (9) becomes

$$\frac{d\alpha}{dt} = k\,\frac{3M}{\rho}\,(4\pi n)^{\frac{1}{2}}\,(1-\alpha) \qquad (11)$$

which is independent of c_o. This independence is confirmed by the data shown in Figures 16 and 20.

When equation (11) is integrated the result is

$$\ln(1-\alpha) = k\left(\frac{3M}{\rho}\right)(4\pi n)^{\frac{1}{2}}\,t \qquad (12)$$

which is seen to be linear in $\ln(1-\alpha)$ and t and, therefore, conforms to the experimentally observed form for the barium and strontium silicates.

The slope of the plot of experimental results of $\ln(1-\alpha)$ versus t is independent of c_o for Sr_2SiO_4 and Ba_2SiO_4. For a given c_o the value of n changes only with changes in specific surface areas. The slope of the plot of $\ln(1-\alpha)$ versus t is a function of the specific surface area and the temperature (see Figures 35, 36, 38 and 39). The value of k should be independent of the value of specific surface area, assuming that the particles of each fineness fraction have the same shape. If the shapes of the particles are different for the different fineness fractions, then k

will involve a geometric factor and will be different for different geometries.

The value of n, the number of particles in the sample, can be determined from its weight and specific surface area.

From the experimentally determined slopes of the relationship between $\ln(1-\alpha)$ and t, the values of k (equation (12) and (13) can be obtained. The density values used in the calculation were 5.42 g/cm^3 for Ba_2SiO_4 and 4.25 g/cm^3 for Sr_2SiO_4 (7, 8).

The values of k for various size fractions are given in Table 10 for Ba_2SiO_4 and Table 11 for Sr_2SiO_4.

Table 10. Calculated Values of k for Ba_2SiO_4

S_o, cm^2/g	k, min^{-1}
955	2.67×10^{-7}
1540	4.42×10^{-7}
1750	4.85×10^{-7}

Table 11. Calculated Values of k-for Sr_2SiO_4

S_o, cm^2/g	k, min^{-1}
9,150	1.31×10^{-8}
10,380	2.11×10^{-8}

The variation of the values of the rate constants will be discussed later.

The rate is a function of temperature. If the specific rate constant k is measured as a function of temperature and plotted against reciprocal temperature, a straight line

results. The slope of this line is equal to the activation energy of the process divided by R the gas constant. Such plots are given in Figures 40 and 41 for Ba_2SiO_4 and Sr_2SiO_4, respectively. The calculated activation energies are 4.82 Kcal/mole for Ba_2SiO_4 and 9.05 Kcal/mole for Sr_2SiO_4.

The data of Figures 25, 26, 30 and 31 show that the rates of the reactions of β-and γ-Ca_2SiO_4 are not independent of sample size or of the initial hydroxide concentration. To explain these data a rate equation was tried that included a first order dependence on hydrogen ion concentration as follows:

$$\frac{dc}{dt} = k\ S\ [H^+] \qquad (13)$$

This dependence is, naturally, one arrived at after attempting several alternate formulations. It is recognized that a somewhat inverted argument is presented here, of which equation (13) is the pragmatic end point.

The hydrogen ion concentration is related to the amount of anhydrous silicate reacted, c, by the following relationship

$$[2c + 10^{-7}][H^+] = 10^{-14} = K_w \qquad (14)$$

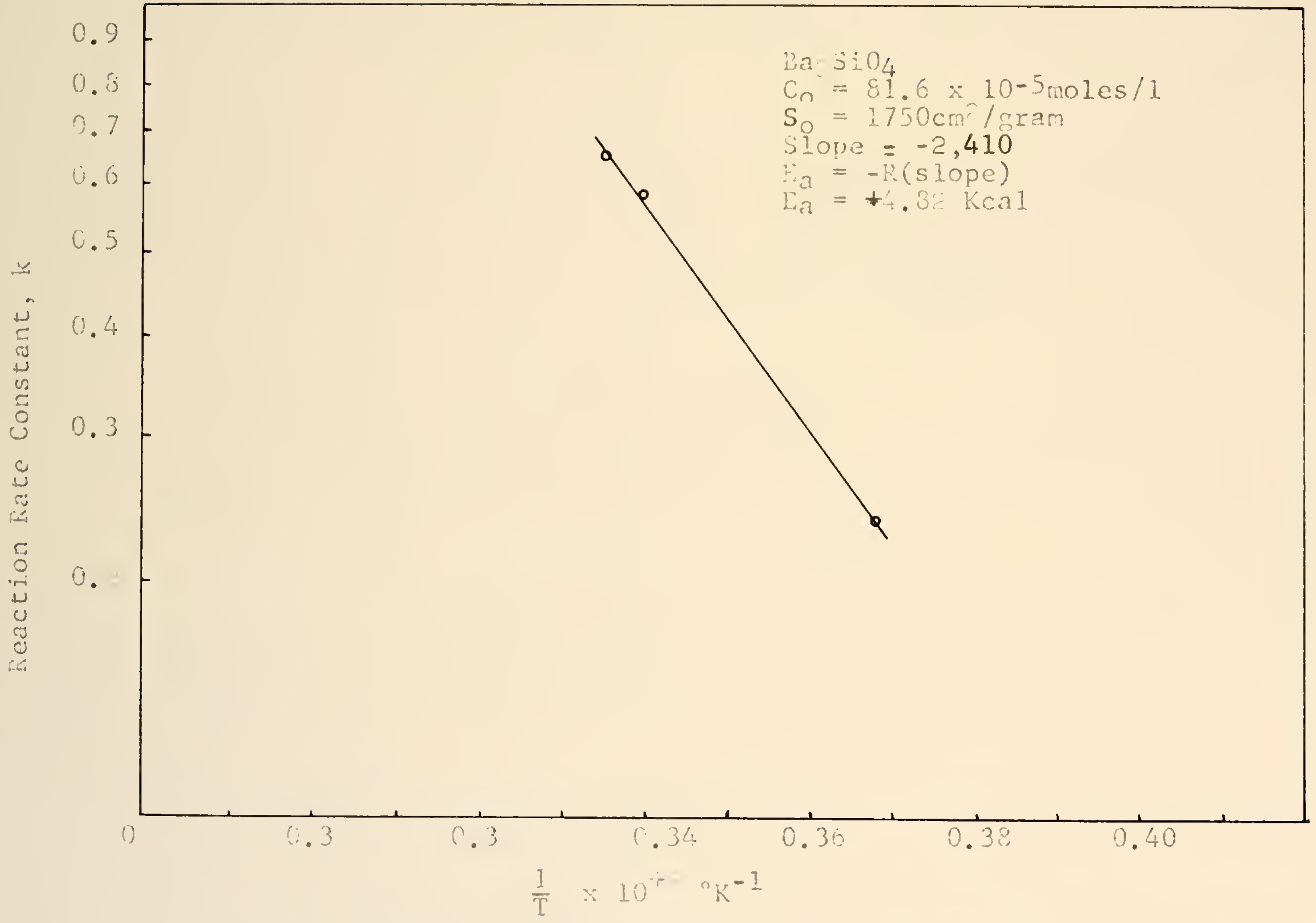

Figure 40. Rate Constant Dependence on Temperature for Ba SiO4

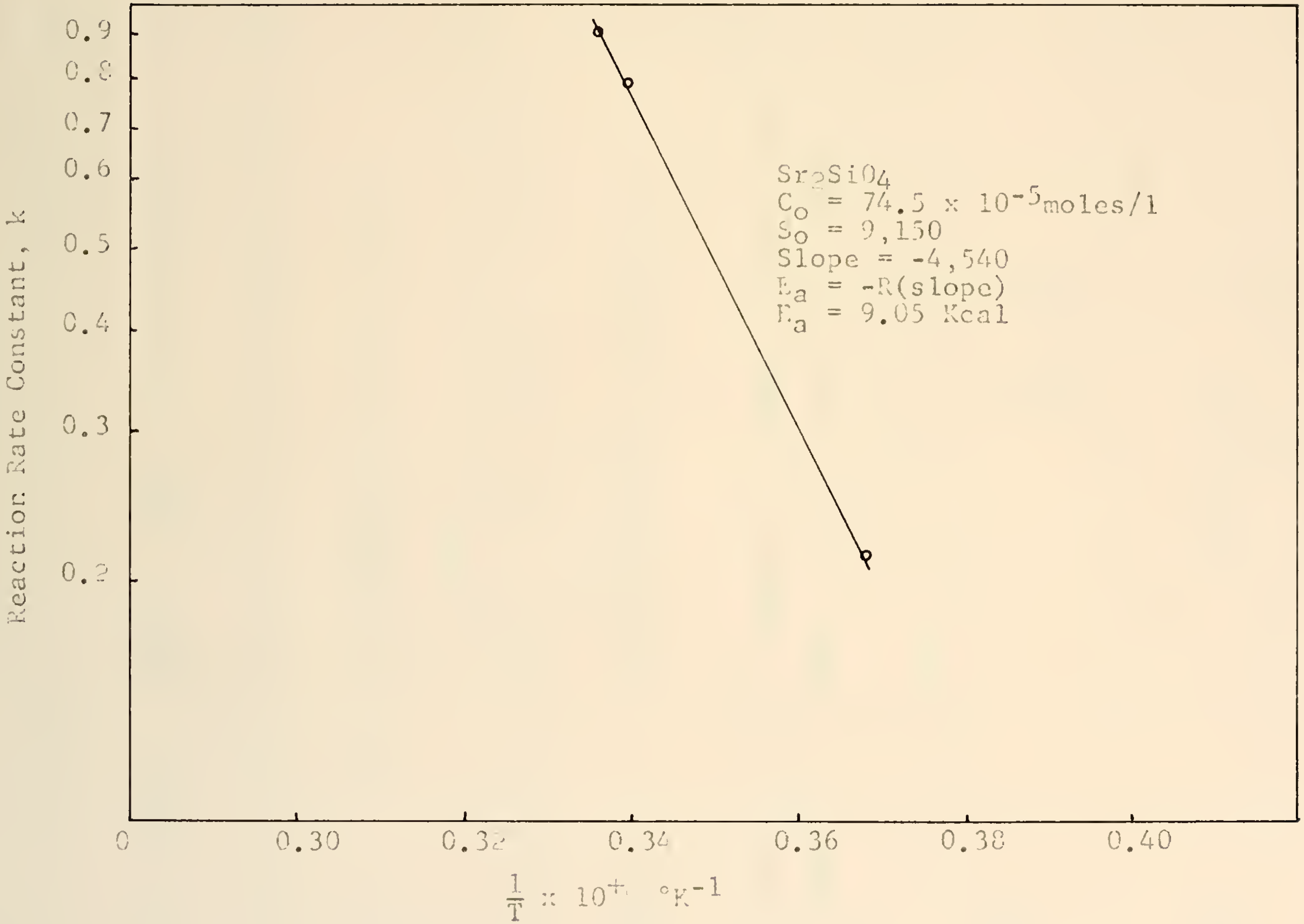

Figure 41. Rate Constant Dependence on Temperature for Sr_2SiO_4

in which 10^{-7} is the $[OH^-]$ at the onset, i.e. in pure water. Equation (14) is rewritten

$$[H^+] = \frac{K_w}{[2c + 10^{-7}]} \qquad (15)$$

and this value is substituted in (13) to give

$$\frac{dc}{dt} = \frac{kSK_w}{2c} \qquad (16)$$

if $C \gg 10^{-7}$, as is the case in these experiments at any except the very earliest times.

As before, the surface area is related to the amount of anhydrous material remaining unreacted by the relationship

$$S = (4\pi n)^{1/3} \left(\frac{3M\,(c_o - c)}{\rho}\right)^{2/3} \qquad (17)$$

The rate law, equation (13), in terms of concentration of reactants and products, is therefore

$$\frac{dc}{dt} = k\,(4\pi n)^{1/3} \left(\frac{3M\,(c_o - c)}{\rho}\right)^{2/3} \frac{K_w}{2c} \qquad (18)$$

If $\alpha = c/c_o$ is substituted into equation (18) the result is

$$\frac{d\alpha}{dt} = \frac{k}{2}\,(4\pi)^{1/3} \left(\frac{3M}{\rho}\right)^{2/3} \frac{(K_w n)^{1/3}}{c_o{}^{4/3}} \frac{(1-\alpha)^{2/3}}{\alpha} \qquad (19)$$

When this equation is integrated and the initial value of $\alpha = 0$ when $t = 0$ is inserted the result

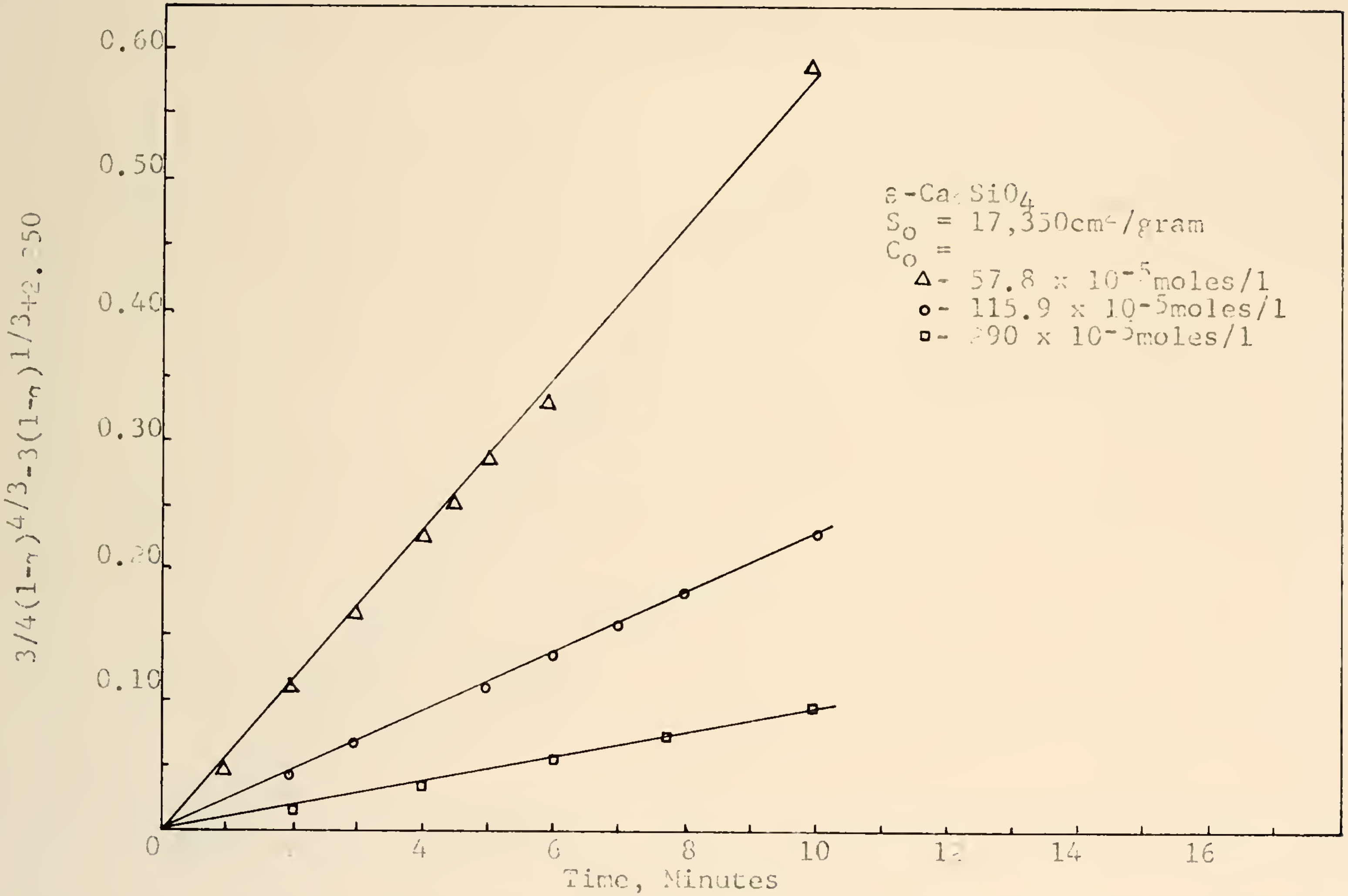

Figure 4[illegible]. Reaction of β-Ca SiO$_4$ with Water at 25.0°C, Effect of Sample Size

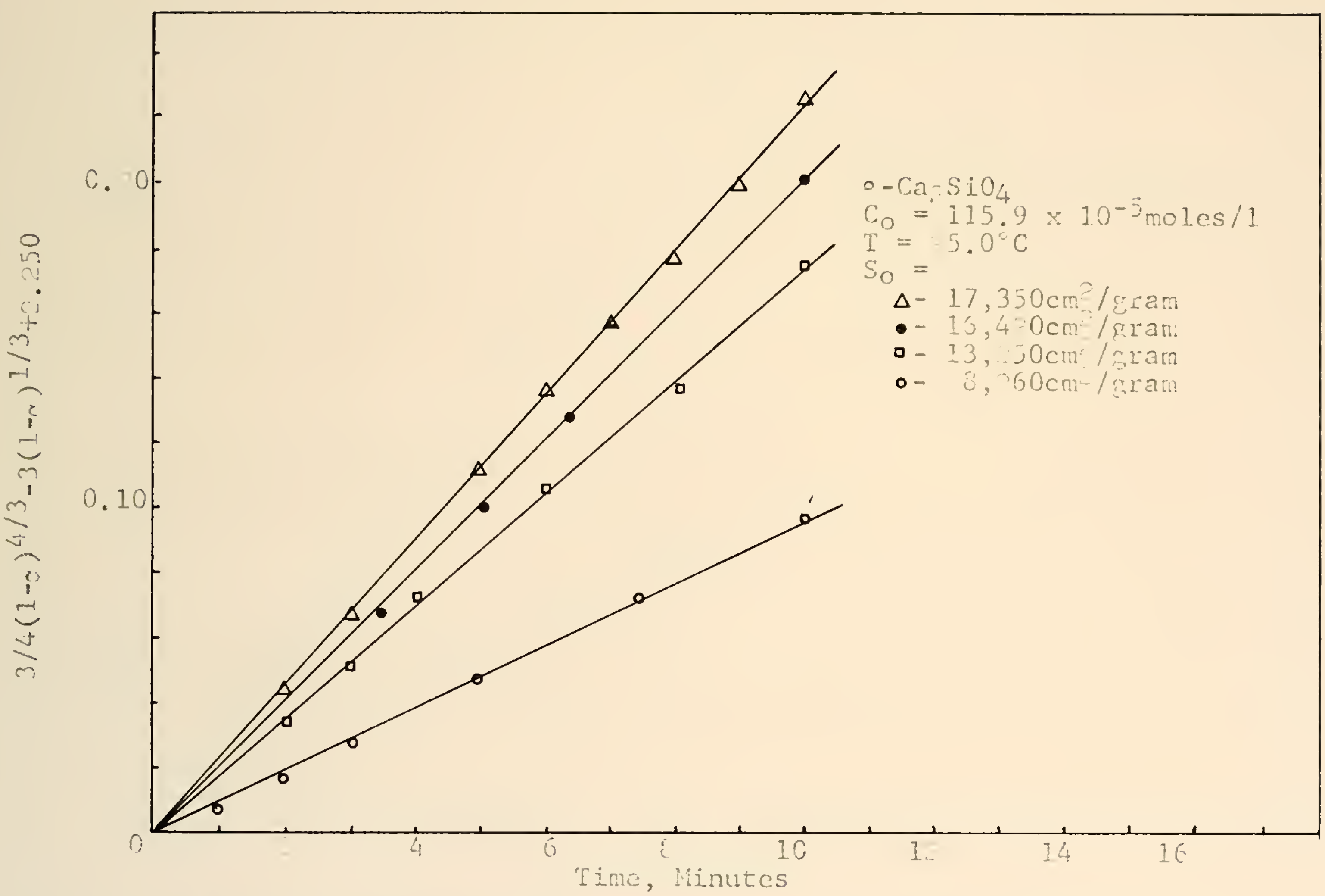

Figure 43 . Reaction of β-Ca_2SiO_4 with Water at 25.0°C, Effect of Surface Area

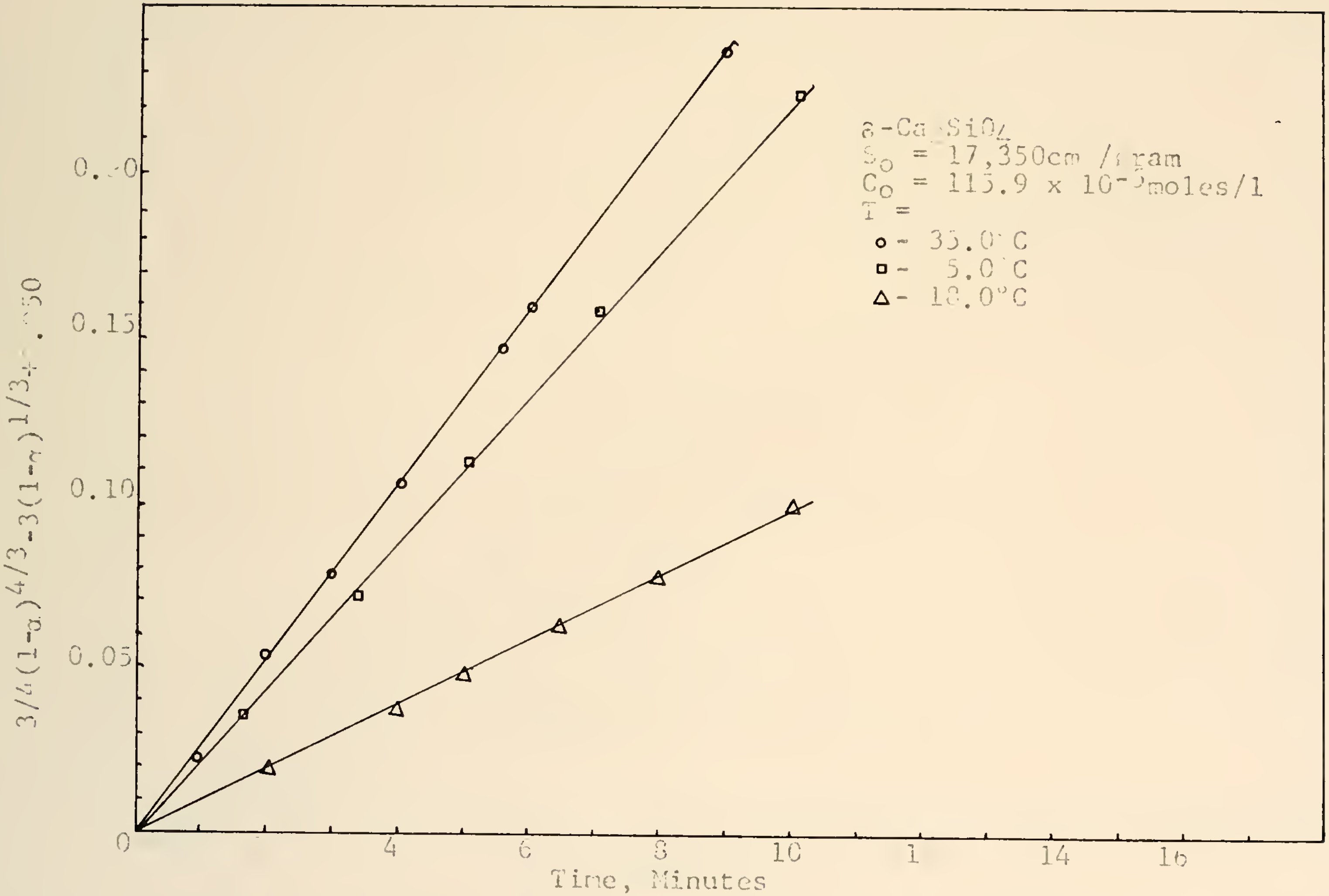

Figure 44. Reaction of β-Ca SiO$_4$ with Water, Effect of Temperatures

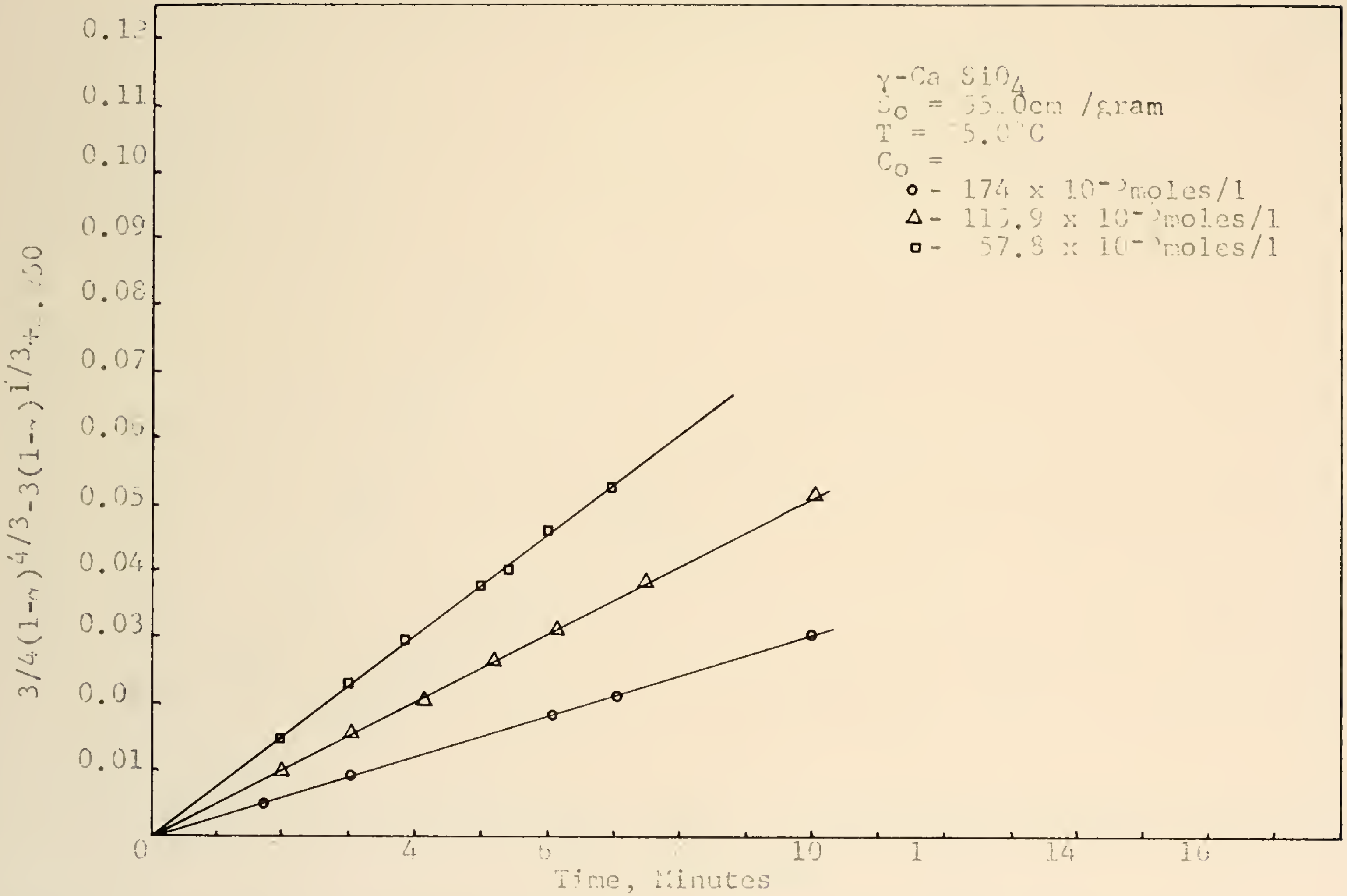

Figure 45. Reaction of γ-Ca$_2$SiO$_4$ with Water, Effect of Sample Size

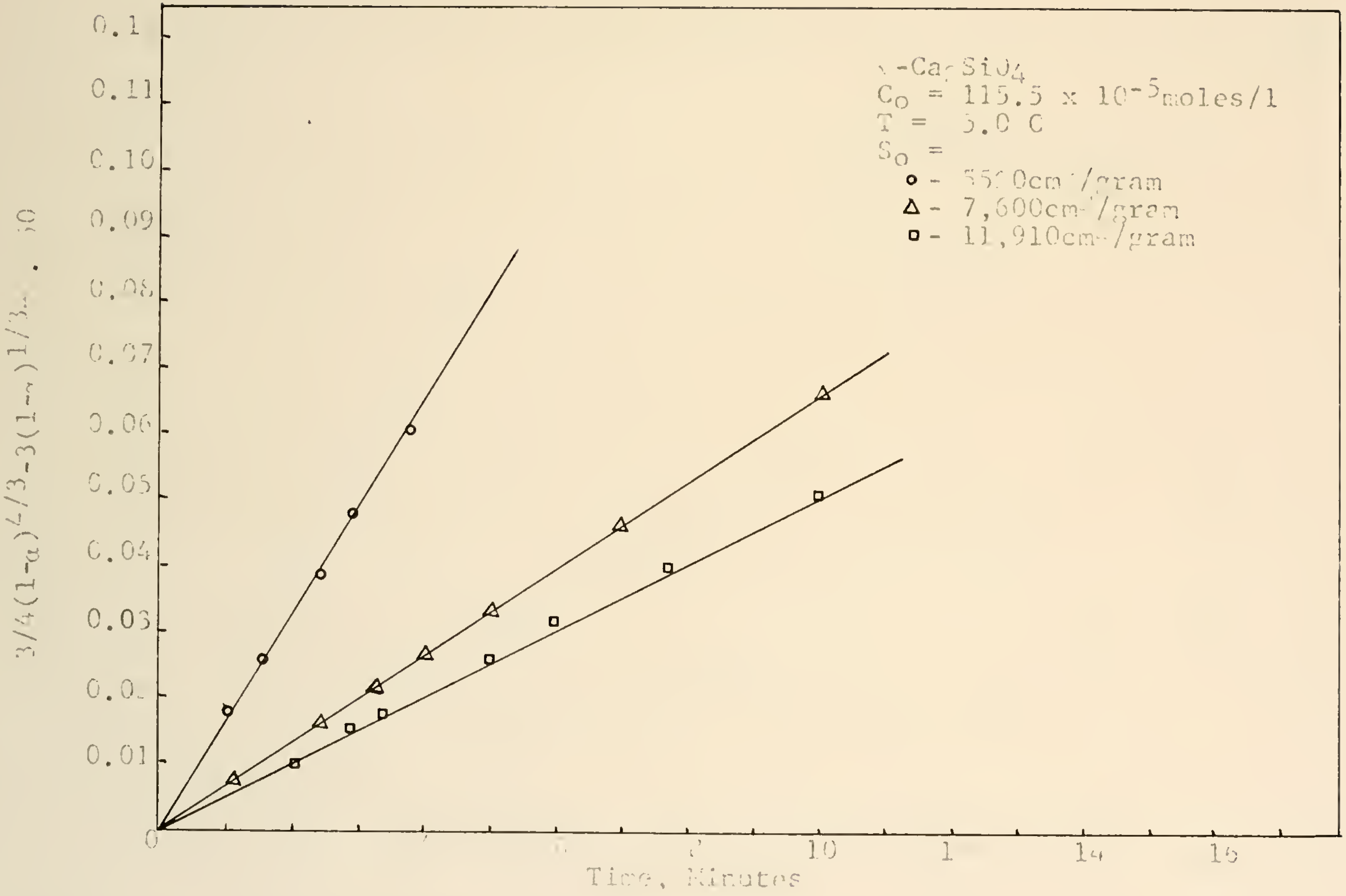

Figure 46. Reaction of γ-Ca_2SiO_4 with Water, effect of Surface Area (C_o)

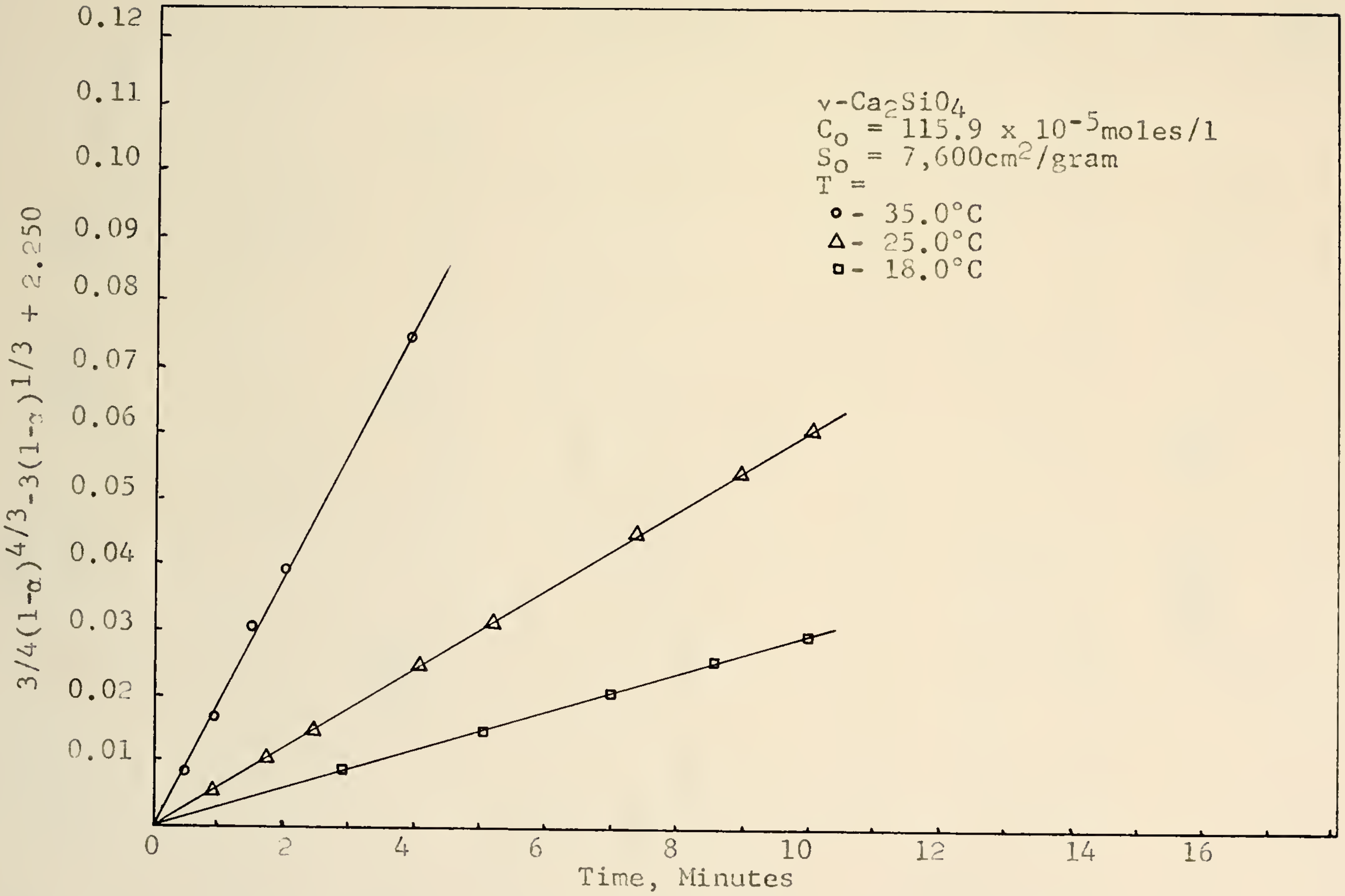

Figure 47. Reaction of γ-Ca_2SiO_4 with Water, Effect of Temperature

$$tk'' = \frac{3}{4}(1-\alpha)^{4/3} - 3(1-\alpha)^{1/3} + \frac{9}{4} \qquad (20)$$

where

$$k'' = \frac{k}{2}(4\pi)^{1/3}\left(\frac{3M}{\rho}\right)^{2/3}\frac{(K_w n)^{1/3}}{c_o{}^{4/3}} \qquad (21)$$

Figures 42-47 show a plot of the right hand side of equation (20) vs. t for β -and γ-Ca_2SiO_4. The values of k'', and therefore of k', can be obtained from the slopes of these curves.

If some $Ca(OH)_2$ is in solution at t = 0, then

$$c = c_t - c_i \qquad (22)$$

where c is the amount of anhydrous silicate reacted, c_t is the concentration of $Ca(OH)_2$ at time t, and c_i is the initial concentration of $Ca(OH)_2$.

For such conditions the rate law can be rewritten as

$$\frac{dc}{dt} = \frac{k}{2}(4\pi)^{1/3}\left(\frac{3M}{\rho}\right)^{2/3}(K_w n)^{1/3}\frac{(c_o-c)^{2/3}}{c_o-c_i} \qquad (23)$$

When this equation is integrated, the initial condition of $c = c_i$ at $t = 0$ is applied, and $\alpha = c/c_o$ is inserted where applicable the result is

$$\frac{tk}{2}(4\pi)^{1/3}\left(\frac{3M}{\rho}\right)^{2/3}\frac{(K_w n)^{1/3}}{c_o{}^{4/3}} = \frac{3}{4}(1-\alpha)^{4/3} - 3(1-\alpha)^{1/3} - 3\left[\frac{c_i}{c_o}\right](1-\alpha)^{1/3} + \frac{9}{4} \qquad (24)$$

Figures 48 and 49 show a plot of the right hand side of equation (24) vs. time, from the slopes of which the values of k can be obtained. Since the ordinate includes the variable c_i, the plots (for each silicate starting material) should fall on a single line. It can be seen that the data are reasonably good in this regard.

Values of activation energies can be obtained from a plot of ln k vs. 1/T or, alternately, from a plot of the right hand side of equation (24) vs. 1/T since the slope is proportional to k. Figures 50 and 51 show such (latter) plots for β- and γ-Ca_2SiO_4 respectively.

The measured activation energies for the reaction of β-Ca_2SiO_4 and for γ-Ca_2SiO_4 are 11.4 Kcal/mole and 16.6 Kcal/mole, respectively.

The values of the rate constant k, determined as outlined above, are given for the various size fractions of β- and γ-Ca_2SiO_4 in Tables 12 and 13, respectively.

Table 12. Calculated Values of k for β-Ca_2SiO_4

So, cm^2/g	k, min^{-1}
8,260	36.3
13,250	48.6
16,420	42.7
17,350	48.6

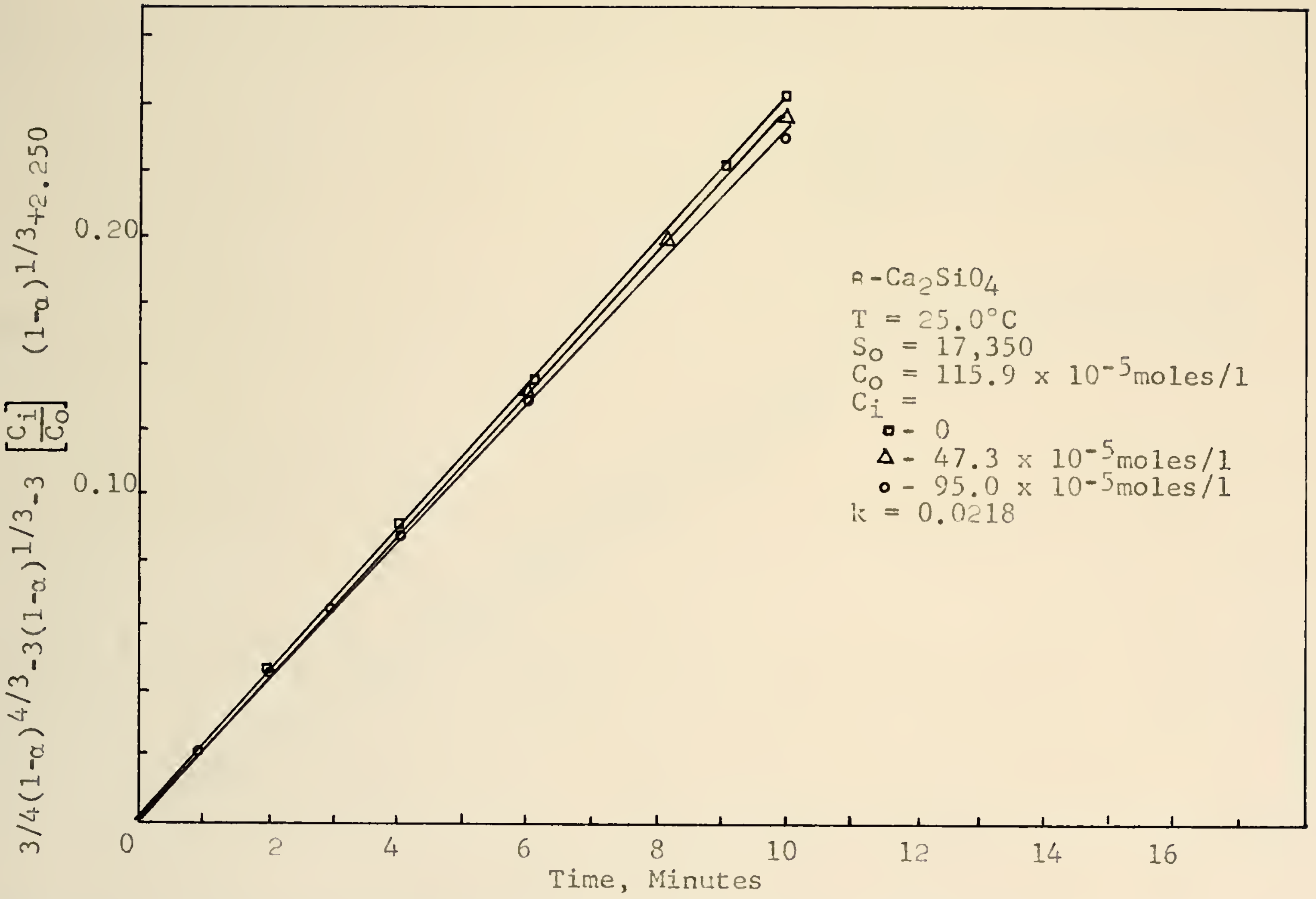

Figure 48. Reaction of β-Ca_2SiO_4 with $Ca(OH)_2$ Solutions at 25.0°C

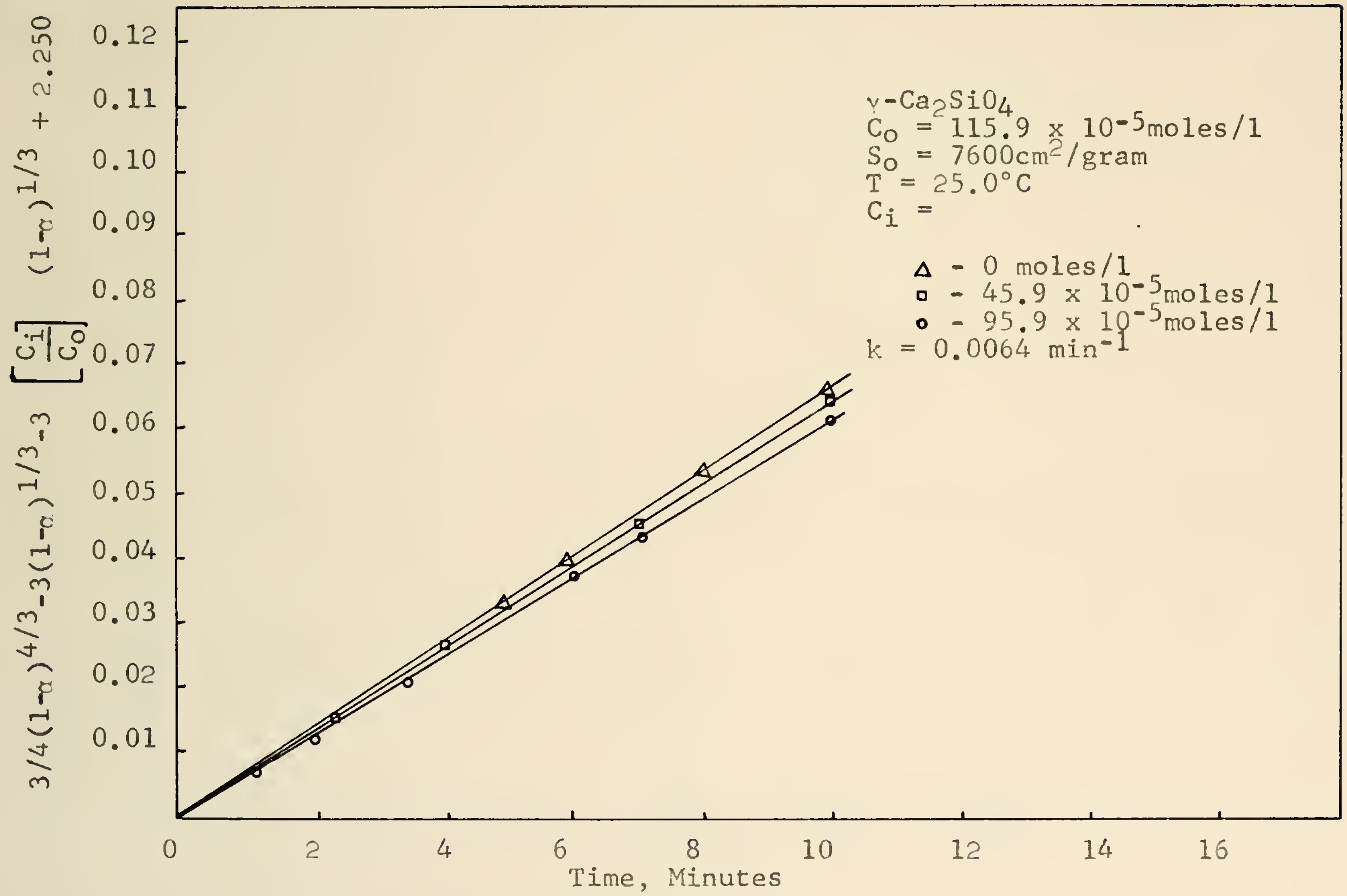

Figure 49. Reaction of γ-Ca_2SiO_4 with $Ca(OH)_2$ Solutions at 25.0°C

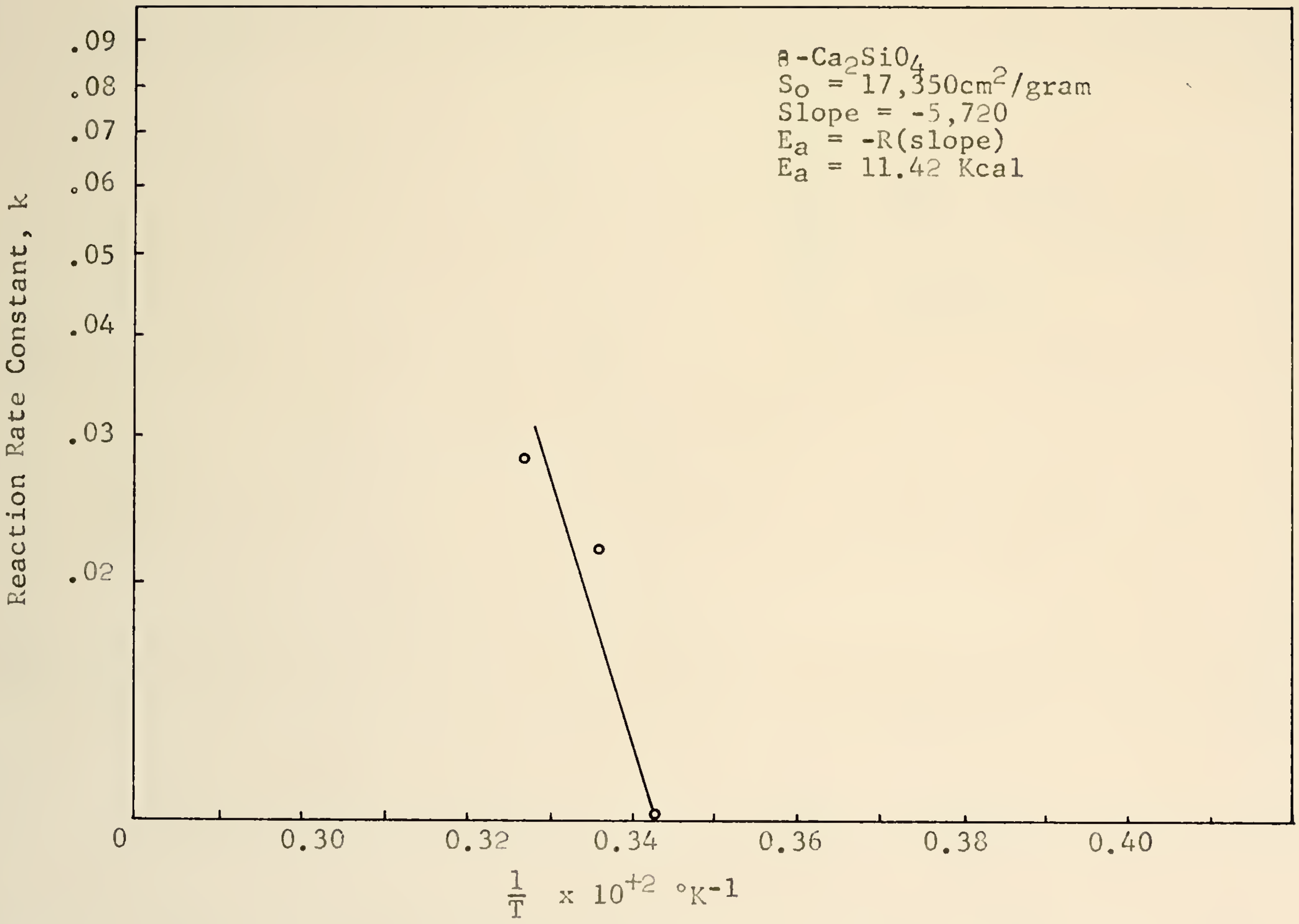

Figure 50 . Rate Constant Dependence on Temperature for °-Ca_2SiO_4

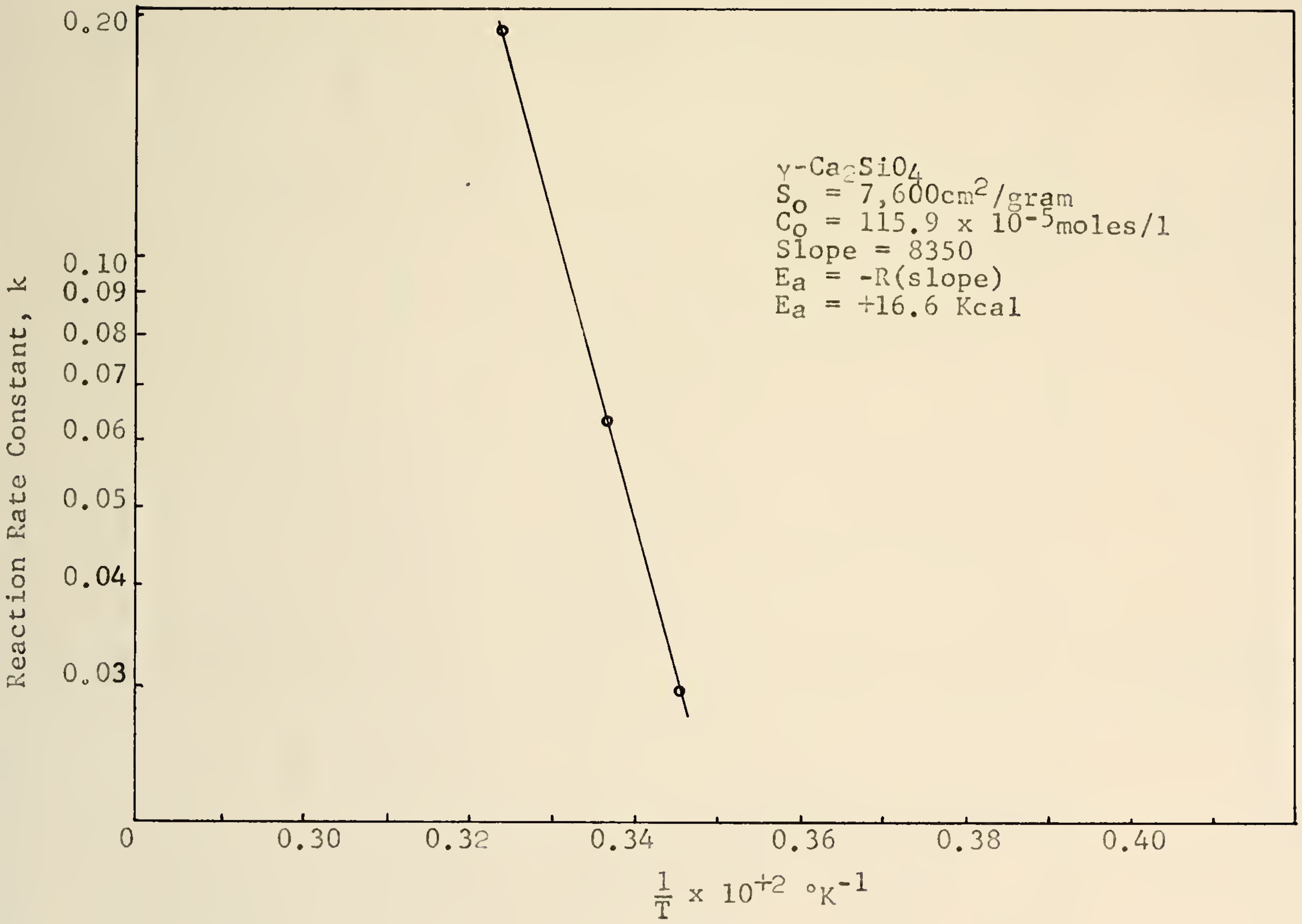

Figure 51. Activation Energy for $\gamma\text{-}Ca_2SiO_4$

Table 13. Calculated Values of k for γ-Ca_2SiO_4

So, cm^2/g	k, min^{-1}
5,520	27.3
7,600	31.1
11,910	47.7

Theoretically, k should be constant, for a given reaction, and independent of the specific surface area. Inspection of Tables 12-13 shows that this is not strictly true for the data developed in this work. If a variability in particle shape existed among various size fractions, it would account partly for such a variation. Since the measured values of k for β- and γ-Ca_2SiO_4 are so close to each other the activation energies given above may be better measures of their relative reactivities, since they were determined for a constant size fraction of starting material, than are the k values.

The kinetic rate law for Ba_2SiO_4 and Sr_2SiO_4 shows a 3/2 order for surface area dependence. The kinetics are determined by the slowest of a series of reaction steps. The steps are, for these hydration reactions studied here, postulated to be diffusion of the reactants to the surface, bond formation and reaction on the surface, bond breaking, and diffusion of the products away from the reaction surface.

If the rate determining step for the reaction of Ba_2SiO_4 and Sr_2SiO_4 were bond formation the question arises,

why is the rate not dependent on the hydroxyl or hydrogen ion species present in solution? To gain some insight into this question the hydrolysis of silicate ions by bases is first considered. Edwards (57) stated that $H_2SiO_4^{=}$ ions exchange oxygen rapidly with water in basic solution, but that the mechanism of this reaction involves an expanded five-fold coordinate intermediate. This kind of process is impossible for the hydrolysis of an ion confined to the surface of a solid, because of the severe volume restrictions. Hydrolysis by a proton to a silicate anion would, however, involve no volume change. For either of these cases the pH of the reaction medium should influence the rate directly, but for the case of attack by a water molecule, the effect of pH should be catalytic. For any of these hydrolysis steps the predicted rate law should be first order in surface area.

The absolute rate law of Eyring (59), applied to chemical kinetics, states that the order of the reactant in the rate law gives its contribution to the composition of the activated complex.

The surface area of a material is proportional to the number of sites on its surface, which are SiO_4^{-4} ions in this case. If the reaction proceeds as follows:

Step 1: $M_2SiO_4 + H_2O \longrightarrow (\frac{1}{2}M(OH)_2 + \frac{1}{2}M_3(HSiO_4)_2)_{surf.}$

Step 2: $(\frac{1}{2}M(OH)_2 + \frac{1}{2}M_3(HSiO_4)_2)_{surf.} \longrightarrow M(OH)_2 + MH_2SiO_4$

and, if the rate determining process is bond breaking, then each bond to be broken is an active site. If the rate determining step is the dissolution of the $M_3(HOSiO_3)_2$, followed by the rapid hydrolysis of this product to MH_2SiO_4 in solution, then the number of bonds to be broken in dissolving the $M_3(HOSiO_3)_2$ would be three halves times the surface area.

The processes postulated, therefore, for the reactions of Ba_2SiO_4 and Sr_2SiO_4 are the initial formation of $M(OH)_2$ and $M_3(HOSiO_3)_2$, the rate determining dissolution of $M_3(HOSiO_3)_2$ from the surface, and then the very rapid hydrolysis to $H_2SiO_4^{=}$ and M^{+2} and OH^- ions. If this process is valid, the lack of the thermodynamically stable $H_3SiO_4^-$ ions can perhaps be explained by the fact that the $HSiO_4^{-3}$ ion is the intermediate species, and two hydrolysis steps must occur before $H_3SiO_4^-$ ions can be formed. The intermediate ion $HSiO_4^{-3}$ would not be expected to polymerize, which may explain the lack of polymerization of the silica in solution. If $H_3SiO_4^-$ ions were formed, rapid polymerization would be expected to occur.

The relative reactivaties of Ba_2SiO_4 and Sr_2SiO_4 can be explained in terms of the strength of the bond in the reaction intermediate between the cation M^{+2} and the anion on the surface $HSiO_4^{-3}$. The bond in $Ba_3(HSiO_4)_2$ is weaker than in $Sr_3(HSiO4)_2$ and, consequently, should decompose off the surface and into solution more rapidly. If bond

formation were the rate determining step one would predict that the compound that offered the higher density of reactive surface sites would be the more reactive. The strontium ion is smaller than barium, packs closer in the anhydrous orthosilicates, and would therefore be predicted to be more reactive than Ba_2SiO_4 for bond formation. The fact that the observed reaction rate constants are reversed lends support for the bond breaking mechanism.

The process for β - and γ -Ca_2SiO_4 is postulated to be one of bond formation. The observed rate law predicted first order dependence in surface area, or reactive sites, and in proton concentration. The process proposed is, therefore, bond formation by single protonation of a silicate ion on the surface of the anhydrous orthosilicate, followed by more rapid dissolution of $M(OH)_2$ and $M_3(SiO_4H)_2$, and then by very rapid hydrolysis of the $HSiO_4^{-3}$ to $H_2SiO_4^{-2}$.

Alternatively the hydrolysis could occur by H_3O^+ ion, in which case the species produced would be MH_2SiO_4 and $M(OH)_2$. There is not enough evidence to distinguish between the two processes.

The fact that the denser of the crystallographic modifications is more reactive lends support to the bond formation alternative.

This discussion of mechanism can then be summarized as follows. All four of the orthosilicates studied, barium,

strontium and the two calcium phases, are postulated to have the same initial reaction processes with water: protonation of a surface silicate ion to form $HSiO_4^{-3}$, dissolution of $M_3(HSiO_4)_2$ from the surface, and further hydrolysis to produce $H_2SiO_4^{-2}$ in solution. In the cases of the barium and strontium silicates the slow, and therefore rate-determining, step is the second of these. For the calcium compounds the slow step is the first.

SUMMARY OF RESULTS

The hydrates of Ba_2SiO_4, Sr_2SiO_4, β-Ca_2SiO_4, and γ-Ca_2SiO_4 had a molar ratio of $MO:SiO_2$ of approximately 1. The hydrates are composed of M^{+2} ions and $H_2SiO_4^{=}$ ions. The hydrate prepared from the cadmium cation also had a molar ratio of $MO:SiO_2$ of 1:1 and was composed of the $H_2SiO_4^{=}$ ion and the Cd^{+2} ion. The appearance of the hydrates of Sr_2SiO_4 and of β- and γ-Ca_2SiO_4 were small needle or lath shaped crystals. The micrograph of CdH_2SiO_4 showed little structure.

The results of the infrared spectra studies of the anhydrous orthosilicates show similarities for all the spectra and a general shift in frequencies to lower values of the asymmetric stretching mode and higher values of deformation mode for larger cations. The theoretically-predicted triply-split degeneracy did not occur, and the three-fold degenerate modes were only doubly split.

The spectra of the hydrates were similar to those of their anhydrous analogues, except for a slight shift in frequencies and the loss of resolution of some splittings.

When the orthosilicates of barium, strontium and calcium were reacted with water the ions M^{+2}, OH^-, and $H_2SiO_4^{=}$

were produced.

The rates of reaction of Ba_2SiO_4 and Sr_2SiO_4 were independent of pH between values of 7 and 11. The kinetic rate law found to be followed by Ba_2SiO_4 and Sr_2SiO_4 in their reaction with water was

$$\frac{dc}{dt} = kS^{3/2}$$

while that for β-and γ-Ca_2SiO_4 was

$$\frac{dc}{dt} = kS\ [H^+]$$

where S means surface area of the anhydrous silicate.

The activation energies of hydration of Ba_2SiO_4 and Sr_2SiO_4 were 4.82 kcal/mole and 9.05 kcal/mole, respectively. The reactivation energies of hydration of β-and γ-Ca_2SiO_4 were 11.4 kcal. and 16.1 kcal., respectively.

The compounds Mg_2SiO_4 and Cd_2SiO_4 were found to be inert to the reaction of water.

CONCLUSIONS

The following conclusions seem reasonable. They are based on the findings of this study, on the materials used, and on the tests performed.

1. When alkaline-earth orthosilicates react with water the soluble products formed are also orthosilicates. Precipitates form by combination of these orthosilicate anions with cations in solution, and these precipitates are, at least initially, also orthosilicates.

2. The process of the hydration of alkaline-earth orthosilicates is postulated to be 1) protonation of a silicate ion in the surface to form the tribasic orthosilicate ion, followed by 2) dissolution of the tribasic metallic orthosilicate from the surface. Either of these steps can be rate-determining. The tribasic ion is rapidly converted in solution to the dibasic orthosilicate anion.

BIBLIOGRAPHY

BIBLIOGRAPHY

1. Nurse, R. W., "Proceedings of the Third Intern. Symp. on Chem. of Cements" pp. 73, Cement and Concrete Assoc., London (1952).

2. Zhuravlev, V. F., *Izv Sektora Fiz. Khim. Anal., Nat. Obshchei i Neorg. Khim., Akgd. Nauk SSSR*, 16, 47-54, (1948).

3. Gallo, G., *Chem. Age*, *57*, 318, (1947).

4. Warren, B. E., *J. Am. Ceram. Soc.*, *16*, 412, (1933).

5. Toropov, N. A., et al., *Zhur. Neorg. Khim.* *8*, 1342-4, (1963).

6. Glushkova, V. and Keler, F., *Zhur. Neorg. Khim.*, *2*, 1254-8, (1957).

7. Hanna, K., Ph.D., Dissertation University of Illinois; *Dissertation Abstracts*, *25*, (2), 1071-2, (1964).

8. Eskola, P., *Am. J. Sci.*, (5), *4*, 331, (1922).

9. Lehmann, Muller, and Wermbter, *Tonnindustry Zietung*, *86*, 578-84, (1962).

10. Levin, E. M. and Ugrinic, G. M., *J. Res. Natl. Bur. Std.*, *51*, 37, (1953).

11. O'Daniel, H. and Tscheischwili, L., *Z. Krist*, *104*, 348-57, (1942).

12. Funk, H., *Z. Anorg. and Allgemeine Chem. 296*, 46-61, (1958).

13. Hohne, E. and Dornberger-Schiff, K., *Acta Cryst.*, *14*, 1298, (1961).

14. Nurse, R. W., *J. Applied Chem.*, *244*, (1952).

15. Glasser, L. S. and Glasser, F. P., *Acta Cryst.*, *18*, 453-4, (1965).

Government Printing Office, Washington D. C., (1960).

34. Landolt Bornstein, 1, (2), 258.

35. Pepperhoff, W., Eisenhuttenw. 29, 153, (1958).

36. Petch, H. E., Sheppard, N. and Megaw, H. D., Acta Cryst., 9, 29-34, (1956).

37. Nakomoto, K., "Infrared Spectra of Inorganic and Coordination Compounds," John Wiley and Sons, New York, (1963).

38. Fujita, J., et al., J. Am. Chem. Soc., 78, 3963, (1956).

39. Gamo, I., Bull. Chem. Soc. Jap., 34, 760-65, 1430-3, (1961)

40. Sartori, G., et al., J. Inorg. and Nucl. Chem., 8, 119, (1958).

41. Scargill, D., J. Chem. Soc., 1961, 4440, (1961).

42. Eyring, H. Walter, J. and Kimble, G., "Qautum Chemistry," 10th ed. pg. 172, John Wiley and Sons, New York, (1961).

43. Jaffe, S., Orchin, M., "Symmetry in Chemistry," John Wiley and Sons, Inc., New York, (1965).

44. O'Conner, T. L., and Greenberg, S. A., J. Chem. Phys., 62, 1195-98, (1958).

45. Herzberg, G., 'Molecular Spectra and Molecular Structure II, Infrared and Raman Spectra of Polyatomic Molecules," D. Van Nostrand Co., Inc., Princeton, New Jersey, pg. 69, (1956).

46. Iler, R., "Colloidal Silicate Chemistry of Silica and Silicates," Cornell University Press, Ithaca, New York, (1955).

47. Weyl, H., "The Theory of Groups and Qauntum Mechanics," 2nd ed., Dover Publ. Inc., New York, (1931).

48. Fortnum, D. H., Ph.D. Thesis, Brown University, Dissertation Abstract, 19, 2240, (1959).

49. Frydrych, R., Ber., 97, 151-8, (1964).

50. Spring, W., Z. Phys. Chem., 1, 209, (1887).
2, 13, (1888).

16. Carlson, E. T., and Wells, L. S., *J. Res. Natl. Bur. Std.* *51*, 73, (1953).

17. Tornebohm, A., *Tonindustrie-Zeitung*, *21*, 1148-51, (1897).

18. Jeffery, J. W., *Acta Cryst.* *5*, 26, (1952).

19. Smith, D., Majumdar, A. J. and Ordway, F., *J. Amer. Ceram. Soc.*, *44*, 405-11, (1961).

20. Smith, D., Majumdar, A. J. and Ordway, F., *Acta Cryst.* 18, 787-95, (1965).

21. Midgely, C. M., *Acta Cryst.*, *5*, 307, (1952).

22. Heller, and Taylor, "Crystallographic Data for Calcium Silicates and Calcium Silicate Hydrates," Her Majesty's Stationery Office, London, (1956).

23. Taylor, H. F. W., "The Chemistry of Cement Hydration," in Burke, J. E., "Ceramic Science," *1*, pg. 89, Pergamon Press, (1961).

24. Taylor, H. F. W., "The Chemistry of Cements," Academic Press, New York, (1964).

25. Greenberg, S. A. and Chang, T. N., *J. Phys. Chem.*, *69*, 182-188, (1965).

26. Thorvaldson, T., "Proceedings of the Fourth Intern. Symp. on the Chem. of Cement," *1*, pp. 315-20, U. S. Government Printing Office, Washington D. C., (1960).

27. Roller, P.S. and Erwin, G., *J. Am. Chem. Soc.*, *62*, 461, (1940).

28. Kantro, D., et al., "Solid Surfaces and the Gas Solid Interface," "Adv. in Chem. Series," *33*, 199-219, (1961).

29. Tarte, P., *Spectrochim Acta 18*, 467-83, (1962).
Spectrochim Acta 19, 25-47, (1963).
Bull. Soc. France Ceram. 58, 13-54, (1963).

30. Halford, R. S., *J. Chem. Phys.* *14*, 8, (1946).

31. Matossi, F., *J. Chem. Phys.* 17, 679, (1949).

32. Saksena, B. D., *Disc. Faraday Soc.* *1961*, 242-58, (1961).

33. Hunt, C. M., "Proceedings of the Fourth Intern. Symp. on the Chem. of Cement," *1*, pp. 297-305, U. S.

51. Moelwyn-Hughes, E. A., "Physical Chemistry," 2nd ed., Pergamon Press, London, (1961).

52. Glasstone, S., "Physical Chemistry," D. Van Nostrand Co., Inc., New York, (1940).

53. Benson, S. W., "The Foundations of Chemical Kinetics," McGraw Hill Book Co., Inc., New York, (1960).

54. Klug, H. P., and Alexander, L. E., "X-ray Diffraction for Polycrystalline and Amorphous Materials," John Wiley and Sons, New York, (1954).

55. Faeth, P., and Willingham, C., "Technical Bulletin on The Assembly, Calibration, and Operation of a Gas Adsorption Apparatus for the Measurement of Surface Areas of Finely Divided Solids," Mellon Institute of Industrial Research, Pittsburgh, (1955).

56. Edwards, J. O., "Inorganic Reaction Mechanisms," W. A. Benjamin, Inc., New York, pg. 142, (1964).

APPENDIX A

APPENDIX A

Description of BET Method and Apparatus for Krypton Adsorption Isotherms and Surface Areas

Krypton gas has a vapor pressure of between 2 and 3 mm of mercury at liquid nitrogen temperatures. This low vapor pressure makes krypton useful for the investigation of materials with small surface areas. Nitrogen adsorption is impractical for specific surface areas smaller than one square meter per gram. The surface areas of the anhydrous orthosilicates used in this study ranged from 950 to 17,500 square centimeters per gram, so krypton gas adsorption was measured at liquid nitrogen temperatures to determine their surface areas.

The procedure of Faeth and Willingham (55) was used. The apparatus is shown in Figure A-1.

The procedure was modified to preserve the expensive krypton. Faeth and Willingham recommended using a calibrated doser to introduce a known volume of gas at a pressure measured by a mercury manometer. This procedure was modified as follows: the doser was used as a lock to control the amount of krypton allowed into the McCleod gauge system. The volume of the McCleod system was previously measured so

that the amount of krypton added was found by measuring the pressure of krypton in the system before the gas was allowed to equilibrate with the sample.

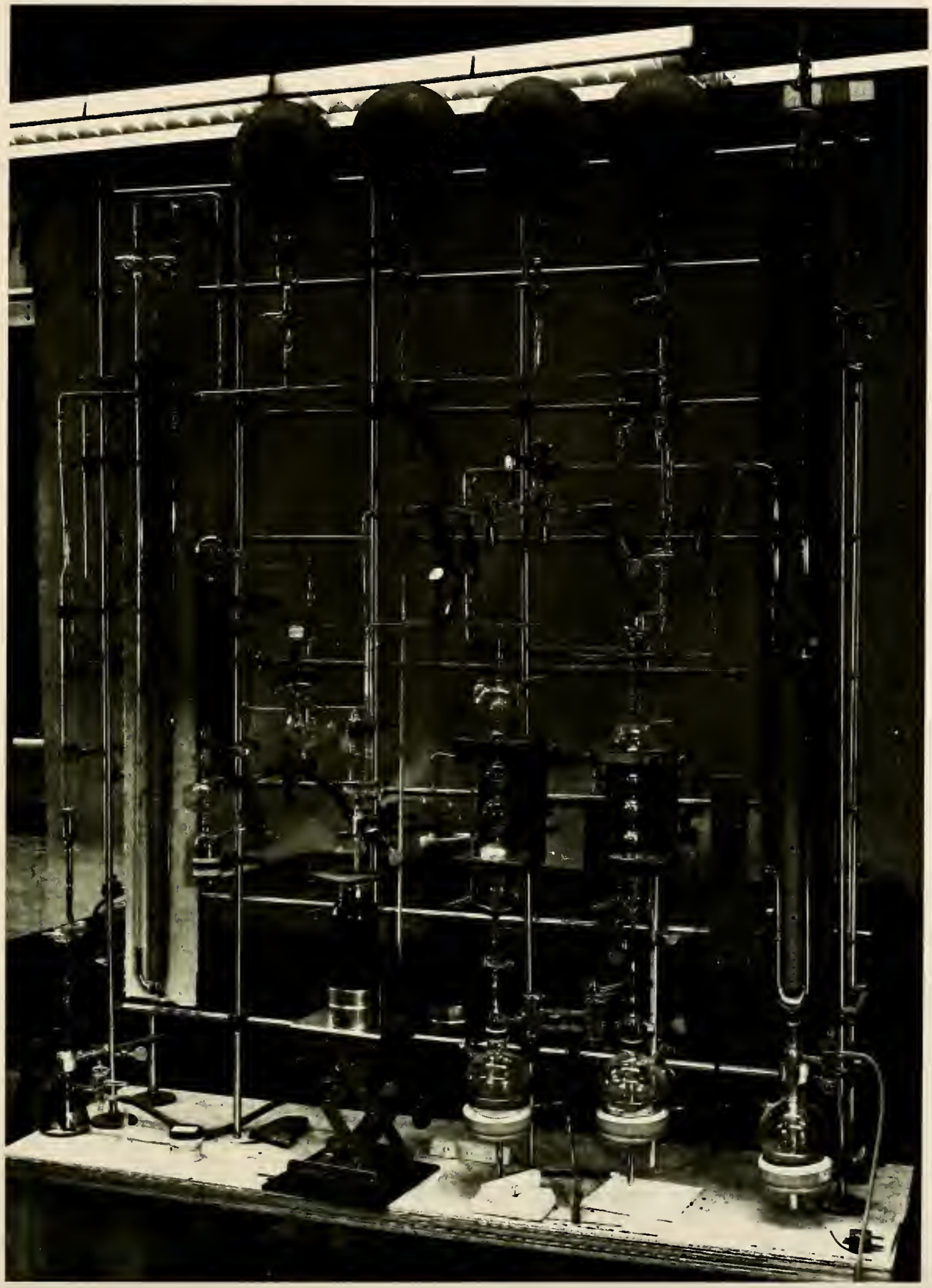

FIGURE A-1. GAS ADSORPTION APPARATUS

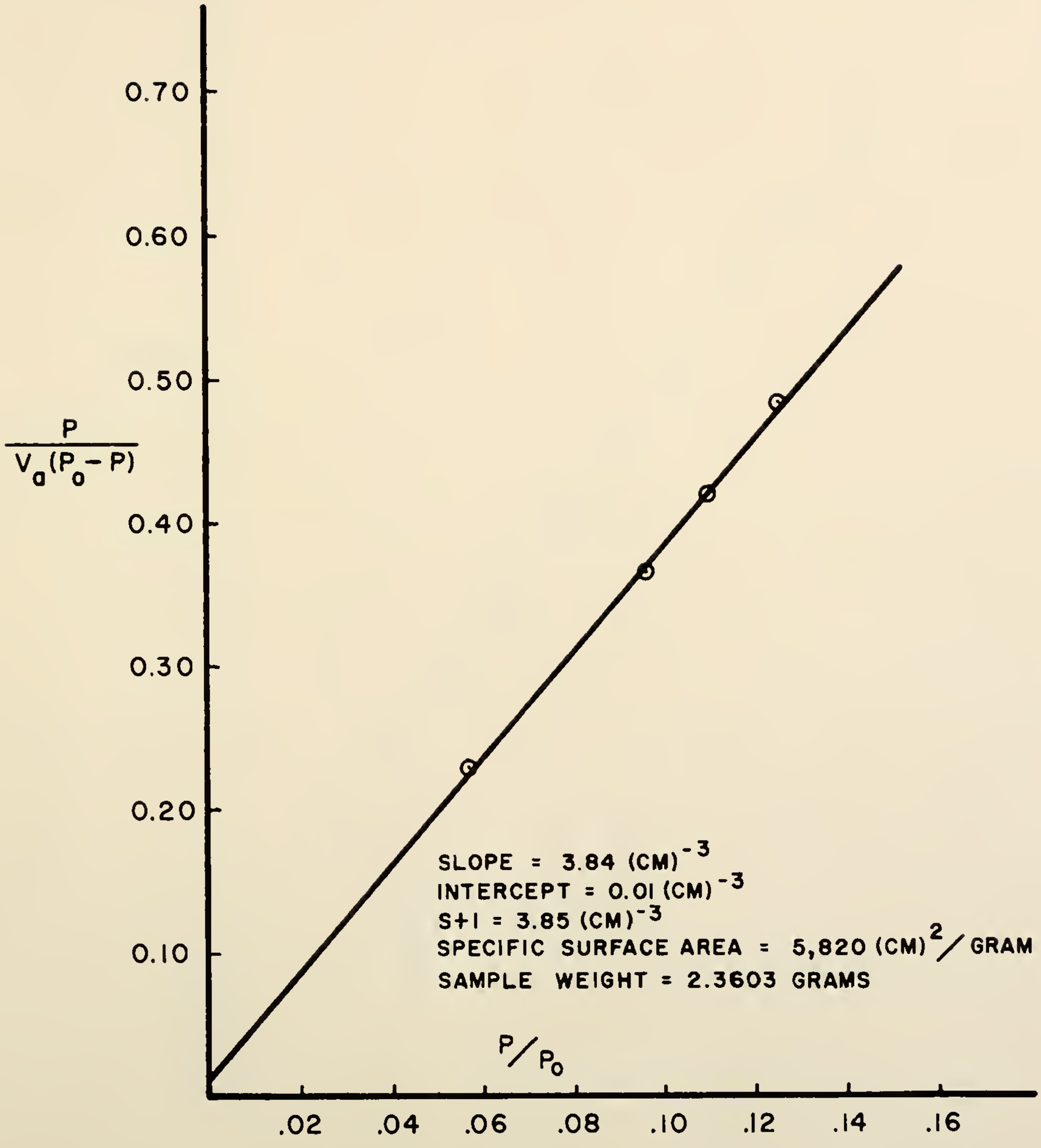

SLOPE = 3.84 $(CM)^{-3}$
INTERCEPT = 0.01 $(CM)^{-3}$
S+I = 3.85 $(CM)^{-3}$
SPECIFIC SURFACE AREA = 5,820 $(CM)^2$/GRAM
SAMPLE WEIGHT = 2.3603 GRAMS

FIGURE A-2. KRYPTON ADSORPTION ISOTHERM FOR Ba_2SiO_4, FINENESS FRACTION NO. 1

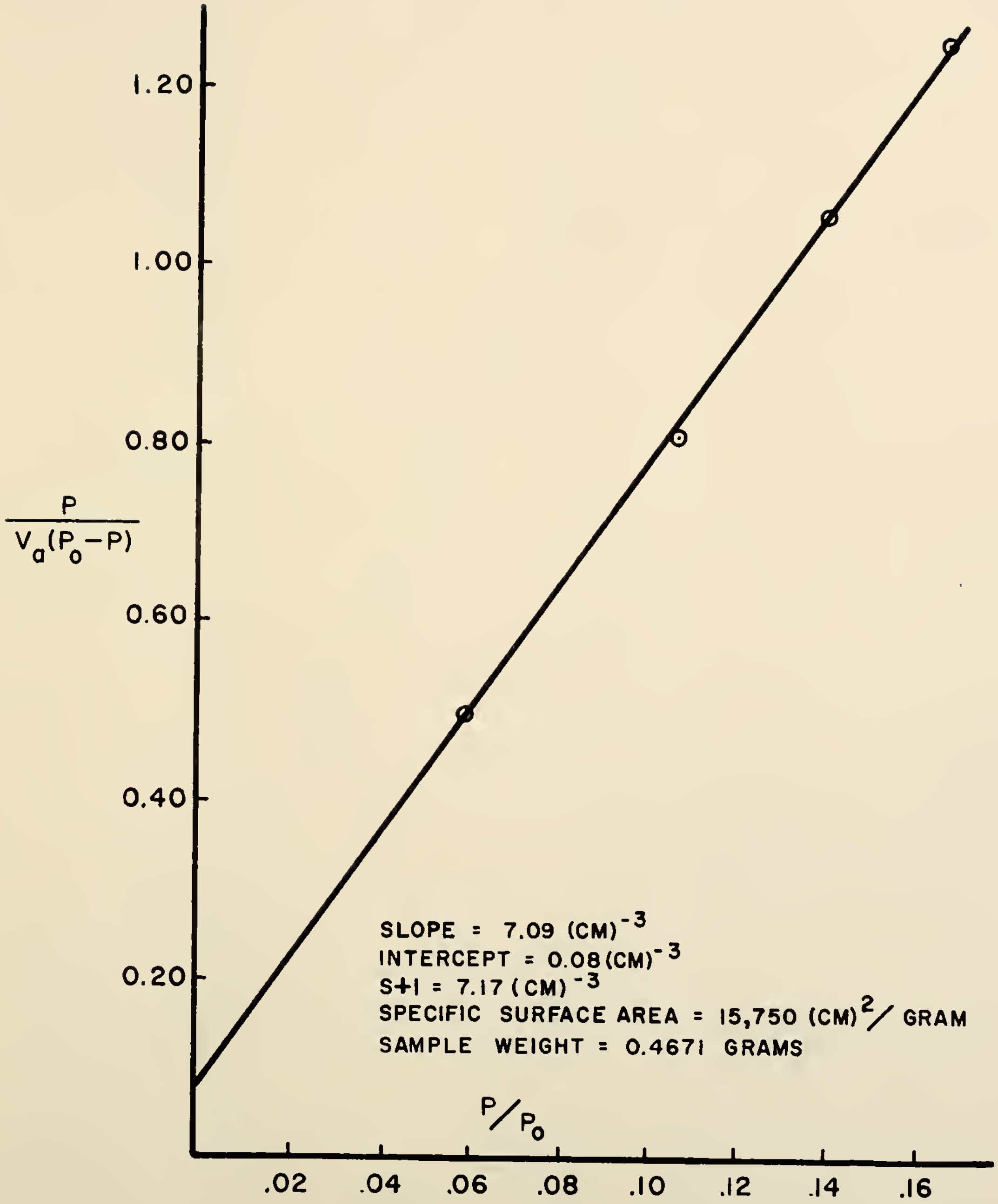

SLOPE = 7.09 $(CM)^{-3}$
INTERCEPT = 0.08 $(CM)^{-3}$
S+I = 7.17 $(CM)^{-3}$
SPECIFIC SURFACE AREA = 15,750 $(CM)^2$/ GRAM
SAMPLE WEIGHT = 0.4671 GRAMS

FIGURE A-3. KRYPTON ADSORPTION ISOTHERM FOR Sr_2SiO_4, FINENESS FRACTION NO. 1

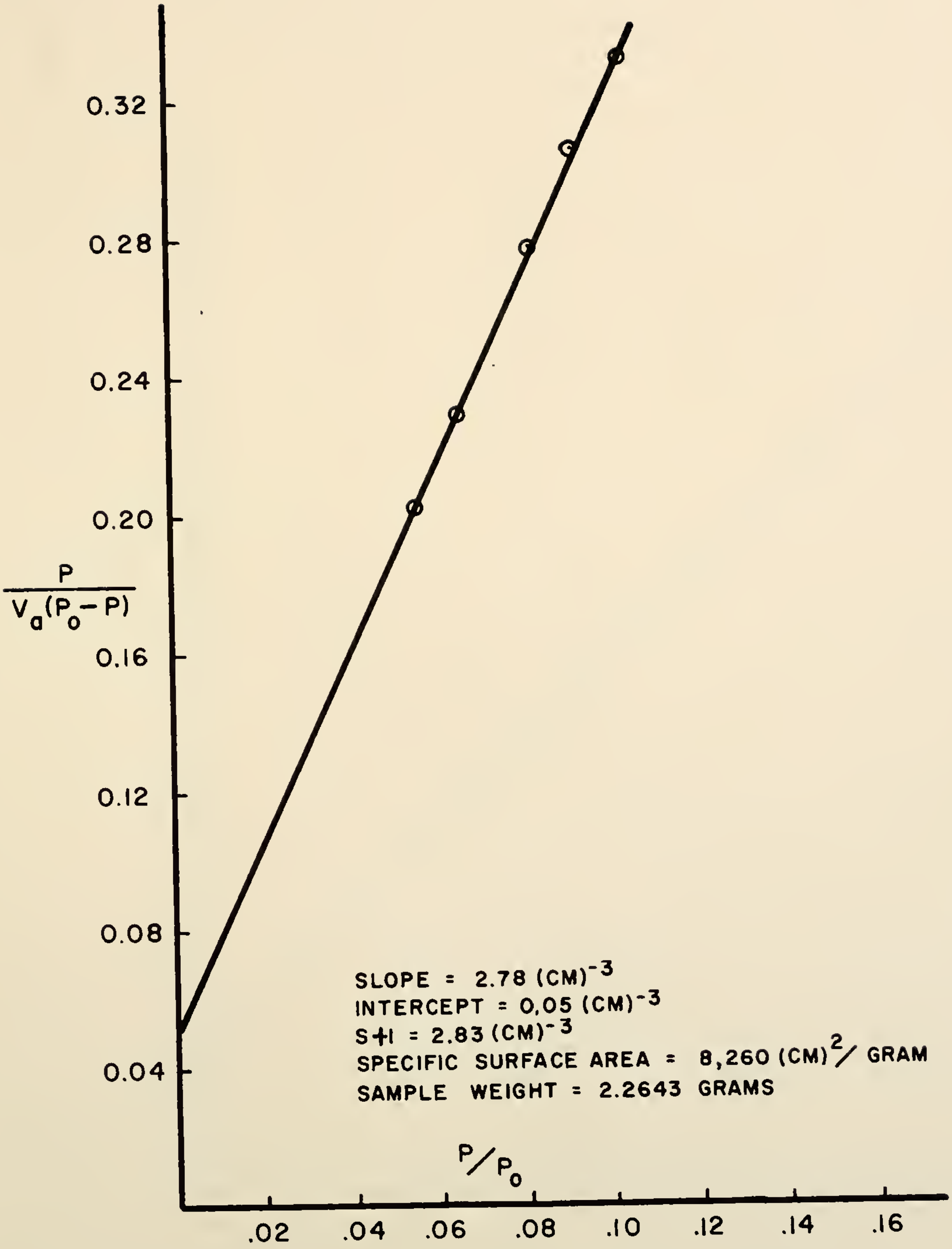

SLOPE = 2.78 $(CM)^{-3}$
INTERCEPT = 0.05 $(CM)^{-3}$
S+I = 2.83 $(CM)^{-3}$
SPECIFIC SURFACE AREA = 8,260 $(CM)^2$/ GRAM
SAMPLE WEIGHT = 2.2643 GRAMS

FIGURE A-4. KRYPTON ADSORPTION ISOTHERM FOR βCa_2SiO_4, FINENESS FRACTION NO. 4

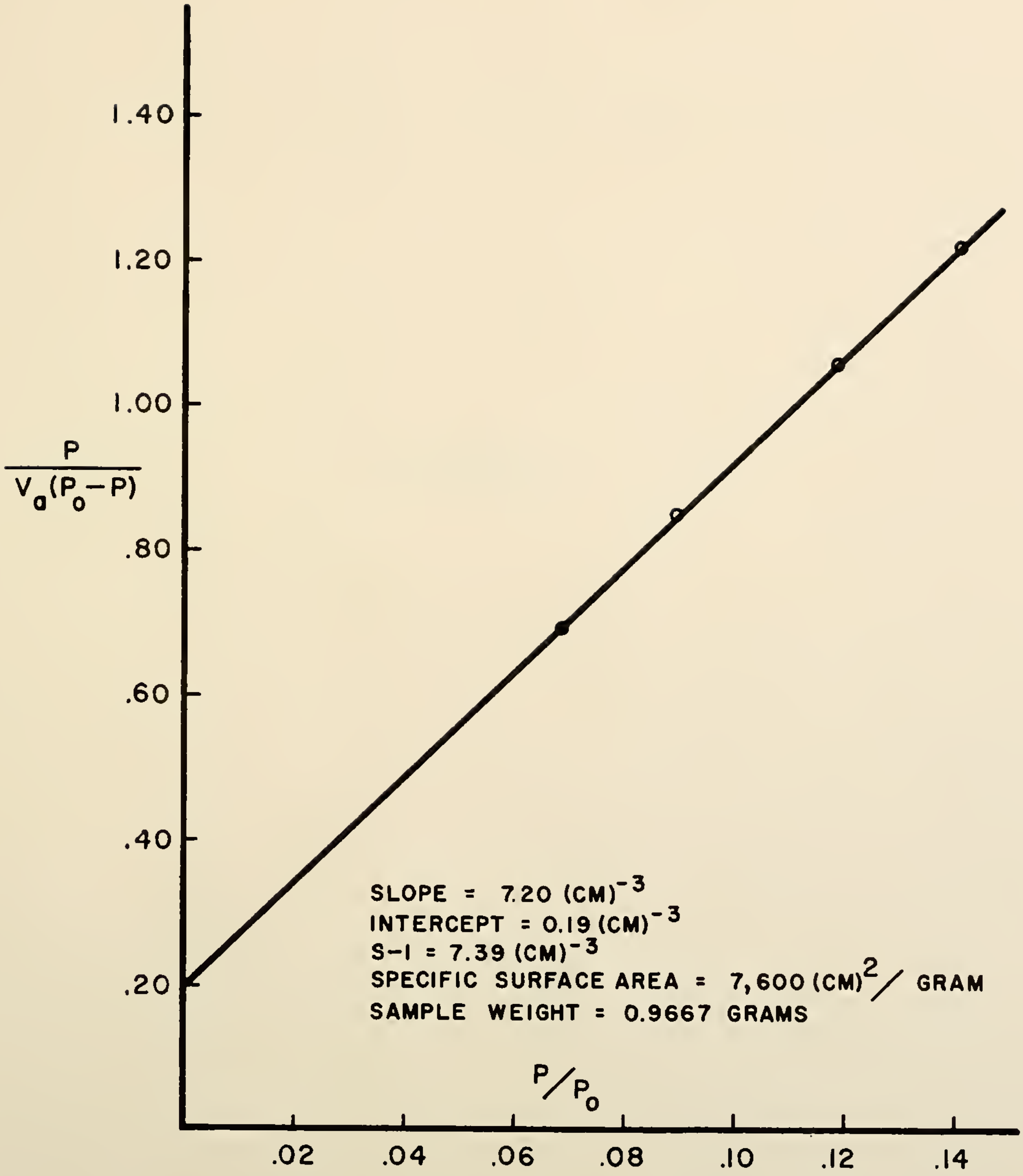

SLOPE = 7.20 $(CM)^{-3}$
INTERCEPT = 0.19 $(CM)^{-3}$
S-I = 7.39 $(CM)^{-3}$
SPECIFIC SURFACE AREA = 7,600 $(CM)^2$/ GRAM
SAMPLE WEIGHT = 0.9667 GRAMS

FIGURE A-5. KRYPTON ADSORPTION ISOTHERM FOR γCa_2SiO_4, FINENESS FRACTION NO. 2

APPENDIX B

APPENDIX B

Description of Circuit for Measuring Resistances and Converting High Frequency A.C. to D.C. Suitable for Sargent SR Recorder

The system was essentially a wheatstone bridge with rectifying and filtering circuits in place of a galvanometer. The circuit is shown in Figure A-2. The rectifying and filtering circuits were of low impedance and loaded the bridge so that the balanced resistances were not the values of the resistors in the bridge but included the impedance of the rectifying circuit.

The fact that current was drawn from the bridge meant that the output was not linear, but this was desirable.

The 0.05μf capacitor was used to block any d.c. level from the rectifying bridge in order to prevent cell polarization. The use of shielded cable and extensive grounding of water bath components and the instrument chassis were measures necessary to obtain precise values of resistance.

The non-linearity of the system enabled any specific resistance range to be expanded logarithmically over full scale of the Sargent SR recorder by nulling the bridge with the highest resistance of interest and then adjusting full scale to read the lowest resistance of interest.

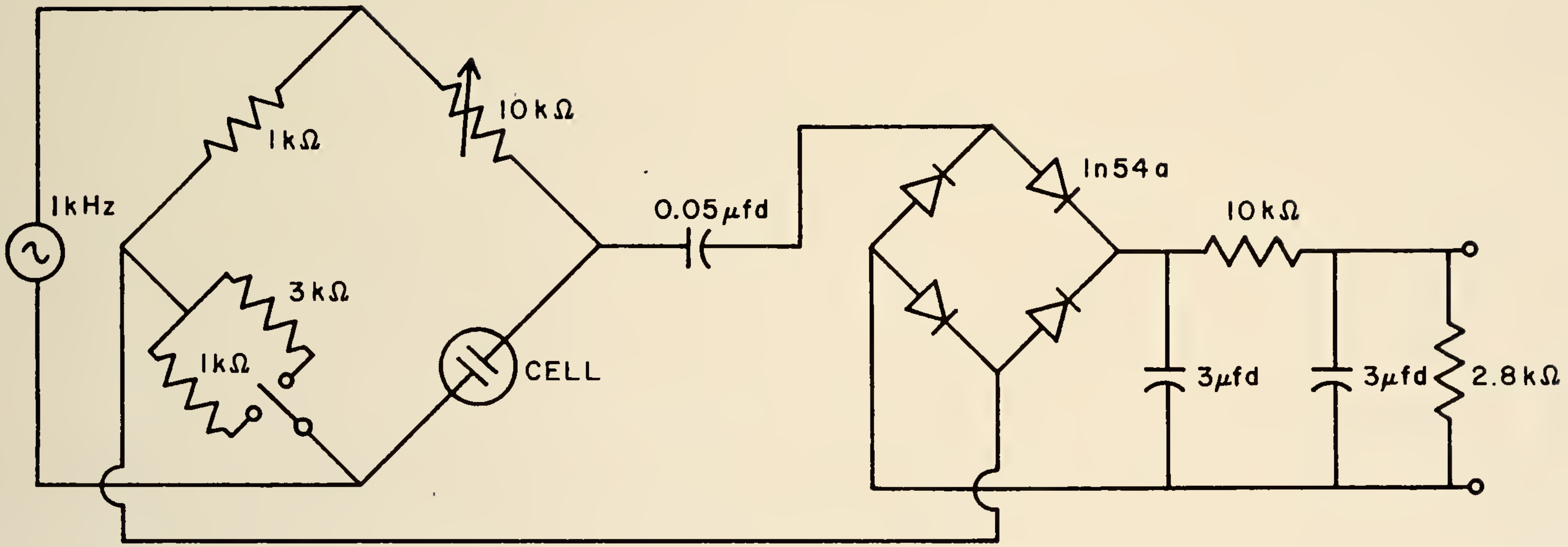
1kHz
1kΩ
10kΩ
3kΩ
1kΩ
CELL
0.05μfd
In54a
10kΩ
3μfd
3μfd
2.8kΩ

FIGURE B-2. BRIDGE CIRCUIT FOR RESISTANCE MEASUREMENT OF SOLUTION

The recorder data can be converted to resistance values by calibrating with a precision potentiometer. Two potentiometers were used to calibrate the recorder; one was 10,000 ohms and the other 100,000 ohms. Their accuracy was found to be better than 1% when checked with an Industrial Instruments Conductivity bridge Model RC 1682.

APPENDIX C

APPENDIX C

Application of Halford's Method to Prediction of Infrared Selection Rules for Orthosilicates

The method of Halford (30) employs the usual group theory analysis of symmetry considerations. The standard treatment of group theory applied to symmetry transformation can be found in books by Eyring, Walter and Kimball (42), Nakamoto (37), Jaffe and Orchin (43), Weyl (44), or Herzberg (45). The book by Nakamoto is of special interest because of its example of internal coordinate analysis.

The method of Halford is applied as follows:

The polyhedron is treated as an unperturbed symmetrical object with the number of atoms it contains. The selection rules are then determined by the normal coordinate transformation operations of group theory.

When the symmetrical polyhedron is confined to a crystal lattice, additional symmetry restrictions are imposed upon it. The imposed symmetry restrictions are almost always a lowering of symmetry, and the results are a change in the selection rules and a splitting of degeneracies.

In crystals the symmetrical environment is such that the polyhedrons almost always sit on sites with special crystallographic symmetry. It is a requirement that the

crystal site symmetry be a subgroup of the molecular symmetry.

Halford states that the molecule in a crystal should be treated as if its maximum symmetry is the subgroup symmetry of the crystallographic site. Physically this means that the crystal and the symmetry of the interactions are governed by crystal symmetry. These arguments cannot predict the magnitude of the energy of the interactions. The intensities of the bands are, therefore, unpredictable.

For orthosilicates of different crystal symmetry Halford's treatment is as follows. A knowledge of the space group and of the unit cell population is necessary. This information is shown in Table A-C-1. The compounds in Table 1 show a variety of four structures: Pmnb(D_{2h}^{24}), P2_1/n, (C_{2h}^{5}), R$\bar{3}$(C_{3i}^{2}).

Halford recognizes the crystallographic principle that the symmetry of the site must be a subgroup of the molecular symmetry and also that the multiplicity of the sites per unit cell must be equal to the number of molecules per unit cell. These principles, with a knowledge of the space group and unit cell populations and a list of the crystallographic space groups and their subgroup multiplicities, enable the prediction of the selection rules of molecules in crystals.

A list of the availabilities and symmetries of the sites in the 230 space groups is included in Halford's paper (30), and a primary reference is Wyckoff (57).

Table A-C-1. Space Group and Unit Cell Population For Some Orthosilicates

Orthosilicate	Space Group	Population of Unit Cell
Cd_2SiO_4	Fddd	8.0
Ca_2SiO_4	$P2_1/n$	4.0
Be_2SiO_4	$R\bar{3}$	18.0
Zn_2SiO_4	$R\bar{3}$	18.0
Mg_2SiO_4	Pmnb	4.0
Ca_2SiO_4	Pmnb	4.0
Sr_2SiO_4	Pmnb	4.0
Ba_2SiO_4	Pmnb	4.0
Co_2SiO_4	Pmnb	4.0
Mn_2SiO_4	Pmnb	4.0
Fe_2SiO_4	Pmnb	4.0
$CaMnSiO_4$	Pmnb	4.0
$CaCoSiO_4$	Pmnb	4.0
$CaMgSiO_4$	Pmnb	4.0

This list is used in the following development:

First, look at the space group V_h^{16}. This space group is called the olivine structure.

From the list of availabilities and multiplicities of crystallographic subgroups we have the following information:

The space group V_h^{16} has two distinct sites of symmetry C_i with four equivalent sites per set and one distinct set of sites with symmetry C_s with four equivalent sites per set.

The isolated silicate tetrahedron has unperturbed symmetry Td. Inspection reveals that Ci is not a subgroup of Td but Cs is a subgroup. The disturbed silicate ion must sit on site Cs. Majumbar, Smith and Ordway (20) have confirmed this site selection by single crystal x-ray measurements.

Normal coordinate analysis using group theory for symmetry Cs gives the selection rules.

The character table for Cs is as follows:

	C_s		E	
x^2, y^2, z^2, xy	R_z, x, y	A'	1	1
xz, yz	R_x, R_y, z	A"	1	-1
		Γm =	15	-3

Decomposing Γ_m we have

$$\Gamma_m = 6A' + 9A''$$

$$\Gamma_{translational} = 2A' + A''$$

$$\Gamma_{rotational} = 2A'' + A'$$

$$\Gamma_{vibrational} = 3A' + 6A'' = \Gamma_m - \Gamma_t - \Gamma_r$$

The analysis of internal coordinates is novel enough to warrant inclusion in detail. The assignment of internal coordinates is explained and illustrated in the book of Nakamoto (37). The stretch coordinates for this isolated tetrahedron are the bond length deformations.

The symmetry transformation A operating on the stretch coordinates gives rise to a matrix M(A) which has a character X(A).

The results show the following:

$A = E$	$X(E) = 4$	$a_1 = \frac{1}{24}(4 + 8 + 12) = 1$
$A = C_3$	$X(C_3) = 1$	$a_2 = \frac{1}{24}(4 + 8 - 12) = 0$
$A = C_2$	$X(C_2) = 0$	$a_3 = \frac{1}{24}(8 - 8 + 0) = 0$
$A = \sigma_d$	$X(\sigma_d) = 2$	$a_4 = \frac{1}{24}(12 - 12 + 0) = 0$
$A = S_4$	$X(S_4) = 0$	$a_5 = \frac{1}{24}(12 + 12) = 1$

or

$$\Gamma_r = A_1 + T_2$$

For the bending coordinates the analysis is similar except that the bending coordinates are defined as angular deformations α_{12}, α_{23}, α_{31}, α_{34}, α_{14}, and α_{24}. The angular deformations are deformations of the interbond angles. The analysis is as follows:

$A = E$ $\quad X(E) = 6$ $\quad a_1 = 1$

$A = C_3$ $\quad X(C_3) = 0$ $\quad a_2 = 0$

$A = C_2$ $\quad X(C_2) = +2$ $\quad a_3 = 1$

$A = \sigma_d$ $\quad X(\sigma_d) = 0$ $\quad a_4 = 0$

$A = S_4$ $\quad X(S_4) = 0$ $\quad a_5 = 1$

$\Gamma = E + T_2 + A_1$, A_1 is redundant.

Internal Coordinate Analysis for Crystal Site Symmetry

For site symmetry C_s the internal coordinate analysis is as follows: For stretch coordinates

$A = E$ $\quad X(E) = 4$ $\quad a_1 = 3$

$A = \sigma_h$ $\quad X(\sigma_h) = 2$ $\quad a_2 = 1$

$\Gamma = 3A' + A''$

For bending coordinates:

$A = E$ $\quad X(E) = 6$ $\quad a_1 = 4$

$A = {}_{n}$ $\quad X(\sigma_n) = 2$ $\quad a_2 = 2$

$\Gamma = 3A_1' + 2A''$

Similar analysis is not applicable directly to site symmetry of C_1, but general lack of symmetry would manifest itself in splitting of all degeneracies.

Thus all degenerate modes of vibration for Td become nondegenerate on the site of C_s symmetry. This splitting is due to the position of the cation in the crystal unit cell. For different structures the cations will be in different positions, and this fact is reflected in the site group symmetry character analysis. The relative effects of this cation on the molecular vibration are two-fold: to change the site symmetry, thereby causing splitting of degenerate vibrations, and to effect a shift in frequency not directly associated with the splitting.

One way to test this assignment would be to use polarized I.R. radiation. Only the A" representation of would be I.R. active with z polarized I.R. radiation.

The character table for C_{2v} is as follows:

C_{2v}	E	$C_2(z)$	$2\sigma_v(x,z)$			
A_1	+1	+1	+1	+1	z	x^2, y^2, z
A_2	+1	+1	-1	-1	r_x	xy
B_1	+1	-1	+1	-1	r, r_y	xy
B_2	+1	-1	-1	+1	y, r_x	yz

The results of internal coordinate analyses are shown in Table A-C-2.

Table A-C-2. Splittings of T_d Modes under Lower Symmetry Restrictions.

Molecular Symmetry	1	2	3	4
T_d	A_1	E	T_2	T_2
Site Symmetry				
C_s	A_1'	$2A''$	$A'+2A''$	$3A''$
Site Symmetry				
C_{2v}	A_1	A_1+A_2	$A_1+B_1+B_2$	$A_1+B_1+B_2$

The mode assignment and the nature of the modes is described in Herzberg. Figure A-C-1 shows the modes and the degeneracies.

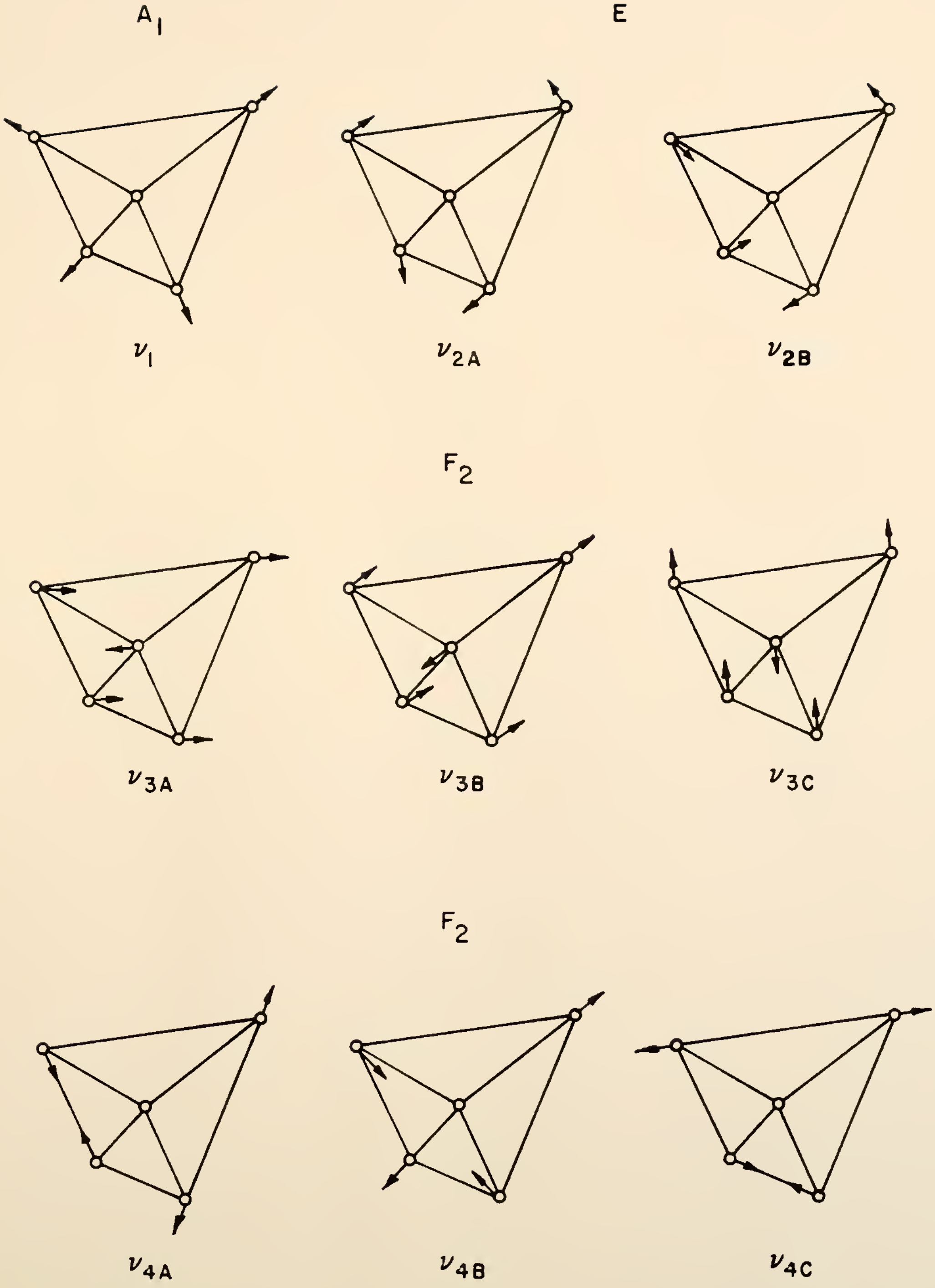
A_1
E
ν_1
ν_{2A}
ν_{2B}
F_2
ν_{3A}
ν_{3B}
ν_{3C}
F_2
ν_{4A}
ν_{4B}
ν_{4C}

FIGURE A-C-1. SYMMETRY MODES FOR AN ISOLATED XY_4 MOLECULE

VITA